



The
University
Of
Sheffield.

**Formalisation and Validation Of a Novel Method Suitable For
Designing Notched Metallic Components Against
Proportional/Non-Proportional Constant/Variable Amplitude
Multiaxial Fatigue**

By

Zuhair Faruq Namiq

A thesis submitted in partial fulfilment of the requirements for the degree
of Doctor of Philosophy

The University Of Sheffield

Faculty of Engineering

Department of Civil and Structural Engineering

April 2019

Declaration of Authorship

I, Zuhair Faruq Namiq, declare that this thesis entitled, (**Formalisation and Validation Of a Novel Method Suitable For Designing Notched Metallic Components Against Proportional/Non-Proportional Constant/Variable Amplitude Multiaxial Fatigue**) and the work presented in it are my own. Where information has been derived from any other source, I confirm that this has been indicated and stated in the thesis.

Signed: _____

Date: _____

ABSTRACT

The construction industry is constantly being challenged to build more complex modern structures using lighter components (thus saving material) but involving not only more complex geometries but also multiaxial loadings. This creates a need to devise an efficient methodology for the design and manufacture of elements that can sustain a wide range of service loads. The investigation of the elasto-plastic deformation of engineering components against multiaxial fatigue load, however, has largely been limited to simple situations where the cyclic load is of a relatively constant amplitude. When both the geometry and load history are more complex, however, inaccuracies might accumulate so that the predicted outcomes end up differing significantly from the experimental result. Multiaxial fatigue is defined as a localised structural problem involving a nominal system of complex cyclic loads that create a corresponding multiaxial local stress/strain history. In addition, any component with a geometrical feature (for instance, notches) under uniaxial fatigue load results in triaxial stress/strain states at any point inside the material. This thesis aims to develop, apply and validate a numerical design technique based on a critical plane theory, suitable to predict the longevity of notched geometries against multiaxial cyclic load involving a random load and the presence of zero/non-zero mean stress. The hypothesis is based on the combination of both the Modified Manson-Coffin Curve Method MMCCM and the Theory of Critical Distances that applied in terms of Point Method (PM) to evaluate fatigue damage in the low/medium-cycle fatigue regime on metallic materials.

Notch geometries with three different notch root radii were modelled and analysed under uniaxial/multiaxial complex fatigue loadings using elasto-plastic finite element ANSYS® software. Both in-phase and out-of-phase fatigue loading were considered. A Kinematic Hardening criterion was used to describe the mechanical behaviour of the material in the plastic regime. The additional non-proportional hardening that accompanies out-of-phase loading was also included in the fatigue model. Then, by taking advantage of the TCD, a local effective stress/strain history was determined in the vicinity of notch root. A key feature of the TCD is that the critical elasto-plastic stress/strain states liable to provoke fatigue damage can be estimated at a specific distance from the notch root for different notch geometry. Such a distance is known as the Critical Distance CD. According to the TCD, the critical distance CD is a material property that changes according to neither the geometrical feature of a component nor the investigated loading paths. To apply the MMCCM correctly, the direction of the critical plane was indicated among that orientation experiencing the Maximum Variance (MV) of the calculated shear strain by using a multi-variable optimisation method called the Gradient Ascent Method. The MMCCM is based on the concept that fatigue cracks initiate on a material plane with the largest shear strain amplitude. The developed approach was then extended to account for the effect of the mean stress/strain and the proportionality of the load sequences. Finally, the number of cycles to failure ($N_{f,e}$) was determined through the Modified Manson-Coffin Curve.

With regard to a Variable Amplitude (VA) cyclic loading, a classic Rainflow method was used as a cycle counting scheme to reduce the complex irregular shear strain history into a series of constant amplitudes. Then, the equivalent shear strain amplitude was used to predict fatigue damage $N_{f,e}$.

The efficiency and reliability of the developed fatigue approach were systematically validated by conducting a series of low/medium-cycle fatigue experimental work using low carbon steel

080M40. Overall, 24 plain samples and 108 notched samples were machined and tested. Three different root radii for the notches (1.5, 3.0, 6.0 mm) were considered and then classified according to the notch root radius type (Sharp, Intermediate & Blunt). The above-mentioned tests were performed under uniaxial/multiaxial, constant/variable amplitude in-phase and out-of-phase loading conditions, with similar/different frequencies. In addition, the experimental fatigue loading signals were described through both zero-mean and non-zero mean stress values.

In conclusion, the validation process exhibited very good agreement between the experimental and estimated results. Interestingly, the physical results achieved were quite satisfying and prove that the developed technique is a powerful engineering tool and a successful design criterion to evaluate multiaxial fatigue damage in cases of notched geometry.

The content of this research work has been reported and published in various publications and conferences by the author as listed in the Publication section of this thesis.

Publications

The following publications have been produced from the work contained in this thesis:

- ***An elasto-plastic model simulation to calculate local stress-strain sequences under uni-axial/multi-axial constant/variable amplitude cyclic loading***
The Annual Postgraduate Research Student Conference - United Kingdom
Author: N. Zuhair Faruq & L. Susmel ISBN 978-88-95940-50-2, P25-31: April 2015
<http://www.gruppofrattura.it/pdf/Sheffield2015/files/assets/basic-html/page-29.html>
- ***An elasto-plastic approach to estimate lifetime of notched components under variable amplitude fatigue loading: a preliminary investigation***
International Journal of Fracture and Structural Integrity (Gruppo Italiano Frattura IGF)
Author: N. Zuhair Faruq, Vol. 10, No. 37 (2016): July 2016
<http://www.fracturae.com/index.php/fis/article/view/IGF-ESIS.37.49>
- ***An alternative elasto-plastic approach to estimate lifetime of notched components under Multi-axial Fatigue Loading***
International Conference on Multi-axial Fatigue & Fracture ICMFF11 - Seville, Spain
Author: N. Zuhair Faruq & L. Susmel, June 2016
<http://www.icmff11.es/q2/cgi.hrb?idexp=Q2UX4&main=homeen>
- ***On the Numerical Modelling of Local Stress-Strain Sequences under Complex Constant/Variable Amplitude Fatigue Loading***
The British Society for Strain Measurement - United Kingdom
Author: N. Zuhair Faruq & L. Susmel, June 2017
http://www.bssm.org/uploadeddocuments/Conf\%202017/2017\%20papers/33_Zuhair_Namiq_formatted.pdf

Acknowledgements

The classic red bricks of the Mapping Building of Sheffield Universitys Engineering Department will never be forgotten in my life since it has been a place where I have met so many lovely people from different cultures and backgrounds.

At the end of my PhD journey, I would like to express my profound gratitude to my supervisors in the Department of Civil and Structural Engineering of Sheffield University, Professor Luca Susmel and Professor Harm Askes.

I would particularly express my deepest gratitude to Professor Luca Susmel, for his invaluable guidance, support and encouragement throughout the course of this research. He has provided me with powerful advice and suggestions, without which the results obtained in this work would not have been possible. Professor Luca, helped me to tackle the many unexpected problems that faced me during this research work. He was always available when I needed him, was always willing to help, and always showed confidence in my work. His efforts and kindness are gratefully acknowledged.

I would also like to acknowledge The Higher Committee for Education Development in Iraq (HCED) for their financial support for my PhD studies.

I would like to thank the members of the Computational Mechanics Group, and my Research Group, without whose friendship my life as a PhD student would not have been so enjoyable and colourful.

Special appreciation is also due to Christopher Todd, Richard Kay and all the staff and technicians in the Lea laboratory at Sheffield University; without their help, my experimental would have been dull and impossible.

I would like to thank all my friends in the UK and elsewhere who shared the happiness, sadness, boredom and excitement of this time with me. Their support and encouragement over these years have been invaluable.

And most importantly, I am grateful to my family. In particular my mother and my brother (Dr. Kadhim), who gave me their endless love and support, allowing me to pursue my dream.

Contents

Declaration	i
Abstract	ii
Publications	iv
Acknowledgements	v
Contents	vi
List of Figures	x
List of Tables	xiv
1 Introduction	1
1.1 Background to the Fatigue Problem	1
1.2 Multiaxial Fatigue Load	2
1.3 The Influence of Notch in Fatigue Problem	4
1.4 Limitations of the Current Approaches on The Evaluation of Multiaxial Fatigue of Notch Components	5
1.5 Statement of the Problem	7
1.6 Aims of the Research Work	8
1.7 Structure of the Thesis	9
2 State of the Art	11
2.1 Historical Overview of Fatigue	11
2.2 Real Engineering Components with Geometrical Features	12
2.2.1 Theory of Critical Distances (TCD)	13
2.3 Critical Review of the Various Current Approaches to the Problem of Multiaxial Fatigue	15
2.4 Γ -Plane Theory For Evaluating Multiaxial Fatigue	16

2.5	Critical Plane Approach (C.P)	17
2.5.1	Stress-Based Approach (<i>S-N</i> Curve)	17
2.5.2	Strain-Based Approach (Manson-Coffin Curve Methods (MCCM))	19
2.6	Material Response under Cyclic Deformation	21
2.6.1	Hardening Rule	23
2.6.2	Nonproportional Cyclic Loading and Nonproportional Additional Hardening	24
2.7	Mean Stress	25
2.8	The Maximum Variance Method (MVM)	26
2.9	Rainflow Cycle Counting Method	27
2.10	Cumulative Fatigue Damage	28
2.11	The main gaps in knowledge	29
3	Scope of the Developed Approach - Methodology	31
3.1	Introduction	31
3.2	Local Triaxial State of Stresses and Strains	32
3.3	The Theory of Critical Distance TCD	33
3.4	Finite Element (F.E model) to Describe the Local Stress-Strain history	34
3.5	The Maximum Variance Method (MVM)	37
3.5.1	Re-Formalisation of the Maximum Variance Method MVM in Terms of Strain ($\gamma - MVM$)	38
3.6	The Modified Manson-Coffin Curve Method	47
3.6.1	Constant Amplitude C.A Cyclic Loading	48
3.6.2	Variable Amplitude V.A Cyclic Loading	50
4	Experimental Work	54
4.1	Introduction	54
4.2	Multiaxial Fatigue Testing Machine	54
4.3	Multiaxial Hydraulic Collet (End Grips)	55
4.4	Axial-Torsional Extensometer - Model 3550	56
4.5	Plane and Notch Specimens	57
4.6	The Test Controlling Parameters	58
4.7	Testing Procedure	61
4.8	Mechanical Properties and Fatigue Parameters of the Material	62

4.8.1	Determination of the Material Fatigue Constants by Running Fully-reversed Axial and Torsional Cyclic Loading of Plane Specimens	62
4.9	Uniaxial Fatigue Test to Find the Critical Distance	63
4.10	Experimental Multiaxial Fatigue Life Evaluation of Notched Components	65
4.10.1	Constant Amplitude Fatigue Test	66
4.10.2	Variable Amplitude Fatigue Test	66
4.10.3	Variable Amplitude Fatigue Tests - Different Frequency	67
5	Elasto-plastic F.E model validation	71
5.1	Introduction	71
5.2	Type of Geometries Used in the FE Model Validation	72
5.2.1	Tubular Geometries - Datasets Taken From Other Literature	73
5.2.2	Plain Cylinder Geometries - Datasets Taken by Running Experiments	75
5.3	Testing Procedure	77
5.4	Formulating the Finite Element Model	77
5.5	Results and Comparison	79
5.5.1	Validation by Using Tubular Specimens	80
5.5.2	Validation by Using Plain Specimens	81
5.6	Conclusions	82
6	Results and Discussion	88
6.1	Introduction	88
6.2	The Index Factor (Stress Ratio ρ) and (ρ_{limit})	89
6.2.1	Numerical Calculation to Find the Index Factor Limit (ρ_{limit}) by Using Experiments:	90
6.3	Determining the Critical Damage by Using Experimental Results	90
6.4	Validating the Strain-Based Algorithm and Matlab Code	91
6.5	Numerical Calculation to find the Critical Distance by Using the TCD Theory	93
6.6	Validation of the Proposed Approach for Different Notch Geometries	93
6.7	Validation of the Proposed Approach against Different Loading Conditions	94
6.7.1	Constant Amplitude Fatigue Loading	95
6.7.2	Variable Amplitude Fatigue Loading	97
6.7.3	Multiaxial Fatigue Loading Taking Account of Mean Stress/Strain	99

6.8	Observed Cracking Behaviour and Surface Failure	100
6.9	Review the Results and Discussion	102
7	Conclusions	107
8	Recommendations for Future Work	109
	References	110
A	Developed Matlab Code to find CP and relative Stresses/strains	117
B	Fatigue Fracture Surface	125

List of Figures

1.1	Fatigue Failures in Modern Structures And Industries Versus the Existing Numerical Approaches (Chowdhury & Sehitoglu 2016)	2
1.2	Fatigue Failures Under Cyclic Loading	3
1.3	Multiaxial Fatigue Loading: a. In-phase (Proportional) b. Out-of-phase (Non-proportional)	4
1.4	Crack Orientation and Fatigue Fracture	5
1.5	Multiaxial Fatigue Fracture at Notch geometry Under Variable Amplitude Cyclic Loading with involving Mean Stress	6
2.1	Fatigue Failures of Railway Wheels and Axle	12
2.2	Theory of Critical Distances Mechanism	14
2.3	Theory of Critical distances - Three Different Formalisation	15
2.4	The Wöhler curve for ferrous and non-ferrous material	18
2.5	Classic Manson-Coffin Curve in terms of Axial and Shear Strain Amplitudes	20
2.6	Modified Manson-Coffin Curve (MMCCM)	22
2.7	Modified Manson-Coffin Curve MMCCM with different ρ values	22
2.8	Stabilized Stress-Strain Curve - Hardening Phenomenon	23
2.9	Stabilized Stress-Strain Curve - Softening Form	23
2.10	Harding rules of materials in the plastic regime	25
2.11	Non-proportional Additional Hardening - Effective Strain Amplitude	26
2.12	Rain Flow Cycle Counting Rules	27
2.13	Example procedure of Rainflow Cycle counting, adopted from Lee et al. (2005)	28
2.14	Palmgren-Miner rule to evaluate damage of variable amplitude loading	29
3.1	Local Triaxial Stress-Strain State of notch component	32
3.2	Shear Strain value of a cubic element	33

3.3	The Corresponding stress/strain under Uniaxial nominal stress	34
3.4	Flow Chat: Methodology to find the Critical Distance (CD) by using TCD theory	35
3.5	Three-Dimensional FE Model Solved by Using ANSYS® -Mechanical APDL . .	36
3.6	Local Stress-Strain State at a Critical Point in Notch sample	37
3.7	Finding the Element Size of FE Model at Notches to Get a Convergence Level . .	38
3.8	Flow Chart presenting algorithm to determine Orientation of the Critical Plane by using the Maximum Variance Method	39
3.9	Notch Geometry Subjected to Combined Tension and Torsion	40
3.10	Flow Chat: application of the formalised approach under Constant Amplitude C.A Multiaxial Fatigue Load	49
3.11	Flow Chat: In-field application of the developed approach against Variable Amplitude VA. Multiaxial Fatigue Load	53
4.1	Multiaxial (Axial-Torsion) Fatigue Testing Machine	55
4.2	Multiaxial End Grips of Fatigue testing Machine	56
4.3	Axial-Torsional Extensometer - Epsilon MODEL: 3550-025M	57
4.4	Axial-Torsional Digital Calibrator of Extensometer - Epsilon MODEL: 3590AT .	57
4.5	Picture of the Tested Samples	59
4.6	Details & Dimensions of the Specimens	59
4.7	Stabilized Uniaxial Stress-Strain Curve	63
4.8	Stabilized Torsional Stress-Strain Curve	64
4.9	Fully-reversed Tension-Compression Manson-Coffin Curve of the Plane material (080M40 Steel)	64
4.10	Fully-reversed Torsion Manson-Coffin Curve of the plane material (080M49 Steel)	65
4.11	Investigated Load employed to test the notched samples 080M40Steel	67
5.1	All the applied Loading paths	73
5.2	Tubular Geometry	75
5.3	Stabilized Uniaxial Stress-Strain Curve	76
5.4	Dimensions of the Specimen	77
5.5	Three Dimensional Finite Element Model of Plain Specimens by Using ANSYS .	79
5.6	Boundary conditions and applied loads (Displacement and Rotation)	79
5.7	Uniaxial and Pure Torsion Hysteresis loop	80
5.8	Axial and Shear Stress-strain Hysteresis loop - Loading Path C	80

5.9	Axial and Shear Stress-strain Hysteresis loop - Loading Path K	81
5.10	Axial and Shear Stress-strain Hysteresis loop - Loading Path H	81
5.11	Axial and Shear Stress-strain Hysteresis loop - Loading Path E	81
5.12	Axial and Shear Stress-strain Hysteresis loop - Loading Path N	82
5.13	The Predicted versus Experiment Elasto-plastic Stresses - Constant Amplitude Loading	82
5.14	The Predicted versus Experiment Elasto-plastic Stresses - Variable Amplitude Loading	83
5.15	Hysteresis Loop - Uniaxial, Constant Amplitude, Zero Mean Stress Fatigue Loading	83
5.16	Hysteresis Loop - Biaxial, Constant Amplitude, Zero Mean Stress, In-phase Fatigue Loading	84
5.17	Hysteresis Loop - Biaxial, Constant Amplitude, Zero Mean Stress, Out-of-phase Fatigue Loading	84
5.18	Hysteresis Loop - Biaxial, Constant Amplitude, Non-Zero Mean Stress, In-phase Fatigue Loading	85
5.19	Hysteresis Loop - Biaxial, Constant Amplitude, Non-Zero Mean Stress, Out-of-phase Fatigue Loading	85
5.20	Hysteresis Loop - Biaxial, Variable Amplitude, Zero Mean Stress, In-phase Fatigue Loading	86
5.21	Hysteresis Loop - Biaxial, Variable Amplitude, Zero Mean Stress, Out-of-phase Fatigue Loading	86
5.22	Hysteresis Loop - Biaxial, Variable Amplitude, Non-Zero Mean Stress, In-phase Fatigue Loading	86
5.23	Hysteresis Loop - Biaxial, Variable Amplitude, Non-Zero Mean Stress, Out-of-phase Fatigue Loading	87
6.1	The Modified Manson-Coffin Curve for Different ρ values and ρ_{limit}	91
6.2	The Predicted Number of Cycles to Failure $N_{f,e}$ versus Experimental Number of Cycles N_f under Multiaxial Constant Amplitude Cyclic Loading	93
6.3	The Predicted Number of Cycles to Failure $N_{f,e}$ versus Experimental Number of Cycles to Failure - Sharp Notch	95
6.4	The Predicted Number of Cycles to Failure $N_{f,e}$ versus Experimental Number of Cycles to Failure - Intermediate Notch	95
6.5	The Predicted Number of Cycles to Failure $N_{f,e}$ versus Experimental Number of Cycles to Failure - Blunt Notch	96

6.6	The Predicted Number of Cycles to Failure $N_{f,e}$ versus Experimental Number of Cycles under Constant Amplitude Fatigue Loadings	98
6.7	The Predicted Number of Cycles to Failure $N_{f,e}$ versus Experimental Number of Cycles under Variable Amplitude Fatigue Loadings	99
6.8	The Predicted Number of Cycles to Failure $N_{f,e}$ versus Experimental Number of Cycles under Variable Amplitude Fatigue Loadings - Different Frequencies	99
6.9	The Predicted Number of Cycles to Failure $N_{f,e}$ versus Experimental Number of Cycles under Variable Amplitude Loading and involving mean stresses	100
6.10	Fatigue Crack Initiation and Propagation (Chowdhury & Sehitoglu 2016)	101
6.11	Fatigue Fracture Surface Appearance of Notched component	102
6.12	Crack Orientation and Fracture Surface from Cyclic Load	103
6.13	Crack Initiation and Fatigue Fracture of Notched Geometry	104

List of Tables

4.1	Mechanical properties of the tested material	58
4.2	Summary of the tested specimens, type of loading, and purpose of the test	60
4.3	Summary of the experimental results generated by testing Sharply notched specimens $r_n=1.5\text{mm}$ under uniaxial constant amplitude cyclic load	63
4.4	Uniaxial and Torsional Fatigue Properties of the investigated material	65
4.5	Experimental test of Sharp Notch Specimens under Uniaxial Constant Amplitude Fatigue Load to Find the Critical Distance	65
4.6	Summary of the Experimental Results Generated by Testing the Sharp Notch Specimens $r_n=1.5\text{mm}$	67
4.7	Summary of the Experimental Results Generated by Testing the Intermediate Notch Specimens $r_n=3\text{mm}$	68
4.8	Summary of the Experimental Results Generated by Testing the Blunt Notch Specimens $r_n=6\text{mm}$	69
4.9	Summary of the Experimental Results of the Notches Generated by Testing under Different Frequencies	70
5.1	Fatigue constant of materials from other technical literatures	74
5.2	Type of materials, Loading paths with Stress and Strain value (Constant Amplitude)	75
5.3	Type of materials, Loading paths with Stress and Strain value (Variable Amplitude)	76
5.4	Mechanical properties of the tested material	76
5.5	Summary of the applied Stress and Strain on the Plain Specimens	78
6.1	Experimental Test to Find the Material Index Factor Limit ρ_{limit}	90
6.2	Experimental fatigue test of plain samples under VA to determine the experimental critical damage D_{cr}	91
6.3	Summary of the experimental N_f generated by testing Plane specimens under multiaxial constant amplitude cyclic load and estimated $N_{f,e}$ & $N_{f,Socie}$	92

6.4	Summary of determining a critical distance C.D by testing Sharply notch specimens $r_n=1.5\text{mm}$ under uniaxial constant amplitude cyclic loading	94
6.5	Summary of the Numerical Results of the Sharp Notch Specimens $r_n=1.5\text{mm}$. .	96
6.6	Summary of the Numerical Results of the Intermediate Notch Specimens $r_n=3.0\text{mm}$	97
6.7	Summary of the Numerical Results of the Blunt Notch Specimens $r_n=6.0\text{mm}$. .	98
B.1	Fatigue Fracture Surfaces of Notches under multiaxial CA/VA load with zero mean stress	125
B.2	Fatigue Fracture Surfaces of Notched Specimens under Multiaxial V.A Fatigue load with involving mean stresses	126
B.3	Fatigue Fracture Surfaces of Notched Specimens under Multiaxial V.A Fatigue load - Different Frequencies	126

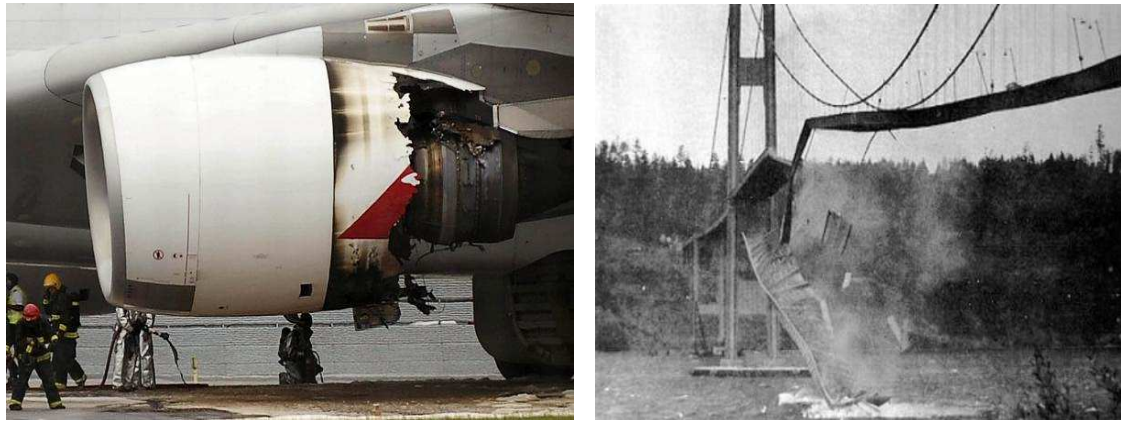
Chapter 1

Introduction

1.1 Background to the Fatigue Problem

In today's world spanning, recent advanced construction and manufacturing technology are ultimately aimed at manufacture engineering elements/components with superior safety and economy. Within these two significant parameters, not only modern industry attempts to build/manufacture an optimised complex geometries, leading to develop a localised stress/strain concentration phenomena, but also tried to consider a complex in-service fatigue loadings that has a detrimental effect on the components. Since the beginning of the last century, elasto-plastic multiaxial Fatigue damage of components with a geometrical features have been centre of attention in the international scientific community, and such an issue remains as a crucial engineering challenge to date (Fig.1.1). In the light of above mentioned promising developments, Multiaxial Fatigue damage of complex geometries become a significant problem that need to be addressed properly. Such a complexity in fatigue rising need for establishing a combination between state-of-art and physical examinations in the laboratory. A revisit to the current predictive literature explained that Fatigue Failure can be considered as one of the most challenging problem and a principal cause of many structural and mechanical failures (Fig. 1.2). Sometimes, such a failure ended by causing death, injury and financial loss (Stephens et al. 2000).

Fatigue has been recognised since the industrial revolution, with the first recorded case of fatigue failure was found occurring on an axle of a railway in 1840. At that time, as there was no physical understanding of fatigue damage by the researchers/designers, a legal action was taken against the engineers (Socie 1997). From a fracture mechanics point of view, fatigue is defined as a localized structural damage that occurs in a material when a component is subjected to a repeated load. Evaluating fatigue damage needs a complete knowledge of the developed stress/strain states at the critical location inside a material. Fatigue failure involves a series of a complex interactions of cyclic loads, time and geometry that occurs as a result of movement in the atomic structure of a material at a stress level much lower than the ultimate stress limit that would be required to cause failure in a single load application (Jiang 2000). Fatigue damage cumulates with each cycle of the applied load and such damage is not recovered even when the material is rested or unloaded. The fatigue-related fracture of a component can happen without any prior warning (Suresh 1991), because sometimes they can fail even under relatively low yield strengths and without any evi-



(a) Fatigue Failure on engine skin of aircraft (Feroz 2014) (b) "Tacoma Narrows" Bridge Failure Under Random Fluctuations by Wind (Variable Amplitude Load)-1940 (Woo n.d.)

Figure 1.2: Fatigue Failures Under Cyclic Loading

or square patterns. In the multiaxial fatigue load, either magnitude of the principal stress changes with time or orientation of the principal axes rotates with respect to the component. However, in many practical situations, both principal stress and axes are rotated. This means that, when evaluating multiaxial fatigue, it is crucial to consider the combination of multiaxial cyclic loads to produce the corresponding stress/strain states of a component. These multiaxial cyclic loads can be proportional (in other words, in-phase, where the orientation of the principal axes is fixed), but often such loads are applied in non-proportional (out-of-phase) form, as shown in Fig.(1.3). Purely axial or torsional fatigue loads are considered as a proportional loading. Out-of-phase loading, meanwhile, happens when there is a shift between the cyclic load wave on one of the axes in respect to a load on the other axes. Non-proportional loadings significantly complicate the problem of fatigue compared to proportional loadings, due to the likelihood of experiencing plastic deformation, and the potential for damage across more planes in the material in addition to the critical plane (Jayaraman & Ditmars 1989). From a mathematical point of view, in a few materials, the degree of non-proportionality produces additional plastic hardening that is not observed in proportional loading (Socie & Marquis 2000). A 90° out-of-phase cyclic load accommodates the largest level of additional non-proportional plastic hardening compared to other smaller angles and gives the shortest component lifetime in respect to fatigue (Kanazawa et al. 1977).

Furthermore, in most cyclic load instances, engineering structures and components are under random amplitude or periodic overloading conditions that further complicate the process of identifying cycles and thus calculating cumulative fatigue damage. In such a loading case, the damage slowly accumulates with each cycle resulting in the development of small nucleate cracks. Estimating the accumulated damage from such variable amplitude loadings require an advanced software to efficiently calculate the fatigue damage arising from each cycle. Last point that deserve to recall here, sometimes, the reason of discrepancy between predicted and experimental fatigue estimation is that the fatigue loading of many real components and structures are not applied in the regular and convenient way that researchers use in the laboratory.

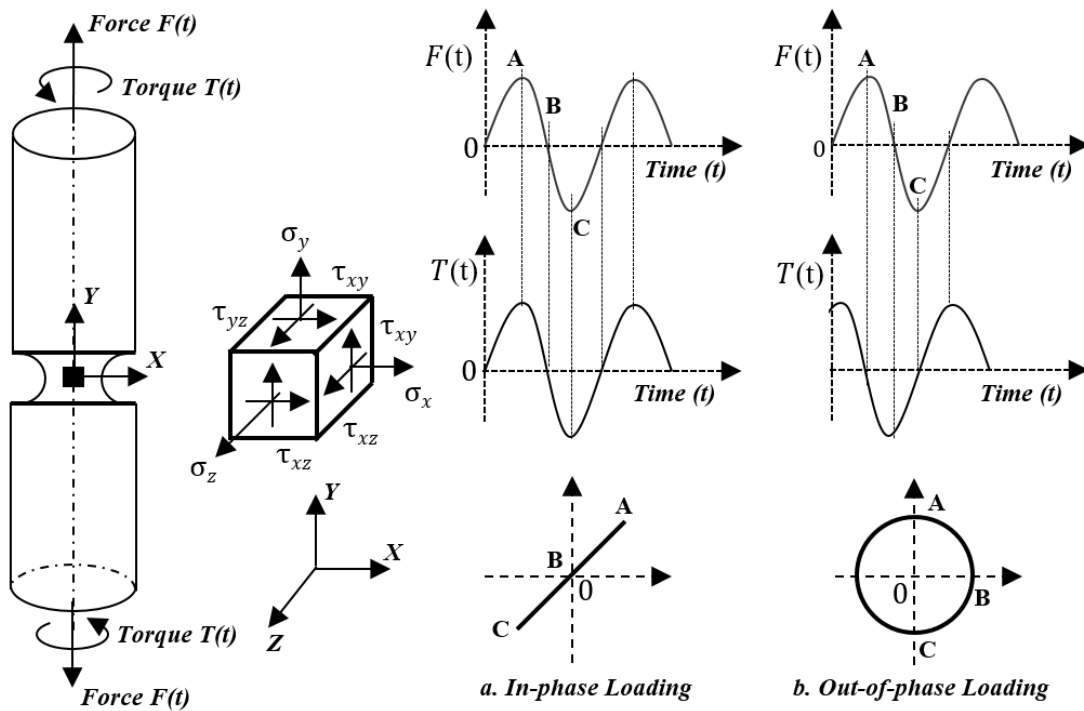


Figure 1.3: Multiaxial Fatigue Loading: a. In-phase (Proportional) b. Out-of-phase (Non-proportional)

1.3 The Influence of Notch in Fatigue Problem

Real engineering components and structures are rarely manufactured with a simple or uniform geometry. Normally, they have either complex geometry or artificial notches such as corners, screw, holes, and even welding, and, under fatigue loading, these features reveal much more complex responses than in the case of simple geometry due to the phenomenon of stress concentration as well as the multi-axiality of the local stresses. Notches are therefore always considered to be a matter of concern in respect to mechanical and structural elements under fatigue load. This is the reason why the scientific community has extensively investigated notches (Susmel 2009). There are two significant differences between notched geometry and plane components. Firstly, notches complicate the stress/strain distribution inside a material, creating a stress concentration zone where the local peak stress at the notch root is relatively higher than the average net stress. Secondly, this frequently results in multi-axiality of the stress field even if the nominal stress is uniaxial (Socie & Marquis 2000). Ultimately, a fatigue crack is often initiated in the region of stress raisers, for instance, notches, holes, grooves, keyways, fillets and welds. Figure (1.5) shows fatigue failure at notch.

In order to describe the severity of the above-mentioned stress/strain concentration and how seriously such a stress/strain state is violated at notches, a dimensionless factor is used to define the rate of stress concentration in a material due to stress raiser and called stress concentration factor (K_t). This factor can be defined as a ratio of the maximum stress at a notch tip to the reference stress. Another significant point that deserves to be mentioned, is that the root radius of a notch, and its opening angle, are assumed to be the most important parameters controlling the local stress/strain distribution inside a notched component in respect to the fatigue process. Consequently, it is al-

ways recommended to use as large a root radius as possible in the notch geometry (Susmel & Taylor 2012).

In conclusion, notches cause not only a multiaxiality in the corresponding stress-strain states inside a material but also intense plastic deformation in the notch zone, particularly at the notch tip, and this serves to reduce the lifetime of a component. The evaluation of fatigue in notch geometries is therefore highly important in structural engineering and engineers have a deep interest in identifying a reliable methodology to perform the fatigue evaluation of notch components as distinct from plane geometry.

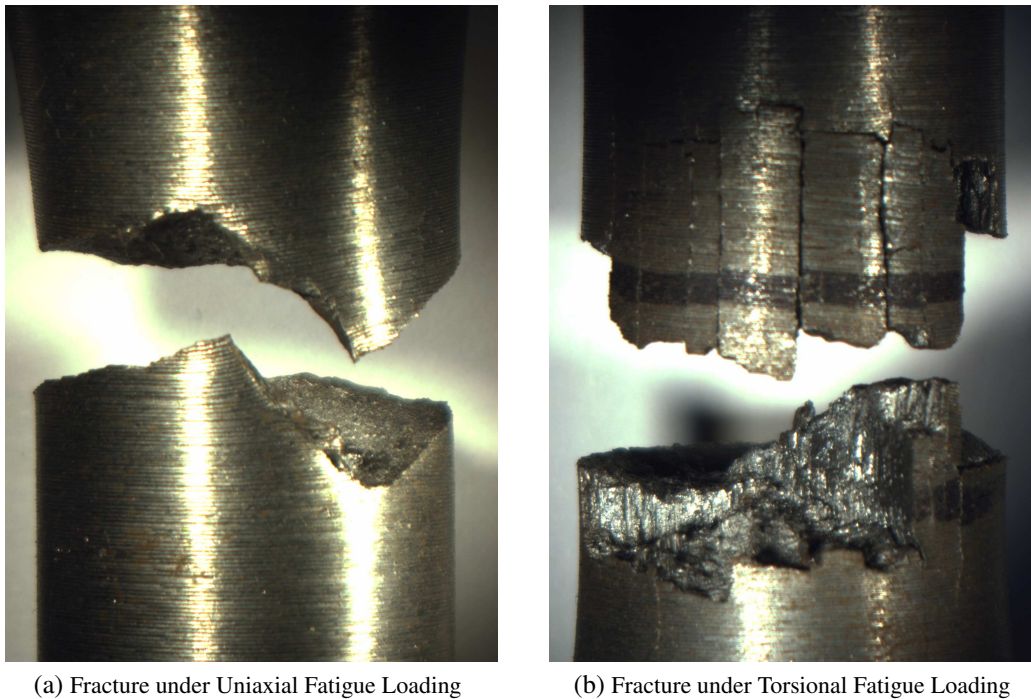


Figure 1.4: Crack Orientation and Fatigue Fracture

1.4 Limitations of the Current Approaches on The Evaluation of Multiaxial Fatigue of Notch Components

Real engineering components under fatigue loading develops non-uniform local stress/strain distribution along cross section of the component that reaches maximum value at stress concentration location. By increasing the magnitude of the applied in-service forces/moments, cyclic plasticity plays a detrimental effect on fatigue damage of the component (Stephens et al. 2000, Susmel 2009 and Socie & Marquis 2000). Under these circumstances, the mechanical behaviour of metallic materials is no longer recommended to model under a simple linear-elastic deformation. Examination of the state of the art shows that, despite the extensive study of fatigue problems that have resulted in several well-developed strategies, according to the best of the authors knowledge, the existing approaches have been developed mainly on the basis of either uniaxial fatigue of a complex geometries or multiaxial fatigue of a plane geometry. Further, for the purpose of simplification, the early studies on fatigue have often been based on reducing the problem to an equivalent uniaxial

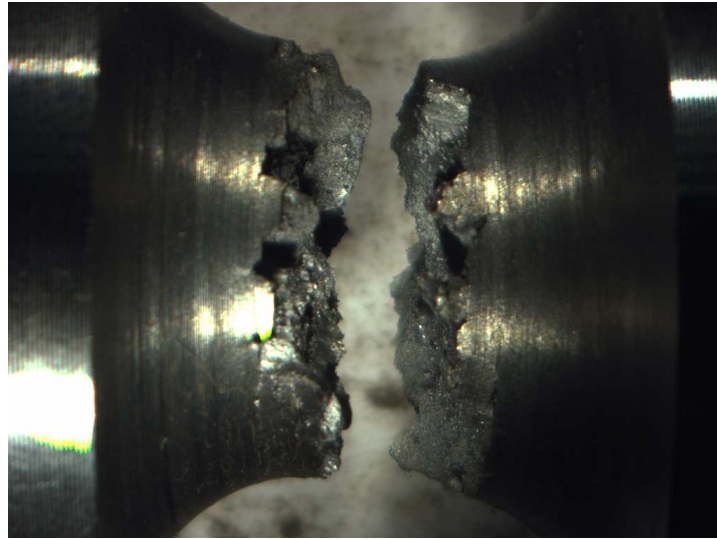


Figure 1.5: Multi-axial Fatigue Fracture at Notch geometry Under Variable Amplitude Cyclic Loading with involving Mean Stress

and/or two-dimensional model without considering whether this assumption is valid for a particular biaxial fatigue load or the complex geometries being evaluated. In addition, a lot of components in engineering applications are subjected to complex multi-axial variable amplitude (V.A.) cyclic loadings, resulting in multi-axial elasto-plastic fatigue damage. Some limited attempts have been made and reported in respect to multi-axial complex fatigue loading of notched components and involving combinations of variable amplitude, proportional/non-proportional, zero/non-zero mean stress cyclic loadings (Susmel & Taylor 2015 and Faruq 2016).

In general though, all the existing design methodologies have their own specific limitations and there is not yet sound agreement and a specific design methodology suitable to evaluate the multi-axial fatigue of complex geometry such as notches under complicated biaxial fatigue load. Specifically, to the author's knowledge, there are currently very few multi-axial fatigue models exist in the literature that consider not only the realistic effective stress concentration of notches but can also do so while taking account of the shape and size of notches, and even load phasing, with/without involving mean stress as a nominal stress, or mean stresses arising from the redistribution of stresses due to plastic deformation.

Moreover, the author's investigation concluded that limitations in computers ability to cope with complex numerical implementations has, until recently, been a significant impediment to the development of an advanced theory to solve very complex multi-axial fatigue problems that are capable of taking account of all the potential complexity.

Finally, according to the authors knowledge of the available literature, there is very limited experimental work in the field of multi-axial fatigue when three dimensional notches are involved, and few of these have been reported. This points to the need to conduct experimental work to validate any developed multi-axial fatigue theory of notches.

To sum up, the increased demand for approaches that correctly estimate the multi-axial lifetime of stress raising components, the interest in meeting minimum safety requirements in the most cost effective way, and the general lack of literature on fatigue arising from multi-axial stresses in complex geometries, the engineering community needs more research into reliable methods that

focus on complex multiaxial fatigue of notch components.

1.5 Statement of the Problem

Engineering structures and elements in service operations are often subjected to multiaxial random loads in various directions at different frequencies with variable phases. Moreover, elements of real structures are characterised by a non-uniform geometry resulting in corresponding stress/strain concentration at a critical location that favours the initiation of fatigue cracks in the stress raiser region. Not only does the presence of such a stress/strain raiser cause a concentration in stresses at the notch tip but also the developed stress-strain states are always multiaxial at the notch area even if the applied load history is uniaxial. The combination all the above aspects makes their analysis in a single model complicated and challenging.

The fatigue problem has been studied extensively in recent decades, resulting in many important techniques and models to estimate the lifetime of a component. Some of the theories have focused on accurately modelling and evaluating fatigue in complex geometry or notches. Others have been developed to consider complex fatigue loadings. Based on the authors review of the literature, the following issues are the most contentious among scientists on material fatigue:

Firstly, the key problem in evaluating multiaxial fatigue is the need to model multiaxial damage as realistically as possible in order to handle the multiaxial complexity described above. Although, in the recent past, a lot of research has been devoted to the study of: i. notches, ii. multiaxial fatigue loading and iii. variable amplitude fatigue loading as individual topics, rather less attention has been given to solving all such issues within a single holistic and reliable approach (Wang & Susmel 2016). The combination of such aspects in one validated model to evaluate multiaxial fatigue is therefore still considered to be an outstanding problem.

Secondly, in classical strain-based applications, the fatigue damage of notch geometry has always been evaluated by directly considering the elasto-plastic root stresses/strains. This can explain by the fact that the use of such root stress/strain magnitudes to perform fatigue evaluation of notched component results in a degree of conservatism and increases the manufacturing cost of a component.

Thirdly, despite the general advice to use as large a root radius for notches as possible, notched components and stress raisers with a small root radius often need to be designed for real-life applications, and these serve to increase the stress concentration factor, thus requiring a safe engineering theory to consider the potential fatigue damage properly, particularly at sharp notches.

Fourthly, in any component under in-service operation, as soon as crack is introduced, even within a simple geometry, the resulting uniaxial loading generates corresponding multiaxial stress/strain states near the crack region requiring a robust multiaxial theory to evaluate the resulting fatigue damage.

Another point that deserves to be highlighted is that despite the revolutionary changes that have occurred in industry since the 1970s, it is only very recently that computational power has reached a level capable of modelling the very complex fatigue load histories. This technological obstacle has forced researchers to rely on laboratory experimentation to evaluate complex multiaxial

fatigue of notches but this involves significant time and cost . Nowadays, advances in computer technology and software allow exact notch geometries to be simulated under actual multiaxial complex fatigue loads.

All of the above issues indicate the need for the scientific community to foster a movement towards a fuller understanding of multiaxial complex fatigue loads that will allow the development of a reliable multiaxial fatigue evaluation methodology to cope with notched components against complicated biaxial cyclic loading and involving zero/non-zero mean stresses.

1.6 Aims of the Research Work

Recent advanced technology is leading to manufacture an optimised complex geometry. Complexity in such a modern geometry parallel to the complex multiaxial in-service loads have increased designers and structural engineers need for establishing an advanced lifetime prediction method that is capable of dealing with multiaxial fatigue damage of materials under complicated service loads. A critical review of the elasto-plastic multiaxial fatigue, and the availability of advanced modern computers and software, in conjunction with the development of experimental facilities capable of handling a large number of computational and validation process, this research sets out to investigate the multiaxial fatigue of a component from a number of differing viewpoints and observation levels so as to establish an efficient design methodology suitable to define the durability of the engineering geometry and to predict the multiaxial fatigue lifetime of a material. The detailed aims of this research work are summarised below:

1. Evaluate the multiaxial fatigue of notch components by using a stabilised simple uniaxial test of a material to describe fatigue behaviour under any combination of complex cyclic loads.
2. Develop a validated elasto-plastic three-dimensional finite element (FE) model using ANSYS® software to determine the corresponding infield stress/strain history at any point inside materials against different cyclic loading forms and amplitudes. The FE model was validated based on the available experimental datasets from other technical literature. Then, the FE model was calibrated so as to be used to analyse notch components with different root radii.
3. Determining the local multiaxial stress/strain states that is relevant to a real developed stress/strain states inside a structural and industrial components which is loaded in a complex way.
4. Reformulating the Maximum Variance Method to be used in terms of strain to determine orientation of the critical plane and stress/strain amplitudes relative to the critical plane under complex multiaxial fatigue loadings. The local effective stress/strain state is used as an input data to evaluate multiaxial fatigue damage of a component under complex cyclic loadings.

5. Develop an efficient Matlab Code based on the maximum variance method to determine orientation of a critical plane and estimate normal and shear stress/strain magnitudes relative to the critical plane. The accuracy and efficiency of the Matlab Code were validated using both: The two-dimensional model presented by Socie & Marquis (2000). And, Experimental validation by testing plane specimens under fatigue loading.
6. Validate the effectiveness of the developed approach by assessing the durability of materials against multiaxial fatigue under complex loading condition. This process includes performing 132 experimental tests of plane and notch geometry. Three different notch categories were considered: sharp, intermediate & blunt.
7. Design structural elements and components against fatigue before hardware exists (i.e before the start of the real manufacturing process of a component). Also, edit/solve different geometries easily with a good level of accuracy.

1.7 Structure of the Thesis

This thesis is divided into eight core chapters with additional Appendixes at the end. An overview of each section is given in the following:

- The current chapter has mainly introduced the background to the fatigue problem, multiaxial cyclic loads and the definition of notched component. It has also noted the limitations of existing methods and thus the need for a new approach and has set out the objectives of the research, and the outline of the thesis.
- Chapter 2: Provides an overview of theories on fatigue and the approaches used in this thesis. It also offers a brief review of the fatigue damage mechanisms, particularly those mechanisms that allow a full description of elasto-plastic fatigue. Modifications to the strain-based approach to consider both mean stresses and a level of non-proportionality are also discussed.
- Chapter 3: Presents the proposed method of predicting elasto-plastic multiaxial fatigue of complex geometries such as notches. The chapter demonstrates how existing theories are applied to the developed approach. First, a validated nonlinear FE model is defined. Then, critical plane theory, fatigue damage model, Modified Manson-Coffin Curve (MMCCM), cycle counting, and cumulative damage models are discussed. Stress/strain raisers are included in the form of complex geometries and components containing notches by using the Theory of Critical Distances TCD.
- Chapter 4: Gives attention to the experimental work performed in the Lea laboratory at the University of Sheffield Engineering Department in order to validate the developed approach for notch specimens. In addition, plain samples were tested to determine the uniaxial and torsional fatigue constants of the material.
- Chapter 5: Describes the development of a reliable elasto-plastic FE model to quantify the local elasto-plastic stress-strain states of a component at a specific point on the component

in the case of plain samples. Case studies containing various loading paths were taken from other literature to verify the accuracy of FE. model. Then, this FE model was extended to be used with notch geometry. The FE model results from ANSYS were linked to the algorithm that is presented in Appendix (A).

- Chapter 6: Discusses the results and comparison between the predicted fatigue strength of the material versus the results generated by performing experimental work to further demonstrate the efficacy of the devised approach.
- Chapter 7: This chapter presents comprehensive conclusions from this research work.
- Chapter 8: Presents some of the additional work proposed for the future.
- Appendix A: Develops a reliable numerical Matlab Code to find the direction of the critical plane and relative stress/strain amplitudes, then applies the MMCCM to find the number of cycles to failure. The Matlab code represents an algorithm re-formalised in Appendix (3.5.1).
- Appendix B: Matrix of the observed fatigue fracture surfaces of all notch specimens under different loading conditions.

Chapter 2

State of the Art

Over the last century, enormous and systematic efforts have been made by researchers studying the fatigue problem to propose engineering tools capable of correctly assessing the fatigue life of a component. This chapter is intended to give a comprehensive detail and historical background of the most significant approaches that are generally required when performing fatigue assessment of a component associating a complicated loading condition to a complex geometry. The first part of this chapter gives an overview of the history of the understanding of fatigue as a starting point to the scholarly investigation of fatigue investigation. Then, the chapter defines a significant different approaches to describe fatigue problem including the well-known Critical Plane approach that is used to describe the most damaging plane of a material under fatigue load. Subsequently, several aspects related to multiaxial fatigue are briefly discussed. This is followed by a critical discussion of the theories of fatigue damage that are particularly used in this research.

2.1 Historical Overview of Fatigue

The experience of fatigue damage in structures or operating machinery parts provides a very compelling motivation to develop a more comprehensive understanding of fatigue. Fatigue first started to be noticed in the 1840s in the context of railroad axles failing at their shoulders. This problem inspired the well-known work by Wöhler in Germany, who performed many experimental tests under fatigue loads to try to understand this railway axle failure problem. Wöhlers research is considered to be the starting point of a systematic investigation of fatigue damage (Stephens et al. 2000). Wöhler established the approach of using a safe working stress limit for a material to ensure that fatigue failure would not happen. After Wöhlers physical investigation and establishing a stress-limit approach, In 1887, Lanza is considered as the next researcher presented and reported some preliminary fatigue test results generated by a locally-made rotating bending-torsion test machine.

Generally, the earliest developed fatigue models were based on the elastic estimation, and engineers began deriving the working stress limit of engineering materials and their endurance limit. Despite all this work, the problem of multiaxial fatigue load has been the centre of attention for far too long. Gough & Pollard (1935) performed a set of multiaxial fatigue experiments on different

materials under various load ratios to establish their fatigue limit by plotting a ratio of bending and shear stresses to the bending and torsion fatigue limit (Gough 1950). Subsequently, a pioneering theory of a *Critical Plane* was proposed. According to the theory of Critical Plane CP, the fatigue damage of a material accumulates and reach its maximum value on a specific plane, referred to as the Critical Plane (Brown & Miller 1973). This approach is considered as the best theory to evaluate fatigue damage of materials. The Critical Plane approach hypothesized that fatigue crack initiate on a plane that experiencing a maximum shear strain amplitude. Furthermore, Dang-Van (1993) defined fatigue crack in a material as a local damage process begins in grains of materials that become plastically deformed. Thus, the concept of the micro-stress of material within a critical volume has been proposed to estimate an endurance limit. In addition to the well-known Critical Plane theory, a lot of effort has been expended to determine the nature of the fatigue damage problem and find a relatively simple method for coping with it during the design process (Van et al. 1986, McDiarmid 1991, & McDiarmid 1994).

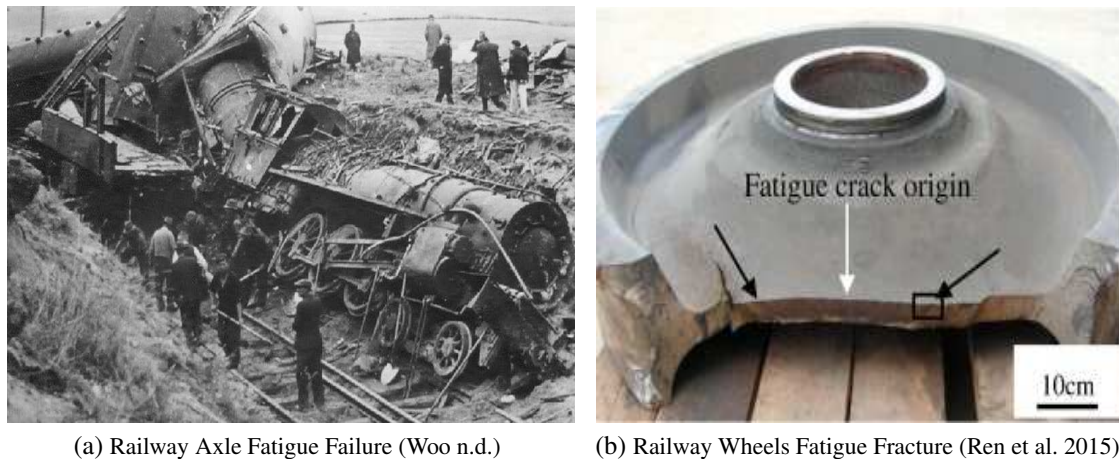


Figure 2.1: Fatigue Failures of Railway Wheels and Axle

2.2 Real Engineering Components with Geometrical Features

As far as complex geometries and notch components are targeted in this thesis, current state of knowledge shows that various approaches have been formalised by considering the pioneering models proposed by Neuber (1958) and Peterson (1959). With knowledge of these two fundamental theories of stress concentration phenomena, the detrimental effect of stress/strain raisers can be modelled either by performing the stress analysis in terms of nominal state of stress quantities (Gough 1949, Tipton & Nelson 1997, Susmel & Lazzarin 2002, & Lazzarin & Susmel 2003) or by directly post-processing the local stress/strain values in the vicinity of the notch tip (stress raiser) far from the notch root by a specific distance (Susmel 2009 & 2010). In this setting, according to the validation exercise presented in the literature, the most successful approach to analyse real engineering components with geometrical features are seen to be those based either on the critical plane theory (Susmel 2004, Susmel & Taylor 2008, Susmel 2008a, and Carpinteri et al. 2013) or energy related parameters (Atzori et al. 2006, Berto et al. 2011, Branco et al. 2018, & Meneghetti et al. 2018).

Based on the critical plane approach that used in this research work, fatigue strength of notched material is a function of the elasto-plastic root deformation. The need for accurately define root stresses/strains is the reason of different attempt since 1980 to devise specific techniques suitable for estimating the elasto-plastic stress and strains at the notch tips (Neuber 1961, Glinka 1985, Hoffmann & Seeger 1985, Köttgen et al. 1995 and Ince & Glinka 2016).

Tipton & Nelson (1989) and Gates & Fatemi (2014) stated that the use of root stress/strain with the critical plane approach is seen to give an accurate estimation of the fatigue damage. However, when the investigated components have a sharp notch, the strain based critical plane approach gives more conservative result in fatigue estimation (Susmel & Taylor 2010). That explain the reason of using fatigue strength reduction factors when notch components are designed by using the stress/strain notch tips (Stephens et al. 2000).

After all the above mentioned stage of developments in determining the local effective stress/strain states of complex geometry, and in order to use the Critical Plane approach in terms of strain to those situation involving sharp notches, in the recent years, a number of successful attempts have been taken place to develop methodologies to use the local elasto-plastic stress/strain of notch components based on the so-called Theory of Critical Distances(Susmel & Taylor 2010, Susmel & Taylor 2015, Gates & Fatemi 2016 & Gates & Fatemi 2018). In the following subsection, detail of the Theory of Critical Distances TCD was described.

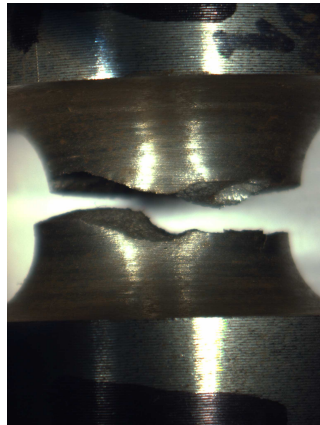
2.2.1 Theory of Critical Distances (TCD)

Numerical analysis indicates that when engineering components are placed under cyclic loading, the corresponding elasto-plastic stress/strain states vary according to the geometrical features of the component. Accordingly, the behaviour of a material can become rather more complex due to the presence of stress raiser. Further, as briefly recalled in subsection (2.5.2), the classical Manson-Coffin curve method hypothesises that the fatigue damage of a geometrical feature component can be evaluated by considering the notch-root stress/strain states. Estimating the fatigue lifetime of notched components by directly considering the root stresses and strains results in an increased level of conservatism (Susmel & Taylor 2015, and 2010), however and thus an inevitable increase in the manufacturing costs. In order to design elements that are optimised to be both safe and economical, the Theory of Critical Distances (TCD) has been proposed to quantify the effective stress/strain state at a critical point inside the material being assessed different than root stress/strain state to predict a reliable fatigue lifetime (Susmel & Taylor 2010). The TCD theory was first developed by Neuber (1958) and Peterson in 1950s to solve the high-cycle fatigue problem of notched components. According to the TCD approach, the effective local stress/strain history to be taken by a distance from the notch tip different than the root stresses, as presented in Fig.(2.2b) (Susmel et al. 2011). The TCD is capable of estimating the corresponding effective stress/strain state of a component containing not only different types of notches but also containing a crack that has already occurred during in-service operation (Susmel 2008b).

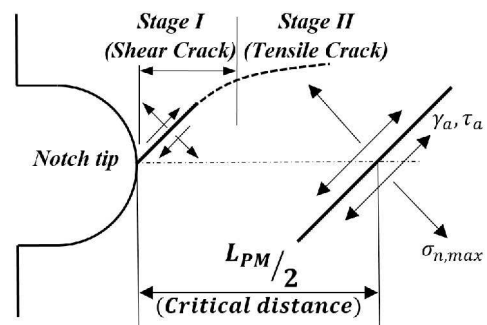
TCD has been formalised into three different forms which includes: i. Point Method P.M. ii. Line Method iii. Area Method, as shown in Fig. (2.3). The point method is considered to be the simplest formalisation of TCD, and assumes that the elasto-plastic stress/strain state damaging the process zone can be taken at a distance from the notch root known as the critical distance and

mathematically expressed as $\frac{L_{PM}}{2}$. The Area Method assumes that the effective stress/strain states that can effectively be used to estimate fatigue strength of a material is calculated by averaging the local stress/strain values over a reference area with L size

The most attractive feature of TCD is how it treats $\frac{L_{PM}}{2}$ as a material property whose value can be seen to change in different materials but to remain constant in the same material. In a different way, the critical distance is not significantly affected by the sharpness of the notch being evaluated (i.e the size and shape of the notch) or by the profile of the cyclic load being applied (2010). According to the infield experience, the critical length of the assessed notch component can be determined by directly post-processing the cyclic elastoplastic stress/strain definition at a point positioned along the notch bisector on a process zone with a distance far from the notch root by $\frac{L_{PM}}{2}$. Such a distance mainly depends on the local micro-mechanical properties and micro-structural features of materials. The process zone is defined as a part of material that controls the entire fatigue failure of a component, and the Critical Distance of point method $\frac{L_{PM}}{2}$ locates at the centre of the process zone as shown in Fig.(2.2b) (Susmel 2009).



(a) Fatigue Failure - Notches Crack



(b) TCD Concept

Figure 2.2: Theory of Critical Distances Mechanism

Recently, Susmel & Taylor (2010), (2015), have made pioneering contributions to the task of systematically reformulating the theory of critical distances to predict the lifetime of notched metallic materials under elasto-plastic deformations. Evaluation fatigue strength of components by defining the design stress/strain states based on the Theory of Critical Distances were not only addressed by the Manson and Coffin (Manson 1954, & Coffin 1954), but also addressed according to the solutions published by Morrow (1965), Smith (1970), and Socie & Morrow (1980). The reliability and accuracy of this method was validated by testing a large number of ferrous and non-ferrous metallic materials under different fatigue loadings, for instance constant amplitude CA (Susmel & Taylor 2010) and variable amplitudes VA (Susmel & Taylor 2015). The validation process proved that TCD is a successful approach in uniaxial/multiaxial fatigue prediction that is widely accepted to quantify the effective infield stress/strain states to accurately evaluate fatigue damage of elements containing not only different types of notches, for example, sharp and blunt, but also developed cracks.

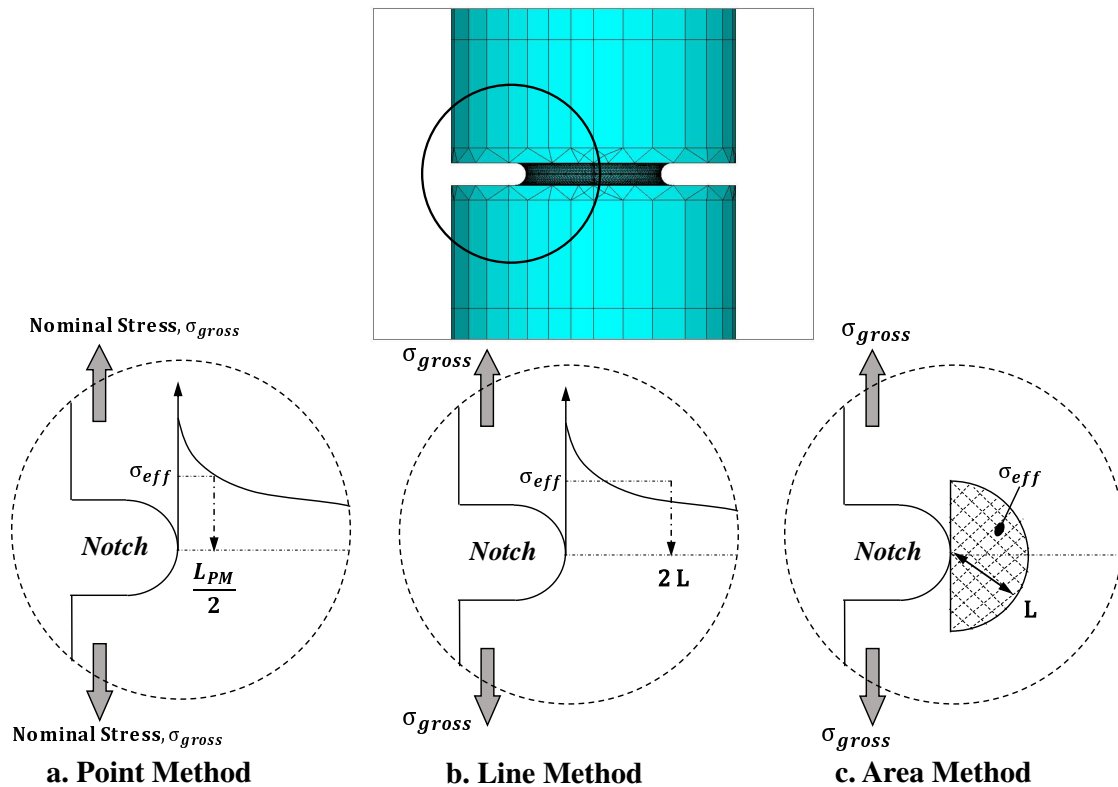


Figure 2.3: Theory of Critical distances - Three Different Formalisation

2.3 Critical Review of the Various Current Approaches to the Problem of Multiaxial Fatigue

Over the past 70 years and particularly with the development of industries, the problem of evaluating multiaxial fatigue damage of components has extremely been investigated to formalise a sound techniques, allowing engineers to design real components against multiaxial fatigue loadings. According to the recent findings in this field, the state of the art shows that plenty of attempts have been made to address multiaxial fatigue damage of components by using different strategies. Multiaxial fatigue can be classified into two regimes. First: low-cycle fatigue that plastic deformation plays a fundamental role in the fatigue crack nucleation. Strain-based approach are always recommended to design low-cycle fatigue (Susmel 2003). Second: high-cycle fatigue, linear-elastic behaviour can be considered with little loss of accuracy, and stress-based methodology can be used in the fatigue evaluation. Generally, design methodology suitable for evaluating multiaxial fatigue is divided by three different groups: Stress-based method, strain-based method, and energy based methodology. The pioneering models proposed by Brown & Miller (1973) took as a starting point the assumption that fatigue damage under multiaxial cyclic loading depends on the local strain state parallel and normal to the crack initiation plane. In order to efficiently consider the detrimental effect of superimposed static stresses, Wang (1993) is used Brown & Miller (1973) criterion with considering mean stresses perpendicular to the critical plane. Socie (1987) and Fatemi & Socie (1988) are developed two different fatigue evaluation techniques by using the stress and strain states relative to the critical plane. The stress/strain-based approach and critical

plane are critically defined in detail in the next sections and the most advantages and disadvantages of the theory was highlighted.

The third fatigue design methodology that suitable for evaluating multiaxial fatigue is based on the assumption that energy is always proportional to fatigue failure of a component. In the philosophical view point, a number of researchers is considered energy-based method as an attractive methodology because it is independent of the degree of multiaxiality of the infield stress/strain states. Among the existing energy-based methods, two approaches deserve to be mentioned. First: method proposed by Guard (1981) and the second approach developed by Ellyin (1991) & Ellyin (1993). The pioneering model formalised by Guard (1981) stated that performing the multiaxial fatigue evaluation of materials by using energy is due to cyclic plastic deformation. However, unfortunately, it has been seen that even this attractive theory has problems resulting inconsistency when uniaxial estimation is compared with those situation under torsional loading. Ellyin (1991) and co-workers argued that not only plastic deformation but also the positive part of the elastic energy should be considered to accurately estimate fatigue damage. That explain fatigue damage is strongly influenced by the elastic energy developed from the tensile stress/strain amplitudes. By revisit all the above mentioned criteria, it can be observed that fatigue damage parameter for evaluating multiaxial lifetime of components is based on the equivalent stress/strain quantity with a unique reference fatigue curve

By following a different fatigue approaches, the present research work in this thesis aims to formalise and validate an alternative multiaxial fatigue design methodology to design an engineering components having a geometrical features with considering a degree of multiaxiality and non-proportionality of the stress/strain state at the assumed crack nucleation field.

2.4 Γ -Plane Theory For Evaluating Multiaxial Fatigue

The Γ -Plane theory was developed by Brown & Miller (1973) to estimate fatigue damage of a component. According to this theory, fatigue life is a function of a developed strain state under multiaxial cyclic loading. In more detail, the maximum shear strain amplitude and the tensile strain normal to the plane of maximum shear controls the process of fatigue cracks. Such a maximum shear-strain plane is known by a Γ -Plane.

Brown & Miller (1973) illustrates a significant role of accurate strain measurement of a component to evaluate multiaxial fatigue by using the Γ -Plane. The author of Γ -Plane concept have shown to some extent how significant the accurate local strain calculation of a material under multiaxial fatigue to reveal the location, orientation and value of the maximum shear strain, γ_a and normal strain $\sigma_{n,max}$ relative to the Γ -Plane. Based on the strain amplitudes, a fatigue crack subsequently initiate and propagate under stage I conditions on the maximum shear-plane. Then, the crack deviate to a propagation mode (stage II). This theory is considered as a useful tool to predict the position, direction and plane of crack initiate based on the maximum shear-plane, and the validation process of Γ -Plane theory shows a satisfactory results in predicting multiaxial fatigue

cracks. However, as stated in section (Future work) of the published Brown & Miller (1973) paper that further work is needed to consider the pre-loading, residual strain and degree of multiaxiality of the applied load. That explains the results from this approach are not always correlate with the experiments, particularly when mean strain and out-of-phase cycle loads are involved, because defining mean stress/strain is a more difficult task compare to the other fatigue loading conditions. Also Γ -Plane Theory was not examined to deal with real engineering components and complex geometries. That mean, Γ -Plane theory have not yet extended to cover engineering components with a geometrical feature leading to localised stress/strain concentration phenomena.

2.5 Critical Plane Approach (C.P)

A critical plane can be simply defined as a material plane in which the damage parameter reaches its maximum value. Generally, in any engineering component subjected to an external system of loading, an infinite number of planes with different orientation pass through any point inside the material. The normal and shear stress/strain amplitudes developed on those planes vary. In order to model fatigue damage correctly, it is important to understand when and where fatigue damage has a maximum value. On the other hand, its widely believed that any component under fatigue loading goes through two subsequent damage stages: First, crack initiation in the plane experiencing the largest shear ranges, followed by, second, a crack propagation that is strongly influenced by the normal stress perpendicular to the critical plane. Such a normal stress favours the growth of the fatigue crack by cyclically opening and closing that crack (Socie 1987).

Examination of the state of the art shows that many different strategies have been investigated so far to evaluate the fatigue damage of a component by using different hypotheses. Amongst the proposed approaches, the *Critical Plane* is the best-known (Susmel 2010, Socie & Marquis 2000). The CP theory was suggested by Brown & Miller (1973) and argues that fatigue cracking in metals is always observed to grow in the plane with the largest shear amplitude under different loading conditions (Fatemi & Socie 1988 & Kim et al. 1999). The critical plane approach is presented in three different forms: i. stress-based, ii. strain-based and iii. strain-stress-based models (Shamsaei et al. 2010). Previous researchers have validated that a stress-based critical plane approach gives an accurate evaluation in a long-life regime in which plastic deformation is small or negligible. In contrast, the strain-based approach is recommended for the elasto-plastic short/medium life fatigue in which plastic deformation is important.

2.5.1 Stress-Based Approach (S-N Curve)

A stress-based approach is a traditional critical plane theory for fatigue prediction that has widely used since Wöhlers time. The hypothesis assumes that the lifetime of a component can be estimated directly through the maximum shear stress amplitude. The S-N curve shows how the fatigue lifetime decreases with higher stress amplitudes. According to this approach, when a stress value decreases to a certain level, the specimen will not fail due to fatigue. This level is referred to as the *endurance limit*. However, some people argued that this fatigue limit does not exist (Sonsino

2007). Although the stress-based approach is old and although the effect of some significant parameters, for instance, mean stress, geometrical features, surface treatment, and many others, are not considered, is still a valid and useful engineering tool.

Basically, to give a clear idea of the Wöhler curve, consider the plane sample in Fig. 2.4 under a uniaxial tension-compression force with a load ratio (R) equal to -1 (i.e. zero-mean stress). The specimen fails after a certain number of cycles that depends on the material properties and fatigue parameters. By testing different samples under various stress amplitudes, the log-log Wöhler curve ($S-N$ curve) can be drawn. There is a specific point that the $S-N$ curve is considered to be horizontal in ferrous material. Any stress below the line can be assumed as not likely to result in fatigue failure. A typical $S-N$ curve is illustrated in Fig. 2.4.

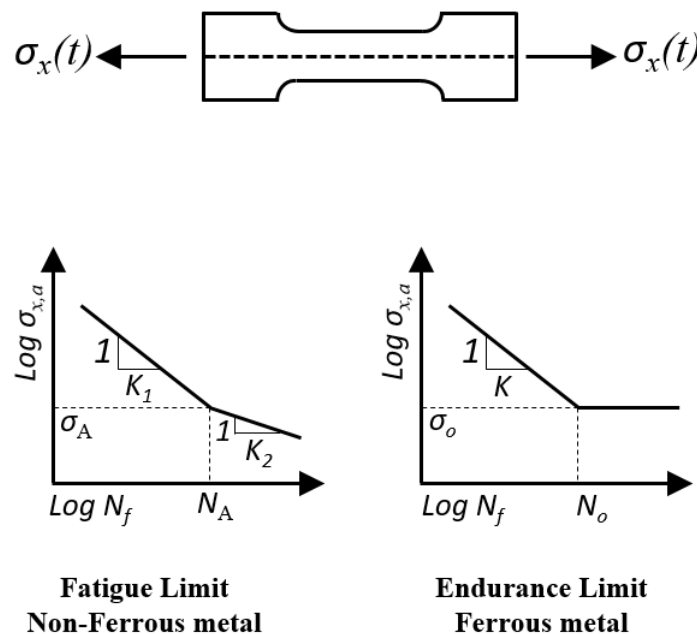


Figure 2.4: The Wöhler curve for ferrous and non-ferrous material

One of the key criticisms of the stress-based approach is that it does not consider the effect of mean stress and the degree of nonproportionality of the applied load. The pioneering modification of the Wöhler curve proposed by Susmel (2009) reformulated the stress-based approach so as to account for both of the above-mentioned damage parameters. This led to the method referred to as the Modified Wöhler Curve Method (MWCM). According to the MWCM, the plane of maximum shear stress amplitude is the plane that fatigue damage reaches the largest level (Susmel & Taylor 2012, & Lazzarin & Susmel 2003). This modified stress-based approach has been validated through several systematic experimental investigations (Susmel & Taylor 2003) & (2010). The validation process demonstrated that the modified Wöhler curve is an extremely powerful tool to predict the lifetime of components. This approach is only recommended for the evaluation of high-cycle fatigue, however (Neuber 1961) because, under these situations, cyclical plastic deformation neglects with little loss of accuracy (Shamsaei et al. 2010). In contrast, when the number of cycles to failure decreases, and the effect of cyclic plasticity cannot be disregarded Manson (1954) and Coffin (1954) concluded that fatigue can be more accurately estimated by solving the problem in terms of an elasto-plastic strain-based critical plane a rather stress-based approach. This strain-

based solution has been shown to have major advantages compared to any form of stress-based approach (Wang & Susmel 2016) and (Susmel & Taylor 2015). This explains that the strain-based theory is accepted as an alternative design tools suitable to be used by design engineers to evaluate low/medium lifetime in the engineering structures and elements (Fatemi et al. 2004) & (Susmel & Taylor 2010).

2.5.2 Strain-Based Approach (Manson-Coffin Curve Methods (MCCM))

Classic Strain-Based Approach (Classic Manson-Coffin Curve Methods (MCCM))

As mentioned in the last section, the accuracy of the stress-based approach is questionable in respect to describing fatigue damage of materials in a low-cycle fatigue regime, because there is no account for plastic deformations. Also, attention needs to be paid to load histories that cause detrimental local notch mean stresses, which can not properly be analysed using the S-N curve. This explains why the Wöhler curve cannot be used directly to address the problems arising from elasto-plastic deformation. The strain-based approach is proposed as being a better technique to predict low/medium-cycle fatigue damage of a component when plastic deformation is significant (Susmel et al. 2009, Susmel 2014).

In the early 1960s, Manson and Coffin independently employed a power law relation between the elasto-plastic strain and number of cycles to failure (N_f), in what is now known as a Manson-Coffin curve (Tavernelli & Coffin 1962). This discovery represented an improved design tool for a class of structures and elements where plastic deformation is important and unavoidable under fatigue load. The MCCM is a strain form of the critical plane parameter that takes as its starting point the assumption that fatigue cracking in low/medium-cycles is controlled directly by the maximum strain range relative to the material plane, known as the critical plane. From a mathematical point of view, such an approach results in a log-log diagram plotting the axial/shear strain of the critical plane versus the number of cycles to failure, N_f . Ever since, despite some weak points being identified, the strain-based approach has been recognised as providing a powerful means of rapidly estimating low-cycle fatigue damage of plane components under uniaxial loading. At the time of developing, the classic Manson-Coffin Curve was described mathematically in terms of axial strain as shown in Fig.(2.5a) and defined according to the following relationship:

$$\varepsilon_a = \frac{\sigma'_f}{E}(2N_f)^b + \varepsilon'_f(2N_f)^c \quad (2.1)$$

Then, the Manson-Coffin Curve was reformulated in terms of shear strain amplitude based on the assumption that fatigue damage maximise on a plain experiencing maximum shear strain amplitude (Wang & Susmel 2016). The shear strain-based relationship was described according to the Eqn.(2.2) and as shown in Fig.(2.5b):

$$\gamma_a = \frac{\tau'_f}{G}(2N_f)^{b_o} + \gamma'_f(2N_f)^{c_o} \quad (2.2)$$

Where ε_a , and γ_a are the axial and shear strain amplitudes on the critical plane. σ'_f , ε'_f ^[i] are fatigue strength coefficient and fatigue ductility coefficient, respectively. τ'_f , γ'_f are the shear fatigue strength coefficient and the shear fatigue ductility coefficient. The terms of b and c are fatigue strength exponent and fatigue ductility exponent. b_o and c_o are shear fatigue strength exponent and shear fatigue ductility exponent. N_f is a number of cycles to failure.

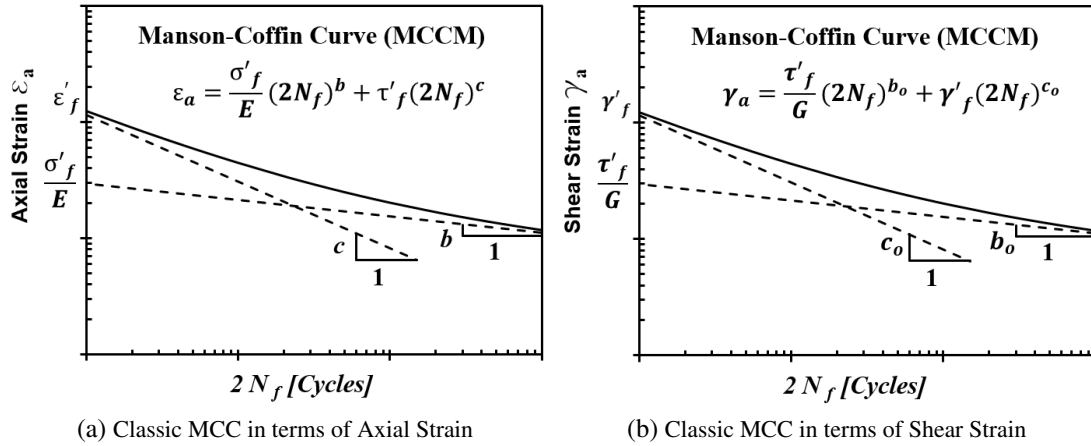


Figure 2.5: Classic Manson-Coffin Curve in terms of Axial and Shear Strain Amplitudes

Modified Strain-Based Approach (Modified Manson-Coffin Curve Methods (MMCCM))

Previous research has established that the classic Manson-Coffin curve shows a relatively a good correlation with experiments in terms of estimating the lifetime of materials. The results from this approach are not always satisfactory, however, particularly when applied to complex geometries (for example notches) and situations involving complex multiaxial cyclic loading. On the other hand, the response of materials under fatigue load is very sensitive to many parameters, for instance, mean stresses, geometrical features and surface treatment. Among those factors, both *i: stress raisers* and *ii: multiaxiality of stress/strain states* have an observable detrimental effect on materials under fatigue and need to be considered when performing lifetime estimation. A significant effort has been made to address these issues, especially through the pioneering modification of the Manson-Coffin Curve proposed by Susmel (2009) for situations involving a degree of multiaxiality and non-proportionality of the stress state at crack initiation sites. The modification is shown in Fig. 2.6 and is based on calculating the index factor (stress ratio ρ) that can be mathematically expressed as:

$$\rho = \frac{\sigma_{n,m} + \sigma_{n,a}}{\tau_a} = \frac{\sigma_{n,max}}{\tau_a} \quad (2.3)$$

Where: $\sigma_{n,m}$ and $\sigma_{n,a}$ are the mean value and the amplitude of the stress normal to the critical plane, τ_a is the shear stress amplitude aligned on the critical plane.

^[i] σ'_f , τ'_f , ε'_f , γ'_f , b , b_o , c , and c_o are the corresponding axial and shear strain-life fatigue properties that can directly be quantified from the uniaxial and torsional Manson-Coffin curve by running an appropriate experiments and zero mean stress (Susmel 2009)

Thanks to this feature, the MMCCM becomes sensitive to the influence of mean stress and degree of multiaxiality and is reformulated mathematically as follows (Wang & Susmel 2016):

$$\gamma_a = \frac{\tau'_f(\rho)}{G} (2N_f)^{b(\rho)} + \gamma'_f(\rho) \cdot (2N_f)^{c(\rho)} \quad (2.4)$$

where:

$$\frac{\tau'_f(\rho)}{G} = \rho \cdot (1 + \nu_e) \frac{\sigma'_f}{E} + (1 - \rho) \frac{\tau'_f}{G} \quad (2.5a)$$

$$\gamma'_f(\rho) = \rho \cdot (1 + \nu_p) \varepsilon'_f + (1 - \rho) \gamma'_f \quad (2.5b)$$

$$b(\rho) = \frac{b \cdot b_0}{(b_0 - b)\rho + b} \quad (2.5c)$$

$$c(\rho) = \frac{c \cdot c_0}{(c_0 - c)\rho + c} \quad (2.5d)$$

The signs b_o and c_o are the shear fatigue strength exponent and shear fatigue ductility exponent, respectively, that directly can determine by running fully reversed pure torsion fatigue test. ν_e and ν_p are an elastic and plastic poisson's ratio.

Based on the above modification, the Manson-Coffin curve progressively moves upwards and downwards based on the ρ value, increasing and decreasing the predicted number of cycles to failure, as shown in Fig. 2.7. For instance, the curve moves downwards as the ratio ρ increases. Typically, the plane components under a uniaxial fully-reversed fatigue load result in a ρ value equal to unity, whereas under torsional loading (fully-reversed), the ρ ratio is equal to zero. In a simple fashion, for a given shear strain amplitude relative to the critical plane, the fatigue damage increases with an increasing ρ value, which explains why it is important to select a critical plane with the largest ρ value among all the potential critical planes. In conclusion, according to the systematic validation exercise (Wang & Susmel 2016), The Modified Manson-Coffin Curve Method, MMCCM is seen to be successful and highly recommended for evaluating the fatigue-related lifetime of metallic materials under cyclic loading.

2.6 Material Response under Cyclic Deformation

In this section, attention is focused towards the plastic behaviour of materials due to cyclic loading. Generally, materials under fatigue load behave either in hardening or softening forms. In some particular materials, however, the plastic deformation remains stable. The investigation of each of the above-mentioned plastic deformation models includes numerous complex constants that need to be determined through experimental work. This can be done by running a constant amplitude fatigue test with strain-controlled deformation. This test is performed in a laboratory with fully reversed uniaxial cyclic tension and compression with zero mean stress. In the case of hardening, at the beginning of each cycle, there is a gradual increase in the developed stresses with each

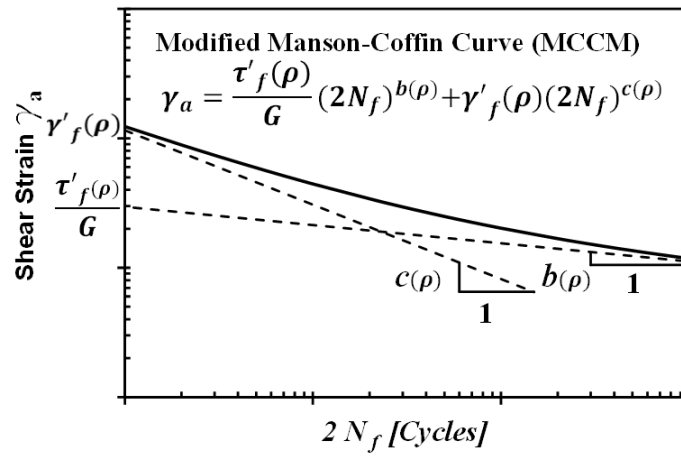


Figure 2.6: Modified Manson-Coffin Curve (MMCCM)

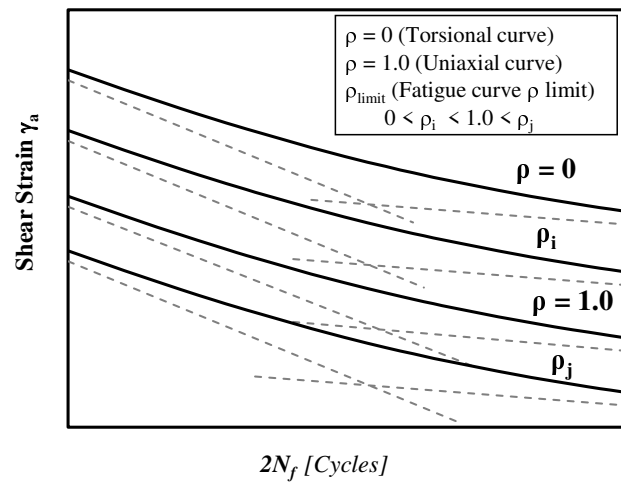


Figure 2.7: Modified Manson-Coffin Curve MMCCM with different ρ values

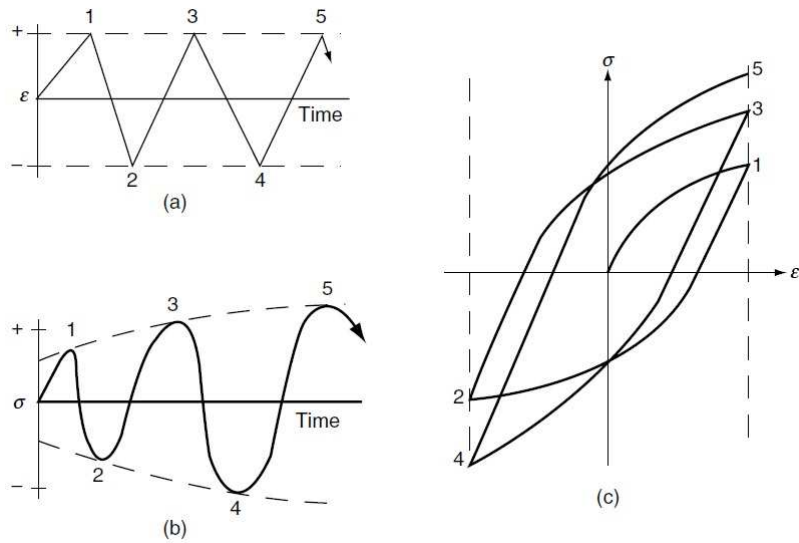


Figure 2.8: Stabilized Stress-Strain Curve - Hardening Phenomenon

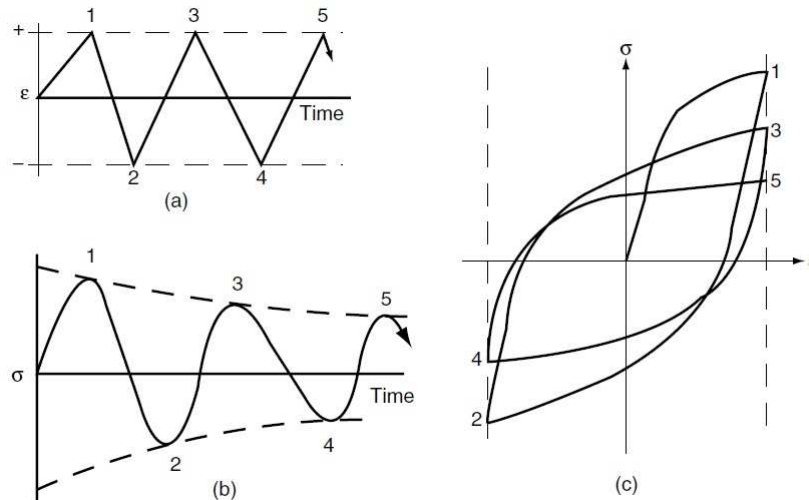


Figure 2.9: Stabilized Stress-Strain Curve - Softening Form

successive strain reversal until a stable stress value is reached for the rest of the fatigue-related life, as shown in Fig (2.8). In the softening case, meanwhile, the developed stresses decrease until a stable level is reached, as presented in Fig (2.9). The hardening and softening evolution of materials has been supported by researchers and can be used as a failure criterion. Lee et al. (2005) concluded that aluminium alloys behave as a soft material and tends to harden under cyclic loads, whereas in contrast, steel is a hard material and tends to soften under reversal loads.

2.6.1 Hardening Rule

Hardening is defined as a material response due to plastic deformation. Alternatively, hardening can be defined as a change in the yield condition of a material as a result of loading in the elasto-plastic regime (i.e evolution of subsequent yield surfaces). Consider a geometry experiencing a

sufficient stress or combination of stresses. After removing the applied loads, the final geometrical configuration may not be the same as the original. From the scientific point of view, the material undergoes a plastic deformation, with a specific change occurring in the yield strength of the material being assessed. All materials have a yield surface with all stress points being located either inside or on the yield surface. In plastic deformation, the stress point moves towards the outside of the yield surface and the material responds by either expanding or translating the yield surface according to the behaviour of the material, this is known as a hardening phenomenon. The cumulative work is obtained by summing the plastic strain occurring over repeated loads (Jiang & Sehitoglu 1996). A complete hardening rule of materials must be able to consider the following deformation characteristics:

Isotropic Hardening

Isotropic hardening is the process of the uniform expansion of an initial yield surface due to the application of stresses greater than the yield stress of the material. Consequently, a new yield surface is obtained, as shown in Fig. 2.10a. In Isotropic Hardening, the initial yield surface expands in all directions during the plastic deformation and a new yield surface is thereby created. The centre of the initial and subsequent yield surfaces are the same. The new surface remains unchanged even when the applied load is removed.

Kinematic Hardening

Kinematic hardening is also known as the Bauschinger effect (Prager 1955). According to the rule of Kinematic hardening, the yield surface of a material under plastic deformation translates in the space of stress as a rigid body without changing the initial form and orientation of the yield surface. The magnitude of unloading in Kinematic hardening equals two times the initial yield stress $2\sigma_y$, as shown in Fig.(2.10b).

2.6.2 Nonproportional Cyclic Loading and Nonproportional Additional Hardening

In real structural elements, many different applications entail multiaxial out-of-phase cyclic loading processes. A nonproportional cyclic load is a term that describes multiaxial fatigue loads that act randomly on a structure. Nonproportional stress, however, is the corresponding stress on a material where the principal axis is continuously rotating during in-service loading. Computation of fatigue damage during nonproportional loading is more complex compared to proportional applications. The simplest example would be a component experiencing, for example, 45° shifting between the applied cyclic tension and torsion, where the principal axis rotates through 45° . During nonproportional loading, the normal stress/strain is bigger than in proportional loading, given the same shear strain amplitude, and this increase in normal stresses accelerates the crack propagation stage. The largest level of non-proportionality of the multiaxial fatigue load equals 90° (Socie & Marquis 2000). Nonproportional stressing can be classified into three forms: 1.

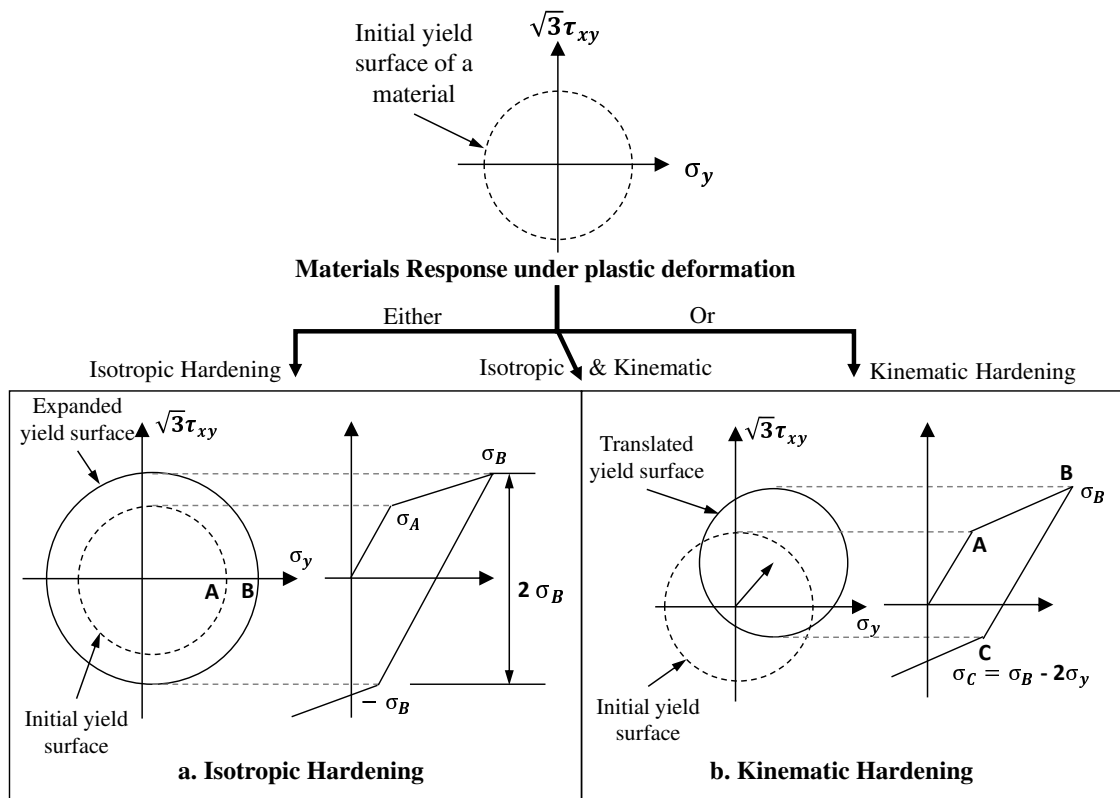


Figure 2.10: Hardening rules of materials in the plastic regime

Proportional cyclic stress with a mean stress; for instance, cyclic uniaxial or pure torsion with a static stress. Here, the static stress results in the principal stress rotating. 2. Nonproportional stress with a fixed principal axis. For example, applying a cyclic load on a plate in two directions. 3. Nonproportional stress with a rotating principal axis.

In addition, a significant point that needs to be remembered here is that many materials under nonproportional fatigue load with a rotating principal stress axis experience additional non-proportional hardening, as shown in Fig.(2.11). Such additional non-proportional hardening is different in different materials and depends to a great extent on the micro-structure of the material being assessed and its load history. For example, while Socie & Marquis (2000) stated that aluminum alloys experiencing a small magnitude of nonproportional additional hardening that can be neglected, steel typically shows a 20% increase in additional hardening.

2.7 Mean Stress

Industrial development has led to a growing interest in understanding the influence of mean stresses on the overall fatigue strength of engineering materials. Mean stress can be applied in different forms. A superimposed static tensile stress $\sigma_{x,m}$ is considered as a kind of mean stress and it can clearly be seen that fatigue damage increases as the superimposed static tensile stress increases. A considerable amount of literature confirms that the presence of superimposed static stress and strain can be neglected in the plane metallic materials under high-cycle fatigue regime

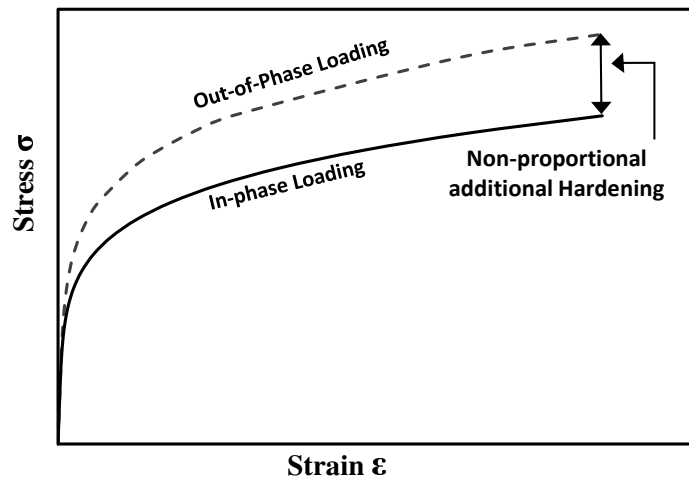


Figure 2.11: Non-proportional Additional Hardening - Effective Strain Amplitude

due to the mean stresses/strains relaxation phenomenon (Socie & Marquis 2000). However, in the low-medium cyclic fatigue, the mean stress has a considerable influence on crack-initiation and propagation, when the nominal mean stress is not fully reversed, it results in a significant influence on the overall fatigue lifetime of a component (Susmel et al. 2011). Thanks to the feature of Modified Manson-Coffin Curve Method, MMCCM that is sensitive in considering the effect of mean stress in the low/medium-cycle fatigue regime.

2.8 The Maximum Variance Method (MVM)

The critical plane (CP) discussed in section (2.5) is the plane experiencing the most fatigue damage that needs to be identified in a realistic numerical calculation. A multi-variable optimisation method is needed to check the infinite potential planes that pass through a critical point inside a material to find the orientation of the most damaging plane (the critical plane). Once the CP is known, then the normal and shear stress/strain mean values and amplitudes are quantified relative to that plane. The Maximum Variance Method is considered to be a worthwhile numerical method to check the critical plane. Advantages of this approach are: (i) it allows all potential critical planes to be examined so as to find the plane experiencing the maximum shear strain amplitude; (ii) it can be solved extremely rapidly.

From a statistical viewpoint, "Variance" is defined as a measure of the amount of variation inside the two extremes defining the maximum range within which the own signal varies ($Var(X) = E(X^2) - m^2$). In this research, the variance of time-variable stress/strain states is the expected value of the square of the deviation of those states from their mean value. The variance is equal to amplitude when the considered signals are sinusoidal. According to the well-documented literature, the fatigue damage of a component is proportional to the variance of the shear strain history relative to the critical plane (Susmel 2010) and the critical plane is indicated through that direction along which the variance of the resolved shear strain history reaches its maximum level. Wang &

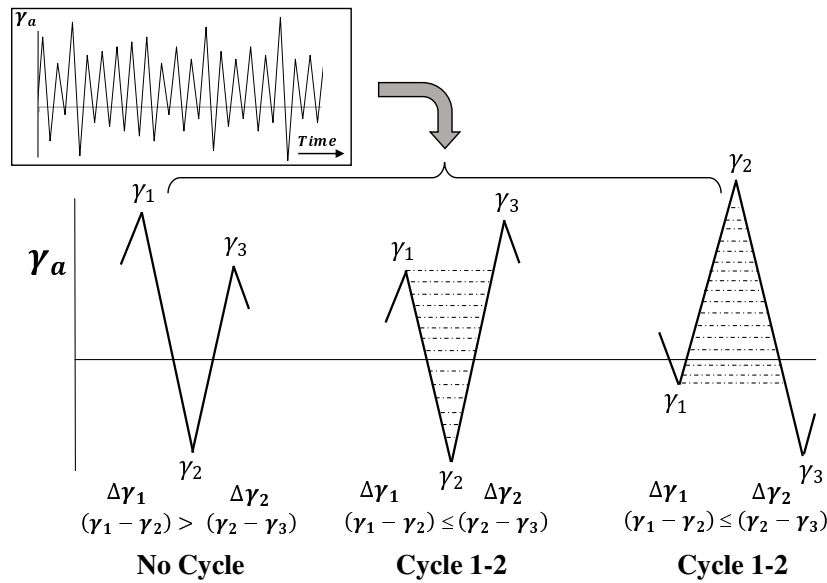


Figure 2.12: Rain Flow Cycle Counting Rules

Susmel (2016) validated that the maximum variance method (MVM) is a successful engineering tool to determine the orientation of the critical plane CP under multiaxial fatigue load.

2.9 Rainflow Cycle Counting Method

In situations of practical interest, most of fatigue loadings on structural elements and components often involve cyclic loads with variable amplitudes. The fatigue evaluation of such loads is not a straightforward exercise. In processing fatigue damage under random loading, a cycle counting technique is required to break down the complex irregular stress/strain histories into a series of individual constant amplitude events. Modern technology has developed many applications to achieve this, using various techniques. The rainflow cycle counting method is the most widely applied and accepted approach within the scientific community (Kim et al. 1999).

According to the rainflow method, a closed shear strain cycle is defined with three points (γ_1 , γ_2 & γ_3) as shown in Fig. 2.12. The method compares a range between ($\Delta\gamma_1 = |\gamma_1 - \gamma_2|$) with a range between ($\Delta\gamma_2 = |\gamma_2 - \gamma_3|$) to check whether the cycle is recording or not. The process of checking cycles is based on the following rainflow rules:

$$\Delta\gamma_1 = |\gamma_1 - \gamma_2| \quad (2.6a)$$

$$\Delta\gamma_2 = |\gamma_2 - \gamma_3| \quad (2.6b)$$

$$\text{If } \Delta\gamma_1 > \Delta\gamma_2 \quad \text{No Cycle Recorded} \quad (2.6c)$$

$$\text{If } \Delta\gamma_1 \leq \Delta\gamma_2 \quad \text{Cycle Recorded (Cycle : 1 - 2)} \quad (2.6d)$$

$$\text{If } \Delta\gamma_1 \leq \Delta\gamma_2 \quad \text{Cycle Recorded (Cycle : 1 - 2)} \quad (2.6e)$$

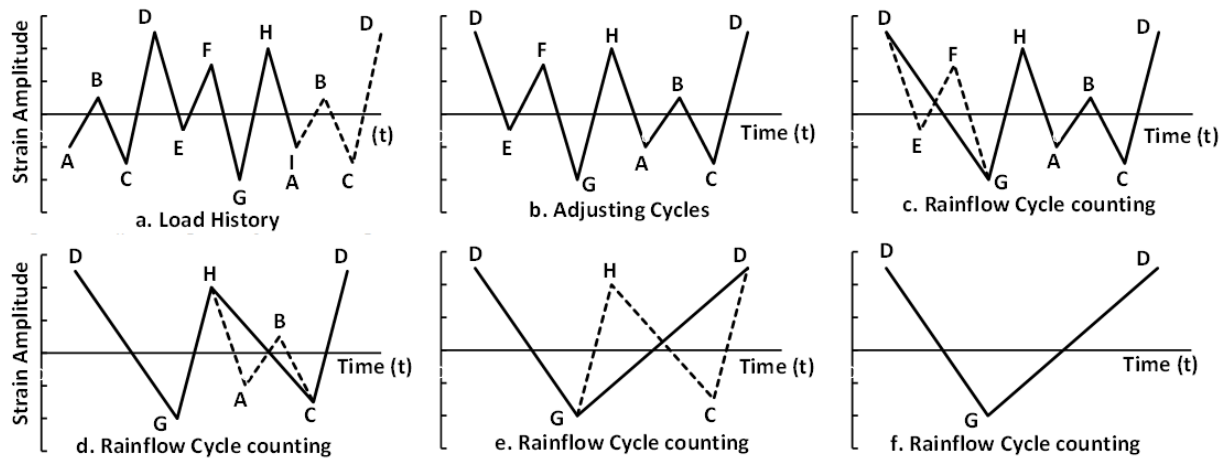


Figure 2.13: Example procedure of Rainflow Cycle counting, adopted from Lee et al. (2005)

Fig. 2.13 represents a shear strain history with variable amplitude range of peaks and valleys. By applying a consensus rainflow method, a cycle is identified to be met using the criteria defined in Fig.(2.12). For any variable amplitude histories, one of the most significant requirements of the rainflow rule is to re-consider the entire event starting at the largest peak or valley amplitude; i.e. so that the counting starts at the maximum peak or minimum valley, whichever is greater in absolute value (Lee et al. 2005). This means that the cycles prior to the extreme peak/valley need to be moved to the end of the history, as shown in (Fig. 2.13 a-b). Then, the first three peak or valley amplitudes are considered, applying the rules and Equation (2.6). If a cycle range and mean is calculated, then the associated peaks and valleys will remove from the history, whereas if they cannot be calculated then the algorithm moves to the next peak or valley cycle, as clearly illustrated in (Fig. 2.13 c-f). This procedure continued until all the cycles are exhausted (Downing & Socie 1982).

2.10 Cumulative Fatigue Damage

In variable amplitude fatigue loading, after identifying variable cycles into a series of constant amplitude episodes using rainflow cycle counting, fatigue damage is accumulated for each cycle in the history. This accumulation of fatigue damage has a direct relationship to the amplitude of the cycles. At the beginning of the applied fatigue load on a component, the damage slowly accumulates with each cycle and small nucleate cracks develop. Then, the nucleate cracks grow (become longer) more quickly (Socie & Marquis 2000). A validated approach requires an understanding of the fatigue damage accumulated in each cycle to be able to estimate the overall lifetime of the material accurately. According to the literature, the Palmgren-Miner (Palmgren 1924 & Miner 1945), rule along with a cycle counting procedure, gives a satisfactory result in estimating the cumulative fatigue damage of a component subjected to cyclic loads of variable amplitude (Wang & Susmel 2016). The Palmgren-Miner rule was proposed for use on ball and roller bearings by Palmgren in 1920, but was not commonly used until after publication by Miner in 1945. Ever since, the method has been widely used by engineers to calculate accumulated damage, and the

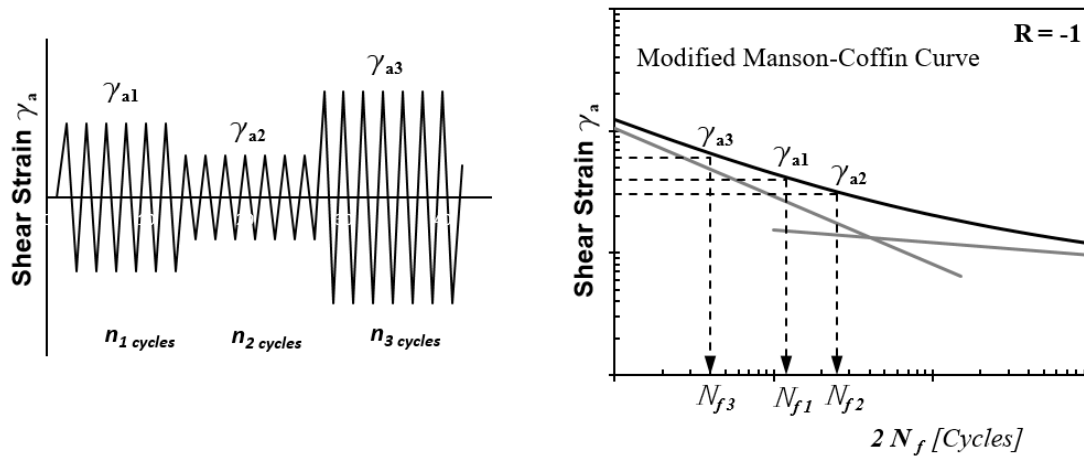


Figure 2.14: Palmgren-Miner rule to evaluate damage of variable amplitude loading

method called Palmgren-Miner rule (Webber 1970).

According to Palmgren-Miners linear damage rule, the total fatigue damage accruing from the loading history is equal to the sum of cycles of each strain level n_i divided by number of cycles to failure at the same strain level $N_{f,i}$, and eventually reaches unity. For instance, consider a variable amplitude shear strain history that changes more than one time during cyclic loading, as shown in Fig. 2.14. If $(n_1, n_2, n_3, \dots, n_i)$ cycles are applied at the $(\gamma_{a1}, \gamma_{a2}, \gamma_{a3}, \dots, \gamma_{ai})$ respectively, using the Modified Manson-Coffin curve, the number of cycles to failure ($N_{f,i}$) can be determined for each shear strain level. According to the experimental investigation, the sum of the life fraction of $\frac{n_i}{N_{f,i}}$ equals one. (Eqn. 2.7).

$$D_{tot} = \frac{n_1}{N_{f1}} + \frac{n_2}{N_{f2}} + \frac{n_3}{N_{f3}} + \dots = 1 \quad \Rightarrow \quad D_{tot} = \sum_{i=1}^j \frac{n_i}{N_{f,i}} \quad (2.7)$$

In the above equation, D_{tot} is the total cumulative fatigue damage. n_i is the number of cycles at the i -th strain amplitude level. $N_{f,i}$ is the number of cycles to failure at the same strain level.

2.11 The main gaps in knowledge

According to the above reviewed theories established in the previous literature to evaluate fatigue of a component and the subsequent modification/development, the following knowledge gap yet not explored and need to be researched:

- According to the literature review in this chapter, the complexity of multiaxial fatigue evaluation of notch component is well demonstrated by the fact that many researchers and experts in this field have worked and proposed various solutions. However, in spite of all their hard works, it still seems impossible to incorporate all these theories into one universal theory for all complex geometries and fatigue loading cases.

- A systematic validation process of the previous literature presented in subsection (2.5.2) confirmed that the classical Manson-Coffin Curve to evaluate fatigue fracture is not correlated with the experiments and need a proper modification by considering the mean stress/strain and degree of non-proportionality of the applied fatigue load.
- The low-cycle multiaxial fatigue under high-strain cyclic load has been investigated during recent years. However, a limited reliable experimental data sets of low-cycle fatigue investigation were presented, and among the suggested criteria for correlating low-cycle multiaxial fatigue, a unique criterion has not yet been confirmed to have a universal applicability.
- The Γ -Plane theory that developed by Brown & Miller (1973) is useful to evaluate multiaxial fatigue of a component. However, according to the state of the art, this theory is particularly relevant to the cases that the applied in service loads are all in-phase and without involving mean stresses/strains. Also Γ -Plane theory has not yet applied on the engineering components with a geometrical features.
- In situation of practical interest, a remarkable number of engineering components are subjected to multiaxial random fatigue loadings. For instance gas turbine, transmission parts, pressure vessels, and automobile suspension, etc. Multiaxial fatigue life prediction against variable amplitude cyclic loading is an extremely complex and intractable problem that only a very limited theories have been developed in the literature due to inherent complexities of crack initiation and propagation. Further, in the validation point of view, physical examination of random fatigue loads in the laboratory are also scarce.

Chapter 3

Scope of the Developed Approach - Methodology

3.1 Introduction

In this chapter, an interpretive summary is presented in order to demonstrate the philosophical assumptions underpinning this research and how the most significant theories have been systematically gathered to develop the proposed approach in the most appropriate way. Then illustrate how the formalised approach is applied on the notch geometries against multiaxial fatigue loads, with involving constant/variable amplitude zero/non-zero mean stresses.

As a general rule, the developed theory is based on the critical plane approach with involving a required modification. Indeed, a successful model requires both the lifetime and the dominant critical plane to be predicted by considering all the parameters that affect fatigue damage mechanisms, these parameters can be classified as: 1. The geometrical features of the component, 2. The cyclic plasticity, 3. The nonproportionality of the applied load, & 4. The presence of mean stresses. A single theory is not enough to consider fatigue problems involving all the above-mentioned parameters, because the mechanisms of describing the stress/strain state and the accumulating fatigue damage are affected by all those parameters. Based on the above-mentioned complexity, several theories are combined in the proposed approach to consider all complex fatigue cases. In order to apply the formalised approach properly, a sophisticated algorithm is designed to predict the multiaxial fatigue of notch components. Then, the developed algorithm is interpreted into a Matlab code. The code is backed up with the corresponding triaxial stress-strain states at a critical point inside the material. The stress/strain components are determined by using the advantage of finite element, ANSYS® software. The validation process concluded that the Matlab script can be assumed to be a successful code and an easy-to-use tool to predict the multiaxial fatigue of notch components under all types of cyclic loading.

3.2 Local Triaxial State of Stresses and Strains

In order to describe methodology of the formalised novel method to evaluate the fatigue lifetime of notch components against multiaxial fatigue load, consider a notch geometry shown in Fig.(3.1) subjected to an external system of complex time-variable forces and moments. Assume point O as a centre of a coordinate system xyz and this as the site where crack initiation is expected to happen. Based on accurate numerical analyses, and the cyclic elasto-plastic behaviour displayed by the investigated metallic material, the time-dependent stress/strain state at the notch zone is found always triaxial, not only under nominal multiaxial conditions, but also under uniaxial loading conditions (refer to chapter (5.1)). Six components of stress and six components of strain are used to fully describe the stress-strain state at any point inside the notch component. Such a stress/strain state consists of six normal and six shear stress/strain vectors. The stress-strain state at the point O is described by the following tensors:

$$[\sigma_o(t)] = \begin{bmatrix} \sigma_x(t) & \tau_{xy}(t) & \tau_{xz}(t) \\ \tau_{xy}(t) & \sigma_y(t) & \tau_{yz}(t) \\ \tau_{xz}(t) & \tau_{yz}(t) & \sigma_z(t) \end{bmatrix} \quad [\varepsilon_o(t)] = \begin{bmatrix} \varepsilon_x(t) & \frac{1}{2}\gamma_{xy}(t) & \frac{1}{2}\gamma_{xz}(t) \\ \frac{1}{2}\gamma_{xy}(t) & \varepsilon_y(t) & \frac{1}{2}\gamma_{yz}(t) \\ \frac{1}{2}\gamma_{xz}(t) & \frac{1}{2}\gamma_{yz}(t) & \varepsilon_z(t) \end{bmatrix} \quad (3.1)$$

where: $\sigma_x(t)$, $\sigma_y(t)$ and $\sigma_z(t)$ are the three normal stress components and $\tau_{xy}(t)$, $\tau_{xz}(t)$ and $\tau_{yz}(t)$ are the shear stresses. $\varepsilon_x(t)$, $\varepsilon_y(t)$ and $\varepsilon_z(t)$ are the three normal strain tensors and $\gamma_{xy}(t)$, $\gamma_{xz}(t)$ and $\gamma_{yz}(t)$ are the shear strain components.

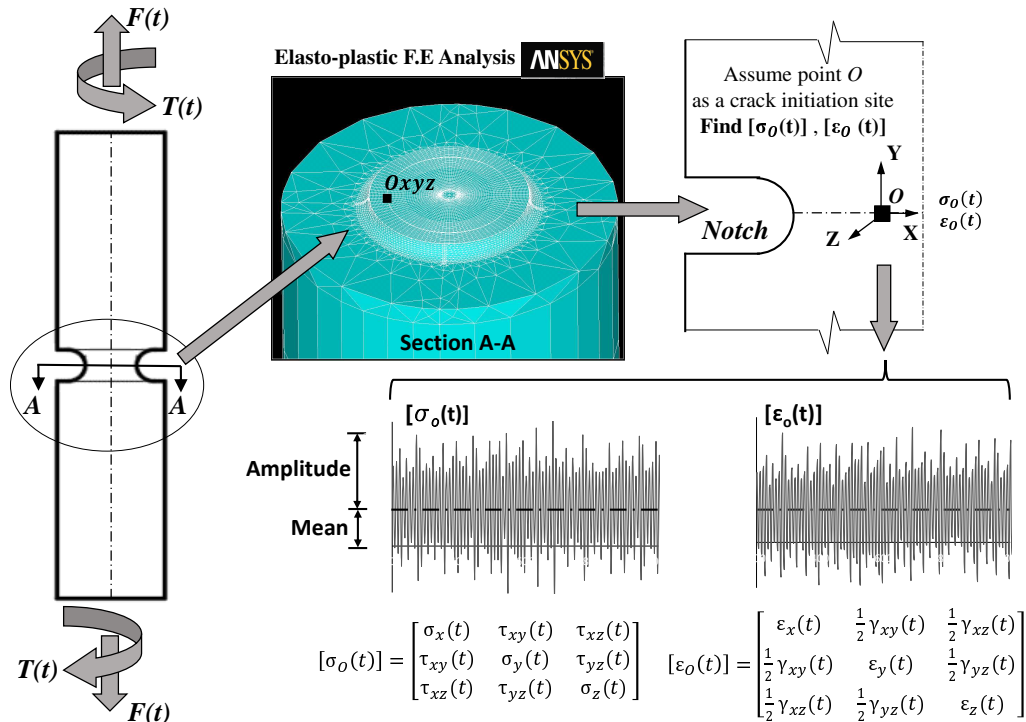


Figure 3.1: Local Triaxial Stress-Strain State of notch component

The strain vectors of, $\varepsilon_x(t)$, $\varepsilon_y(t)$ & $\varepsilon_z(t)$ are related to the stresses $\sigma_x(t)$, $\sigma_y(t)$ & $\sigma_z(t)$ respectively. Half of the shear strains $\gamma_{xy}(t)$, $\gamma_{xz}(t)$ & $\gamma_{yz}(t)$ are analogous to the shear stress vectors, $\tau_{xy}(t)$, $\tau_{xz}(t)$ & $\tau_{yz}(t)$, because each side of the cube holds half of the total shear strain value, as shown in Fig. (3.2) (Socie & Marquis 2000).

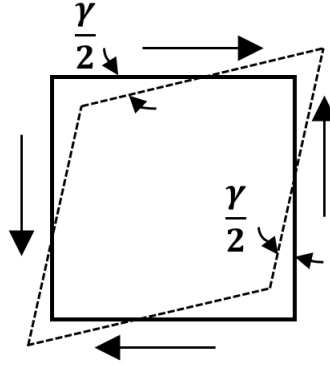


Figure 3.2: Shear Strain value of a cubic element

3.3 The Theory of Critical Distance TCD

As discussed in subsection (2.2.1), the idea of taking notch root stresses to evaluate fatigue lifetime results in an unacceptable increase in the level of conservatism and is no longer valid (2010). The Theory of Critical Distance takes as a starting point the assumption that fatigue lifetime prediction of notch components can be determined by using the corresponding stress-strain state at a certain distance from the notch tip, such a distance called a Critical Distance CD, as shown in Fig.(2.2b). In light of the TCD point method (PM), fatigue strength of metallic materials containing geometrical features can be accurately estimated by directly post-processing the entire elastoplastic stress/strain field acting on a material far from the notch tip with a distance called "Length by using Point Method L_{PM} , and equal to $\frac{L_{PM}}{2}$ ". Susmel & Taylor (2015) validated that in order to define a critical distance by running experiments, it is always advisable to perform several tests of sharply notched specimens under fully-reversed uniaxial fatigue loads with constant amplitude, and using different amplitude values at each test. The reason of using notch specimen as sharp as possible in finding the Critical Distance because TCD is always recommended to assume both extreme cases of plain and cracked specimen. Very sharp notch is seen to be similar to the case of presence cracks. Further, one single calibration test is enough to determine $\frac{L_{PM}}{2}$. However, six sharp notches were tested in this research because the scattering procedure in presenting fatigue data is always advise using several tests.

The procedure of finding a critical distance in the form of point method $\frac{L_{PM}}{2}$ by running experiments is sketched and presented in the flowchart of Fig.(3.4). As illustrated in the flow chart, six sharp U-notched specimens with a 1.5 mm root radius were tested under fatigue force of constant amplitude $F(t)$. Detail of the experiments is presented in chapter (4). The specimens were failed at a specific number of cycles to failure (N_f). By following a relevant finite element FE numerical

analysis, a stabilised local elasto-plastic stress-strain versus distance curves along the focus path of the notch were plotted for all tested specimens. The FE models were solved by using commercial Finite Element (FE) software ANSYS®. Subsequently, by using full advantage of the maximum variance method that reformulated in terms of strain (the reformulation is presented in subsection 3.5.1), the local stress/strain states along the focus path are post-processed based on the Maximum Variance of the resolved shear strain ($\gamma - MV$) relative to the critical plane. Then, all the Shear strain amplitude γ_a , Shear stress amplitude τ_a , Maximum normal stress $\sigma_{n,max}$, and Index factor ρ , relative to the critical plane were determined. Finally, the shear strain amplitude γ_a that calculated by using experimental Number of Cycles to failure N_f is compared with the Shear strain amplitude γ_a that determined by using the local stress/strain states at the assumed critical distance $\frac{L_{PM}}{2}$. The procedure of comparing both calculated shear strain amplitudes γ_a was continue until the experimental number of cycles to failure equals the estimated number of cycles to failure ($N_f = N_{f,e}$), then the assumed $\frac{L_{PM}}{2}$ was recorded. The same procedure was applied on all the 6 specimens, then average of the recorded critical distances were taken and used for all other analysis. In the FE analysis, the plastic deformation was defined by using a multilinear Kinematic Hardening and the stabilised uniaxial elasto-plastic stress/strain was used. A significant point that needs to be highlighted here is that, according to the FE analysis, the local stress/strain state in the vicinity of the notch tip is always triaxial, even if the externally applied load is uniaxial (Susmel et al. (2011)).

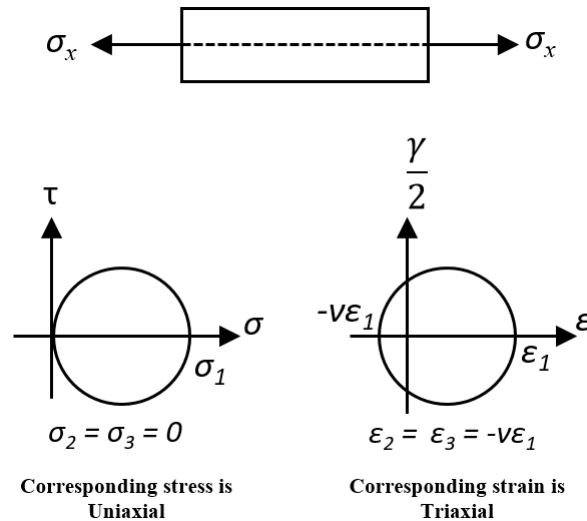


Figure 3.3: The Corresponding stress/strain under Uniaxial nominal stress

3.4 Finite Element (F.E model) to Describe the Local Stress-Strain history

After finding the critical location inside the material by using the Theory of Critical Distance, the next step was to determine the local elasto-plastic stress-strain states at the critical location. The appearance of finite element methods has simplified the process of obtaining the stress field distribution. According to the best of the author's knowledge, neither experimental, nor accurate

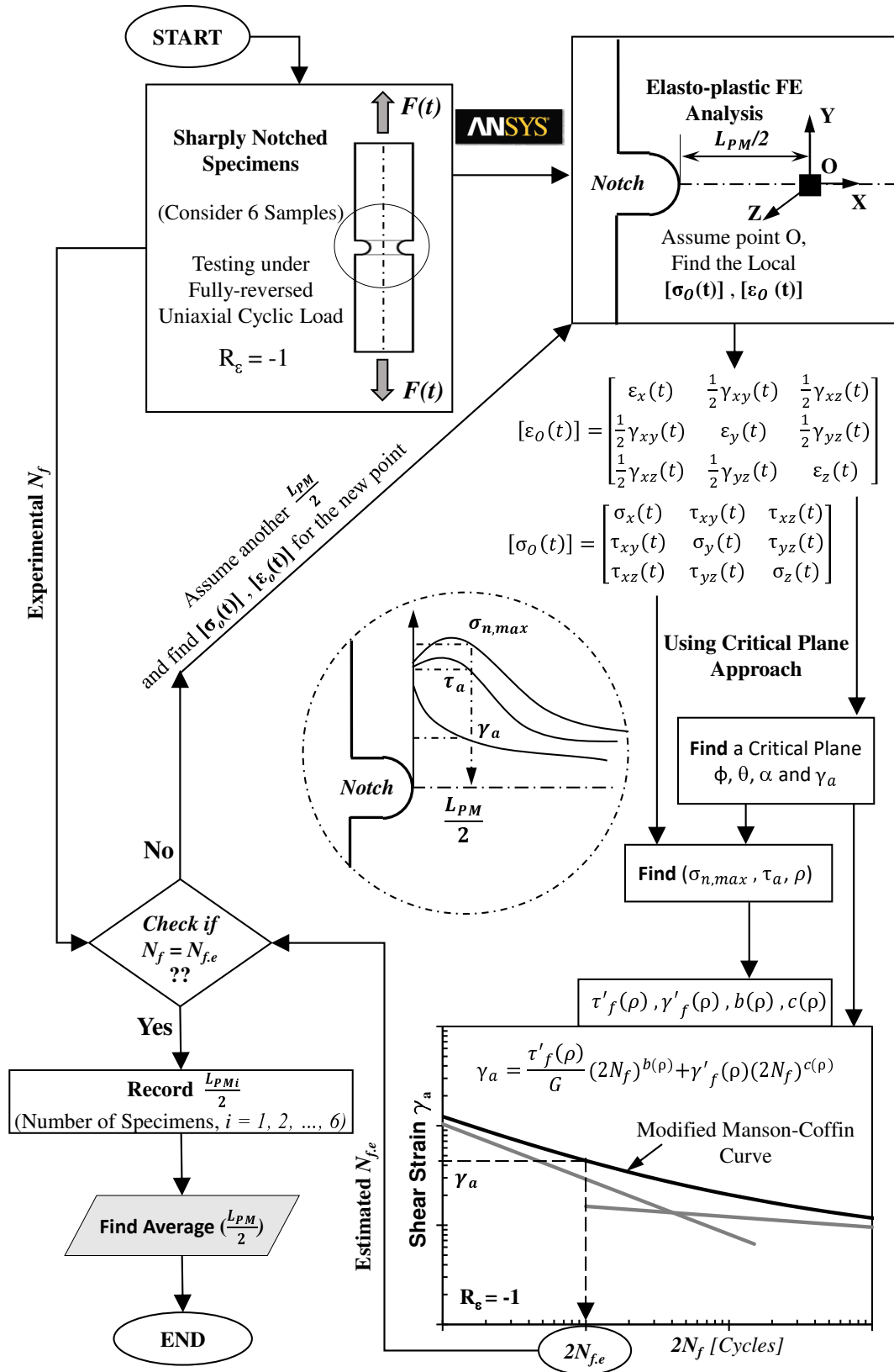


Figure 3.4: Flow Chat: Methodology to find the Critical Distance (CD) by using TCD theory

elasto-plastic models, currently exist that are able to compute the local stress/strain history inside a complex geometry efficiently. The only way to estimate such triaxial states is by using a correct form of a 3D finite element method with a relevant meshing size to reach a convergence level. In order to create an appropriate elasto-plastic three-dimensional finite element model for notch geometry, therefore, a validation exercise was followed in chapter (5) to model a three-dimensional finite element (3D FE) of a plane sample against different fatigue loadings. Then, the plane 3D FE model was extended to be used with notch geometries. The validation process presented in chapter (5) gives a relatively a good indication of the reliability of the developed 3D FE model. The numerical 3D FE calculation was carried out using ANSYS-Mechanical APDL® by employing a three dimensional solid brick 8-node element type SOLID185. The analysis was based on the von Mises yield criterion, and a stabilised uniaxial stress-strain curve was used to define the elasto-plastic description of the material. The plastic deformations were obtained by adopting a multi-linear kinematic hardening rule for the material. The FE model notch geometries were illustrated in Fig.(3.5). In order to decrease the computational time for the FE, three zones of meshing were formed on the geometry as shown in Fig.(3.6): 1. Coarse meshing zone, 2. Fine meshing zone, between the coarse and the very fine region. and 3. Very fine mesh, which was applied in the notch region. To obtain a reliable local stress-strain response at the notch zone, the geometry mesh density was gradually refined until the profile of the determined linear-elastic stress fields were not affected by the mesh density as illustrated in Fig.(3.7). This resulted in elements of the critical zone having dimensions equal to 0.025 mm. To allow the material in the fatigue process zone to reach a stabilised configuration, six virtual cycles were run in the FE model for each investigated constant amplitude level. The numerical results are presented and discussed in detail in Chapter (6).

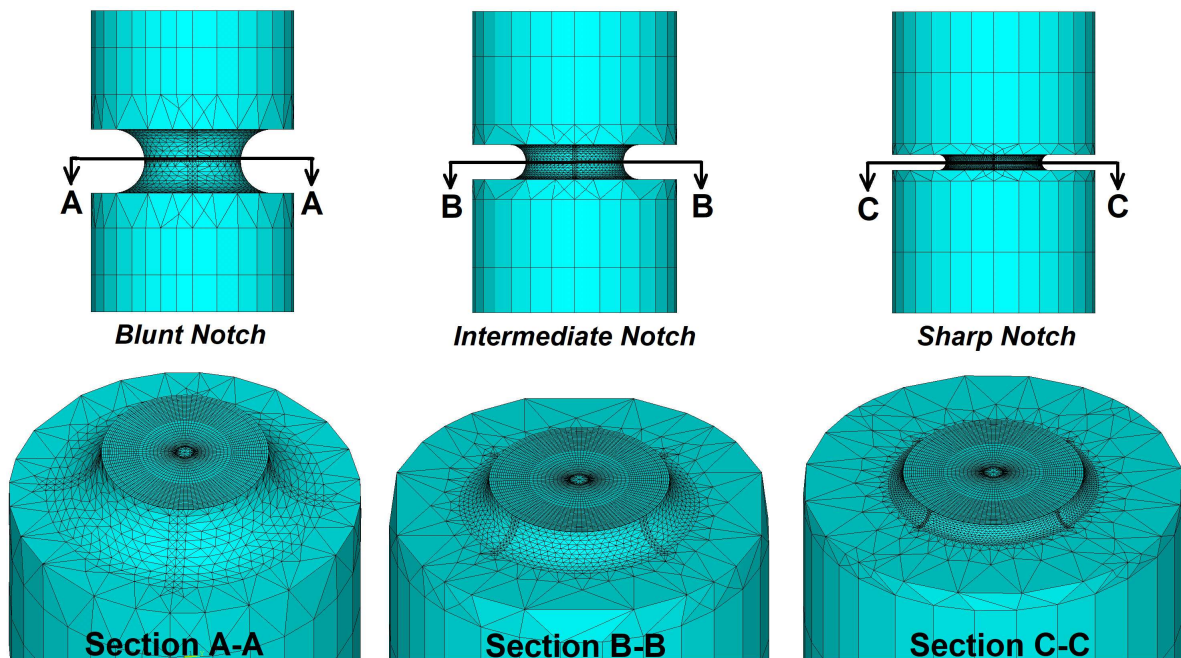


Figure 3.5: Three-Dimensional FE Model Solved by Using ANSYS®-Mechanical APDL

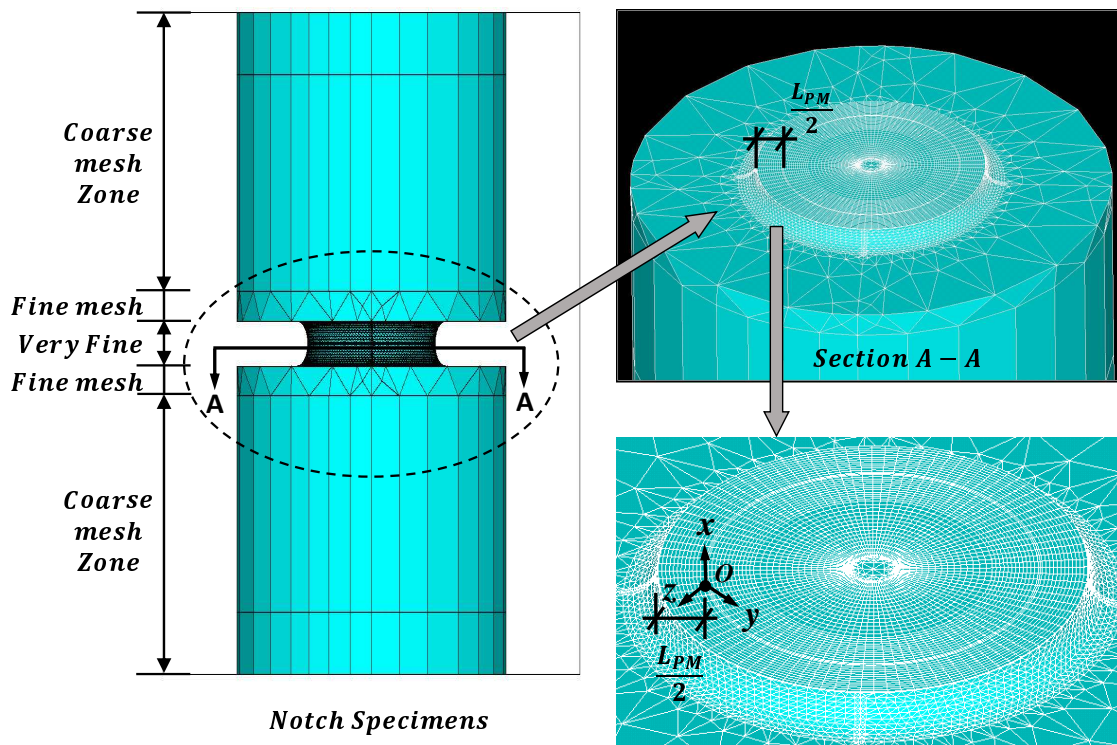


Figure 3.6: Local Stress-Strain State at a Critical Point in Notch sample

3.5 The Maximum Variance Method (MVM)

Once the critical distance was known and the corresponding stress-strain response is plotted at the critical point from the notch tip using the 3D FE model, attention was subsequently focused on the determination of the material plane in which the fatigue damage reaches its maximum value (Critical Plane). As discussed in the last chapter, many different techniques and methods have been investigated and systematically validated to find the critical plane. Among these, the maximum variance method was validated as capable of being successfully applied to determine the critical plane in terms of stress (Susmel et al. 2009) and (Susmel 2014). Thus, the MVM provides an excellent starting point to classify the potential critical plane among the infinite planes that pass through a critical point inside a material, and then finding the exact orientation of the critical plane. In order to apply the Modified Manson-Coffin Curve to evaluate multiaxial fatigue, in this research, the maximum variance method in terms of stress was re-formulated so as to allow the orientation of a material plane experiencing the maximum variation of the shear strain to be determined when a point inside a component is damaged by fatigue. In more detail, to obtain a solution, the post-processing steps of MVM that were formalised inside a well-organised algorithm by Susmel (2010) were re-formulated in terms of strain, as presented in the flowchart of Fig.(3.8). This contained two main steps: First step, determine the potential critical planes by examining all orientation angles with a specific interval (every $\frac{\pi}{12}^\circ$ was recommended in the literature). Then: Second step, perform the optimisation process by applying the Gradient Ascent Method to find the exact critical plane. From the complexity of the input load history, and according to the literature, amongst all the potential critical planes, there always exist only two planes that experience the

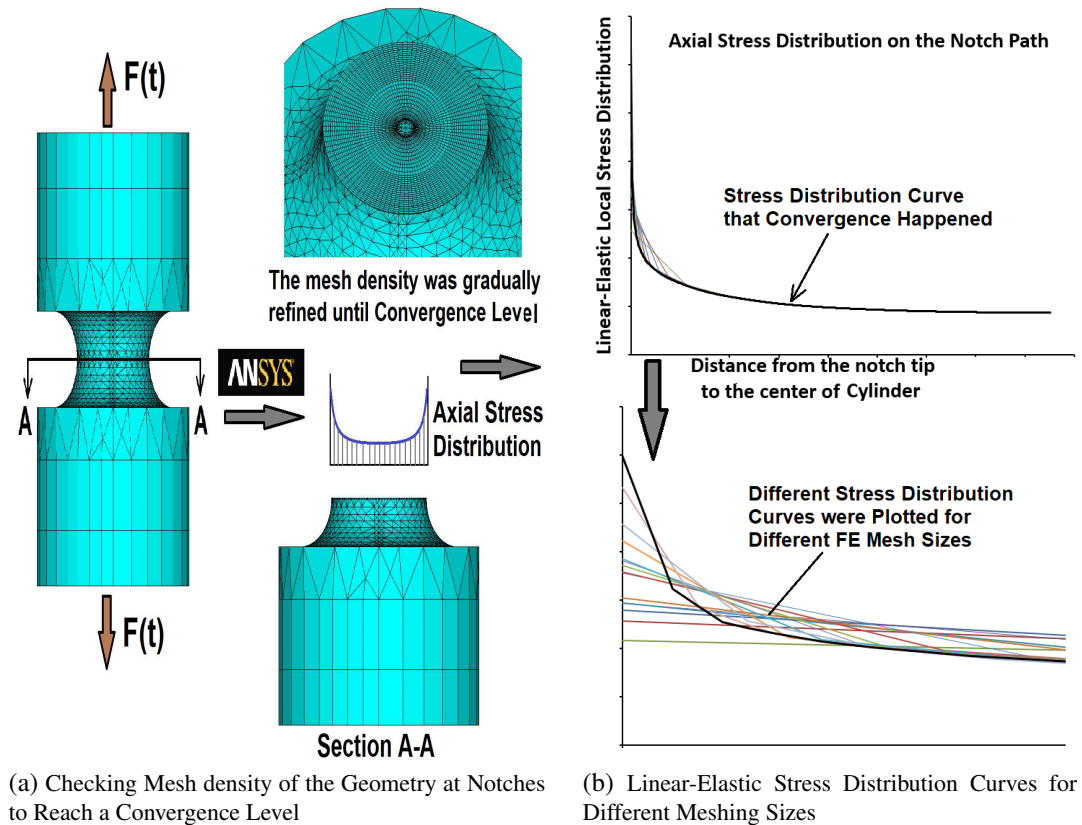


Figure 3.7: Finding the Element Size of FE Model at Notches to Get a Convergence Level

maximum shear strain amplitude. Once the orientation of the critical plane was determined, the developed normal and shear stress/strain amplitudes with the normal mean stresses relative to the critical plane needed to be calculated. Both maximum shear strain amplitude γ_{max} and normal stress σ_n on the critical plane were employed as two basic and significant parameters for fatigue damage (Susmel 2010). From a mathematical point of view, the re-formulated strain-based algorithm required numerical computer software to solve the complex equations. The re-formulated algorithm was therefore successfully re-written into a computer language script by using MATLAB software that is freely available for academic use of Sheffield University. Then, the developed Matlab code was validated by using data from other literature (Wang & Susmel 2016). After determining orientation of the critical plane, the next step was quantifying the mean and amplitude stress/strain relative to the critical plane. The fundamental concept and mathematical re-formalisation of the algorithm, including the Matlab code are provided in the next subsection and (Appendix-A).

3.5.1 Re-Formalisation of the Maximum Variance Method MVM in Terms of Strain ($\gamma - MVM$)

This section re-formulates the stress-based algorithm developed in the published literature of Susmel (2010) to a strain-based formalisation by replacing the stress vectors of (σ and τ) with the strain components of (ϵ and γ) respectively, while considering the effect of the Poisson ratio (ν) and a triaxial local strains even if the nominal stress/strain is uniaxial. For the purpose of re-

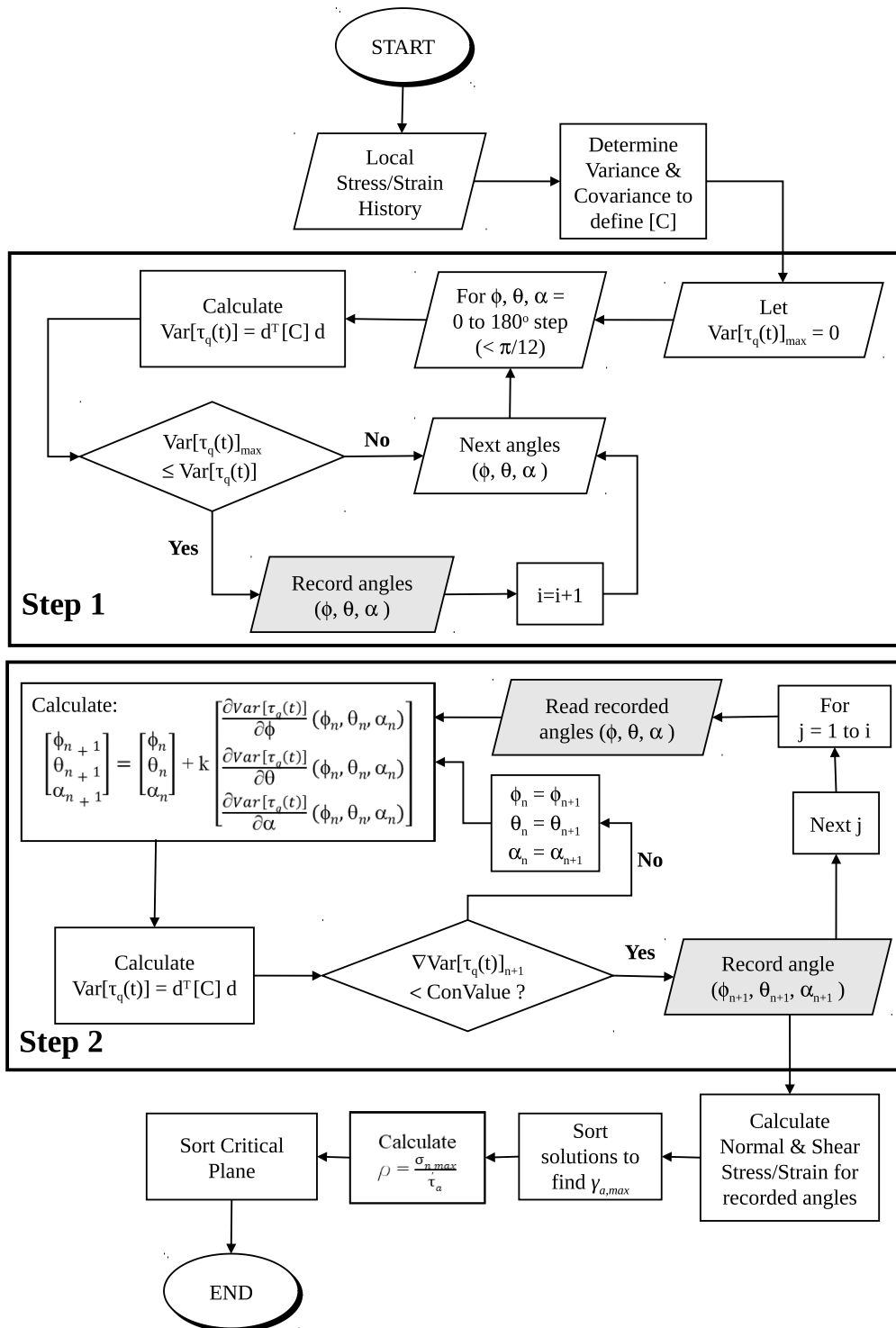


Figure 3.8: Flow Chart presenting algorithm to determine Orientation of the Critical Plane by using the Maximum Variance Method

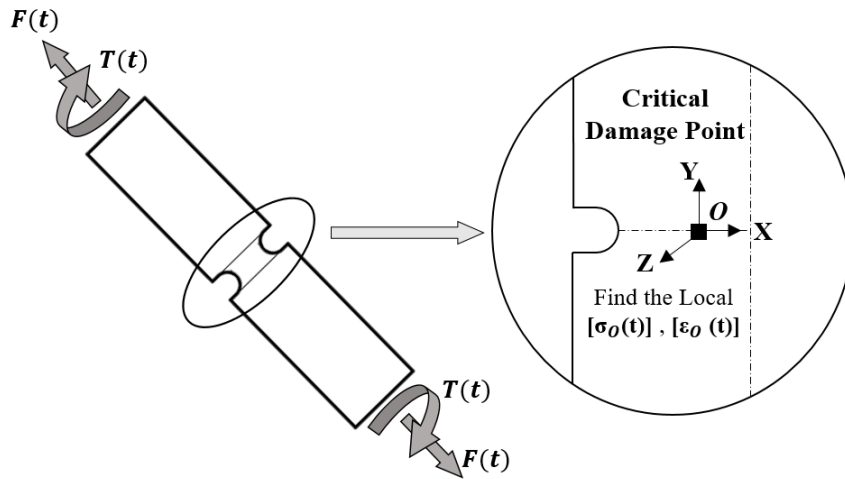


Figure 3.9: Notch Geometry Subjected to Combined Tension and Torsion

formalisation, assume a notch geometry presented in Fig.(3.9), subjected to a complex system of external force and moment resulting in local triaxial stress/strain histories. Let us consider point O inside the geometry as the most critical location to initiate a crack and the same point was taken as a centre of coordinate reference O_{xyz} . The stress-strain states of the aforementioned point are defined by six stress and six strain components as described in Eqns (3.2):

$$[\sigma_o(t)] = \begin{bmatrix} \sigma_x(t) & \tau_{xy}(t) & \tau_{xz}(t) \\ \tau_{xy}(t) & \sigma_y(t) & \tau_{yz}(t) \\ \tau_{xz}(t) & \tau_{yz}(t) & \sigma_z(t) \end{bmatrix} \quad [\varepsilon_o(t)] = \begin{bmatrix} \varepsilon_x(t) & \frac{\gamma_{xy}(t)}{2} & \frac{\gamma_{xz}(t)}{2} \\ \frac{\gamma_{xy}(t)}{2} & \varepsilon_y(t) & \frac{\gamma_{yz}(t)}{2} \\ \frac{\gamma_{xz}(t)}{2} & \frac{\gamma_{yz}(t)}{2} & \varepsilon_z(t) \end{bmatrix} \quad (3.2)$$

Where, $\sigma_x(t)$, $\sigma_y(t)$ & $\sigma_z(t)$ represent the normal stress components. $\varepsilon_x(t)$, $\varepsilon_y(t)$ & $\varepsilon_z(t)$ are the normal strain components. $\tau_{xy}(t)$, $\tau_{xz}(t)$ & $\tau_{yz}(t)$ are the shear stress components and $\gamma_{xy}(t)$, $\gamma_{xz}(t)$ & $\gamma_{yz}(t)$ are the shear strain components.

The strain vectors of, $\varepsilon_x(t)$, $\varepsilon_y(t)$ & $\varepsilon_z(t)$ are related to the stresses $\sigma_x(t)$, $\sigma_y(t)$ & $\sigma_z(t)$ respectively. Half of the shear strains $\gamma_{xy}(t)$, $\gamma_{xz}(t)$ & $\gamma_{yz}(t)$, however, are analogous to the shear stress vectors, $\tau_{xy}(t)$, $\tau_{xz}(t)$ & $\tau_{yz}(t)$ because each side of the cube holds half of the total shear strain value.

If Δ is assumed to be a material plane and \mathbf{n} is a normal unit vector on that plane. Angles ϕ , θ and α are used to define the orientation of plane Δ . According to the above schematisation, ϕ is the angle between the projection unit vector \mathbf{n} on the xy-plane. θ is the angle between the unit vector \mathbf{n} and the z-axis. Now a local axis needs to be defined at point O , which is called O_{anb} . An angle α is the angle between the direction \mathbf{q} and the a-axis (Susmel 2010).

$$n = \begin{bmatrix} n_x \\ n_y \\ n_z \end{bmatrix} = \begin{bmatrix} \sin(\theta)\cos(\phi) \\ \sin(\theta)\sin(\phi) \\ \cos(\theta) \end{bmatrix} \quad (3.3a)$$

$$q = \begin{bmatrix} q_x \\ q_y \\ q_z \end{bmatrix} = \begin{bmatrix} \cos(\alpha)\sin(\phi) + \sin(\alpha)\cos(\theta)\cos(\phi) \\ -\cos(\alpha)\cos(\phi) + \sin(\alpha)\cos(\theta)\sin(\phi) \\ -\sin(\alpha)\sin(\theta) \end{bmatrix} \quad (3.3b)$$

The corresponding normal stress/strain $\sigma_n(t)$, $\varepsilon_n(t)$ relative to the Δ plane, and shear stress/strain $\tau_q(t)$, $\gamma_q(t)$, resolved along direction \mathbf{q} , can be determined directly by the following equations (Wang & Susmel 2016).

- Normal Stress and Strain on Δ plane:

$$\sigma_n(t) = \begin{bmatrix} n_x & n_y & n_z \end{bmatrix} \begin{bmatrix} \sigma_x(t) & \tau_{xy}(t) & \tau_{xz}(t) \\ \tau_{xy}(t) & \sigma_y(t) & \tau_{yz}(t) \\ \tau_{xz}(t) & \tau_{yz}(t) & \sigma_z(t) \end{bmatrix} \begin{bmatrix} n_x \\ n_y \\ n_z \end{bmatrix} \quad (3.4)$$

$$\varepsilon_n(t) = \begin{bmatrix} n_x & n_y & n_z \end{bmatrix} \begin{bmatrix} \varepsilon_x(t) & \frac{\gamma_{xy}(t)}{2} & \frac{\gamma_{xz}(t)}{2} \\ \frac{\gamma_{xy}(t)}{2} & \varepsilon_y(t) & \frac{\gamma_{yz}(t)}{2} \\ \frac{\gamma_{xz}(t)}{2} & \frac{\gamma_{yz}(t)}{2} & \varepsilon_z(t) \end{bmatrix} \begin{bmatrix} n_x \\ n_y \\ n_z \end{bmatrix} \quad (3.5)$$

- Shear Stress and Strain amplitude resolved along direction \mathbf{q} :

$$\tau_q(t) = \begin{bmatrix} q_x & q_y & q_z \end{bmatrix} \begin{bmatrix} \sigma_x(t) & \tau_{xy}(t) & \tau_{xz}(t) \\ \tau_{xy}(t) & \sigma_y(t) & \tau_{yz}(t) \\ \tau_{xz}(t) & \tau_{yz}(t) & \sigma_z(t) \end{bmatrix} \begin{bmatrix} n_x \\ n_y \\ n_z \end{bmatrix} \quad (3.6)$$

$$\frac{\gamma_q(t)}{2} = \begin{bmatrix} q_x & q_y & q_z \end{bmatrix} \begin{bmatrix} \varepsilon_x(t) & \frac{\gamma_{xy}(t)}{2} & \frac{\gamma_{xz}(t)}{2} \\ \frac{\gamma_{xy}(t)}{2} & \varepsilon_y(t) & \frac{\gamma_{yz}(t)}{2} \\ \frac{\gamma_{xz}(t)}{2} & \frac{\gamma_{yz}(t)}{2} & \varepsilon_z(t) \end{bmatrix} \begin{bmatrix} n_x \\ n_y \\ n_z \end{bmatrix} \quad (3.7)$$

If (i=x,y,z), from the stress/strain state of equations (3.2), $\sigma_i(t)$ and $\varepsilon_i(t)$ are the normal stress and

strain components, whereas if (i,j=x,y,z), $\tau_{ij}(t)$ and $\gamma_{ij}(t)$ are the shear stress and strain components.

The variance of a shear strain $\gamma_q(t)$, resolved along direction \mathbf{q} can be calculated directly from the equations below (Susmel 2010):

$$Var [\gamma_q(t)] = d^T [C] d \quad (3.8)$$

where $Var [\gamma_q(t)]$ is the variance of the shear strain resolved along the direction of variance of $\gamma_q(t)$. d is the vector of direction cosines.

According to the equation (3.2), the time variable local strain states of $\varepsilon_i(t)$ and $\varepsilon_j(t)$ were defined over time interval $[0, T]$ and have mean strains equal to $\varepsilon_{i,m}$ and $\varepsilon_{j,m}$. The variance of $\varepsilon_i(t)$ and $\varepsilon_j(t)$ can be determined mathematically by the following equations:

$$Var [\varepsilon_i(t)] = \frac{1}{T} \int_0^T [\varepsilon_i(t) - \varepsilon_{i,m}]^2 dt \quad (3.9)$$

$$Var [\varepsilon_j(t)] = \frac{1}{T} \int_0^T [\varepsilon_j(t) - \varepsilon_{j,m}]^2 dt \quad (3.10)$$

whereas the covariance between $\varepsilon_i(t)$ and $\varepsilon_j(t)$ can be defined according to the following covariance equation:

$$CoVar [\varepsilon_i(t), \varepsilon_j(t)] = \frac{1}{T} \int_0^T [\varepsilon_i(t) - \varepsilon_{i,m}] \cdot [\varepsilon_j(t) - \varepsilon_{j,m}] dt \quad (3.11)$$

The defined equation (3.8) takes full advantage of the mathematical fact that, according to the equations (3.9) and (3.10), if $i=j$ then the $Cov [s_i(t), s_j(t)] = Var [s_i(t)]$. Consequently, the square $[C]$ matrix can be written according to the following form:

$$[C] = \begin{bmatrix} V_x & C_{x,y} & C_{x,z} & C_{x,xy} & C_{x,xz} & C_{x,yz} \\ C_{x,y} & V_y & C_{y,z} & C_{y,xy} & C_{y,xz} & C_{y,yz} \\ C_{x,z} & C_{y,z} & V_z & C_{z,xy} & C_{z,xz} & C_{z,yz} \\ C_{x,xy} & C_{y,xy} & C_{z,xy} & V_{xy} & C_{xy,xz} & C_{xy,yz} \\ C_{x,xz} & C_{y,xz} & C_{z,xz} & C_{xy,xz} & V_{xz} & C_{xz,yz} \\ C_{x,yz} & C_{y,yz} & C_{z,yz} & C_{xy,yz} & C_{xy,yz} & V_{yz} \end{bmatrix} \quad (3.12)$$

Every cell of $[C]$ matrix can be determined by using the following definitions. Let assume (i,j=x,y,z):

$$V_i = Var [\varepsilon_i(t)] \quad (3.13a)$$

$$V_i = Var \left[\frac{\gamma_{ij}(t)}{2} \right] \quad (3.13b)$$

$$C_{i,j} = CoVar [\varepsilon_i(t), \varepsilon_j(t)] \quad (3.13c)$$

$$C_{i,j,i} = CoVar \left[\frac{\gamma_{ij}(t)}{2}, \varepsilon_i(t) \right] \quad (3.13d)$$

$$C_{i,i,j} = CoVar \left[\varepsilon_i(t), \frac{\gamma_{ij}(t)}{2} \right] \quad (3.13e)$$

$$C_{i,j,i,j} = CoVar \left[\frac{\gamma_{ij}(t)}{2}, \frac{\gamma_{ij}(t)}{2} \right] \quad (3.13f)$$

Now equation (3.8) can be rewritten in a simplest form:

$$Var \left[\frac{\gamma_q(t)}{2} \right] = d^T [C] d \quad (3.14)$$

The equation (3.14) can be presented in terms of M :

$$Var \left[\frac{\gamma_q(t)}{2} \right] = \sum_{i=1}^6 d_i M_i \quad (3.15)$$

Vector of direction cosines \mathbf{d} were expressed by using angles ϕ , θ and α (Susmel 2010):

$$d = \begin{bmatrix} d_1 \\ d_2 \\ d_3 \\ d_4 \\ d_5 \\ d_6 \end{bmatrix} = \begin{bmatrix} \frac{1}{2} [\sin(\theta)\sin(2\phi)\cos(\alpha) + \sin(\alpha)\sin(2\theta)\cos(\phi)^2] \\ \frac{1}{2} [-\sin(\theta)\sin(2\phi)\cos(\alpha) + \sin(\alpha)\sin(2\theta)\sin(\phi)^2] \\ -\frac{1}{2}\sin(\alpha)\sin(2\theta) \\ \frac{1}{2}\sin(\alpha)\sin(2\phi)\sin(2\theta) - \cos(\alpha)\cos(2\phi)\sin(\theta) \\ \sin(\alpha)\cos(\phi)\cos(2\theta) + \cos(\alpha)\sin(\phi)\cos(\theta) \\ \sin(\alpha)\sin(\phi)\cos(2\theta) - \cos(\alpha)\cos(\phi)\cos(\theta) \end{bmatrix} \quad (3.16)$$

Consequently, by using the equation (3.14), the directions experiencing maximum variance of the resolved shear strain are determined.

Numerical calculation to determine the direction experiencing the maximum shear strain amplitudes:

To identify the orientation of a critical plane correctly, and despite the relative abundance of multi-variable optimisation methods, it has been confirmed that the *Gradient Ascent Method* is a satisfactory optimisation technique to obtain the correct orientation of the critical plane (Susmel 2010). According to the Gradient Ascent Method, the iterative process used to reach convergence can be determined as follows:

$$\begin{bmatrix} \phi_{n+1} \\ \theta_{n+1} \\ \alpha_{n+1} \end{bmatrix} = \begin{bmatrix} \phi_n \\ \theta_n \\ \alpha_n \end{bmatrix} + k \begin{bmatrix} \frac{\partial Var[\gamma_q(t)]}{\partial \phi}(\phi_n, \theta_n, \alpha_n) \\ \frac{\partial Var[\gamma_q(t)]}{\partial \theta}(\phi_n, \theta_n, \alpha_n) \\ \frac{\partial Var[\gamma_q(t)]}{\partial \alpha}(\phi_n, \theta_n, \alpha_n) \end{bmatrix} \quad (3.17)$$

n is the solution determined at n^{th} step. $n+1$ is the subsequent step in the direction proportional to the gradient of function $Var[\gamma_q(t)]$. k is a number small enough, but greater than zero, to help the iteration process to convergence. A systematic examination of different types of load histories illustrated that accurate results can be obtained by using the $k < 10^{-6}$ and angle steps smaller than $\frac{\pi}{12}$.

$$\frac{\partial Var[\gamma_q(t)]}{\partial \phi} = \sum_{i=1}^6 \left(\frac{\partial d_i}{\partial \phi} M_i + \frac{\partial M_i}{\partial \phi} d_i \right) \quad (3.18)$$

$$\frac{\partial Var[\gamma_q(t)]}{\partial \theta} = \sum_{i=1}^6 \left(\frac{\partial d_i}{\partial \theta} M_i + \frac{\partial M_i}{\partial \theta} d_i \right) \quad (3.19)$$

$$\frac{\partial Var[\gamma_q(t)]}{\partial \alpha} = \sum_{i=1}^6 \left(\frac{\partial d_i}{\partial \alpha} M_i + \frac{\partial M_i}{\partial \alpha} d_i \right) \quad (3.20)$$

$$\frac{\partial [M]}{\partial \phi} = \begin{bmatrix} \frac{\partial M_1}{\partial \phi} \\ \frac{\partial M_2}{\partial \phi} \\ \frac{\partial M_3}{\partial \phi} \\ \frac{\partial M_4}{\partial \phi} \\ \frac{\partial M_5}{\partial \phi} \\ \frac{\partial M_6}{\partial \phi} \end{bmatrix} = \begin{bmatrix} V_x & C_{x,y} & C_{x,z} & C_{x,xy} & C_{x,xz} & C_{x,yz} \\ C_{x,y} & V_y & C_{y,z} & C_{y,xy} & C_{y,xz} & C_{y,yz} \\ C_{x,z} & C_{y,z} & V_z & C_{z,xy} & C_{z,xz} & C_{z,yz} \\ C_{x,xy} & C_{y,xy} & C_{z,xy} & V_{xy} & C_{xy,xz} & C_{xy,yz} \\ C_{x,xz} & C_{y,xz} & C_{z,xz} & C_{xy,xz} & V_{xz} & C_{xz,yz} \\ C_{x,yz} & C_{y,yz} & C_{z,yz} & C_{xy,yz} & C_{xy,yz} & V_{yz} \end{bmatrix} \begin{bmatrix} \frac{\partial d_1}{\partial \phi} \\ \frac{\partial d_2}{\partial \phi} \\ \frac{\partial d_3}{\partial \phi} \\ \frac{\partial d_4}{\partial \phi} \\ \frac{\partial d_5}{\partial \phi} \\ \frac{\partial d_6}{\partial \phi} \end{bmatrix} \quad (3.21)$$

$$\frac{\partial [M]}{\partial \theta} = \begin{bmatrix} \frac{\partial M_1}{\partial \theta} \\ \frac{\partial M_2}{\partial \theta} \\ \frac{\partial M_3}{\partial \theta} \\ \frac{\partial M_4}{\partial \theta} \\ \frac{\partial M_5}{\partial \theta} \\ \frac{\partial M_6}{\partial \theta} \end{bmatrix} = \begin{bmatrix} V_x & C_{x,y} & C_{x,z} & C_{x,xy} & C_{x,xz} & C_{x,yz} \\ C_{x,y} & V_y & C_{y,z} & C_{y,xy} & C_{y,xz} & C_{y,yz} \\ C_{x,z} & C_{y,z} & V_z & C_{z,xy} & C_{z,xz} & C_{z,yz} \\ C_{x,xy} & C_{y,xy} & C_{z,xy} & V_{xy} & C_{xy,xz} & C_{xy,yz} \\ C_{x,xz} & C_{y,xz} & C_{z,xz} & C_{xy,xz} & V_{xz} & C_{xz,yz} \\ C_{x,yz} & C_{y,yz} & C_{z,yz} & C_{xy,yz} & C_{xy,yz} & V_{yz} \end{bmatrix} \begin{bmatrix} \frac{\partial d_1}{\partial \theta} \\ \frac{\partial d_2}{\partial \theta} \\ \frac{\partial d_3}{\partial \theta} \\ \frac{\partial d_4}{\partial \theta} \\ \frac{\partial d_5}{\partial \theta} \\ \frac{\partial d_6}{\partial \theta} \end{bmatrix} \quad (3.22)$$

$$\frac{\partial[M]}{\partial\alpha} = \begin{bmatrix} \frac{\partial M_1}{\partial\alpha} \\ \frac{\partial M_2}{\partial\alpha} \\ \frac{\partial M_3}{\partial\alpha} \\ \frac{\partial M_4}{\partial\alpha} \\ \frac{\partial M_5}{\partial\alpha} \\ \frac{\partial M_6}{\partial\alpha} \end{bmatrix} = \begin{bmatrix} V_x & C_{x,y} & C_{x,z} & C_{x,xy} & C_{x,xz} & C_{x,yz} \\ C_{x,y} & V_y & C_{y,z} & C_{y,xy} & C_{y,xz} & C_{y,yz} \\ C_{x,z} & C_{y,z} & V_z & C_{z,xy} & C_{z,xz} & C_{z,yz} \\ C_{x,xy} & C_{y,xy} & C_{z,xy} & V_{xy} & C_{xy,xz} & C_{xy,yz} \\ C_{x,xz} & C_{y,xz} & C_{z,xz} & C_{xy,xz} & V_{xz} & C_{xz,yz} \\ C_{x,yz} & C_{y,yz} & C_{z,yz} & C_{xy,yz} & C_{xy,yz} & V_{yz} \end{bmatrix} \begin{bmatrix} \frac{\partial d_1}{\partial\alpha} \\ \frac{\partial d_2}{\partial\alpha} \\ \frac{\partial d_3}{\partial\alpha} \\ \frac{\partial d_4}{\partial\alpha} \\ \frac{\partial d_5}{\partial\alpha} \\ \frac{\partial d_6}{\partial\alpha} \end{bmatrix} \quad (3.23)$$

$$\frac{\partial d_1}{\partial\alpha} = \frac{1}{2}(-\sin\theta \cdot \sin 2\phi \cdot \sin\alpha + \cos\alpha \cdot \sin 2\theta \cdot \cos^2\phi) \quad (3.24a)$$

$$\frac{\partial d_1}{\partial\theta} = \frac{1}{2}(\cos\theta \cdot \sin 2\phi \cdot \cos\alpha + 2\sin\alpha \cdot \cos 2\theta \cdot \cos^2\phi) \quad (3.24b)$$

$$\frac{\partial d_1}{\partial\phi} = \frac{1}{2}(2\sin\theta \cdot \cos 2\phi \cdot \cos\alpha - 2\sin\alpha \cdot \sin 2\theta \cdot \cos\phi \cdot \sin\phi) \quad (3.24c)$$

$$\frac{\partial d_2}{\partial\alpha} = \frac{1}{2}(\sin\theta \cdot \sin 2\phi \cdot \sin\alpha + \cos\alpha \cdot \sin 2\theta \cdot \sin^2\phi) \quad (3.24d)$$

$$\frac{\partial d_2}{\partial\theta} = \frac{1}{2}(-\cos\theta \cdot \sin 2\phi \cdot \cos\alpha + 2\sin\alpha \cdot \cos 2\theta \cdot \sin^2\phi) \quad (3.24e)$$

$$\frac{\partial d_2}{\partial\phi} = \frac{1}{2}(-2\sin\theta \cdot \cos 2\phi \cdot \cos\alpha + 2\sin\alpha \cdot \sin 2\theta \cdot \sin\phi \cdot \cos\phi) \quad (3.24f)$$

$$\frac{\partial d_3}{\partial\alpha} = -\frac{1}{2}\cos\alpha \cdot \sin 2\theta \quad (3.24g)$$

$$\frac{\partial d_3}{\partial\theta} = -\sin\alpha \cdot \cos 2\theta \quad (3.24h)$$

$$\frac{\partial d_3}{\partial\phi} = 0 \quad (3.24i)$$

$$\frac{\partial d_4}{\partial\alpha} = \frac{1}{2}\cos\alpha \cdot \sin 2\phi \cdot \sin 2\theta + \sin\alpha \cdot \cos 2\phi \cdot \sin\theta \quad (3.24j)$$

$$\frac{\partial d_4}{\partial\theta} = \sin\alpha \cdot \sin 2\phi \cdot \cos 2\theta - \cos\alpha \cdot \cos 2\phi \cdot \cos\theta \quad (3.24k)$$

$$\frac{\partial d_4}{\partial\phi} = \sin\alpha \cdot \cos 2\phi \cdot \sin 2\theta + 2\cos\alpha \cdot \sin 2\phi \cdot \sin\theta \quad (3.24l)$$

$$\frac{\partial d_5}{\partial\alpha} = \cos\alpha \cdot \cos\phi \cdot \cos 2\theta - \sin\alpha \cdot \sin\phi \cdot \cos\theta \quad (3.24m)$$

$$\frac{\partial d_5}{\partial\theta} = -2\sin\alpha \cdot \cos\phi \cdot \sin 2\theta - \cos\alpha \cdot \sin\phi \cdot \sin\theta \quad (3.24n)$$

$$\frac{\partial d_5}{\partial\phi} = -\sin\alpha \cdot \sin\phi \cdot \cos 2\theta + \cos\alpha \cdot \cos\phi \cdot \cos\theta \quad (3.24o)$$

$$\frac{\partial d_6}{\partial\alpha} = \cos\alpha \cdot \sin\phi \cdot \cos 2\theta + \sin\alpha \cdot \cos\phi \cdot \cos\theta \quad (3.24p)$$

$$\frac{\partial d_6}{\partial\theta} = -2\sin\alpha \cdot \sin\phi \cdot \sin 2\theta + \cos\alpha \cdot \cos\phi \cdot \sin\theta \quad (3.24q)$$

$$\frac{\partial d_6}{\partial\phi} = \sin\alpha \cdot \cos\phi \cdot \cos 2\theta + \cos\alpha \cdot \sin\phi \cdot \cos\theta \quad (3.24r)$$

Once the orientation of the critical plane is known, the next step is finding normal and shear

stress/strain amplitudes on the critical plane. The mean and amplitude value of the shear stress and shear strain component on the critical plane can directly be calculated as follow:

1. In case of Constant Amplitude C.A Cyclic Loading:

$$\gamma_a = \frac{1}{2}(\gamma_{MV,max} - \gamma_{MV,min}) \quad (3.25)$$

$$\gamma_m = \frac{1}{2}(\gamma_{MV,max} + \gamma_{MV,min}) \quad (3.26)$$

Where, γ_a and γ_m are the shear strain amplitude and mean shear strain on the critical plane, respectively. $\gamma_{MV,max}$ and $\gamma_{MV,min}$ are the maximum and minimum value of shear strain, resolved along the direction of maximum variance.

$$\tau_a = \frac{1}{2}(\tau_{MV,max} - \tau_{MV,min}) \quad (3.27)$$

$$\tau_m = \frac{1}{2}(\tau_{MV,max} + \tau_{MV,min}) \quad (3.28)$$

$\tau_{a,max}$ and τ_m are the maximum amplitude and mean of shear stresses relative to the critical plane. $\tau_{MV,max}$ and $\tau_{MV,min}$ are the maximum and minimum shear stresses, resolved along the direction of maximum variance, respectively.

$$\sigma_{n,a} = \frac{1}{2}(\sigma_{n,max} - \sigma_{n,min}) \quad (3.29)$$

$$\sigma_{n,m} = \frac{1}{2}(\sigma_{n,max} + \sigma_{n,min}) \quad (3.30)$$

$\sigma_{n,a}$ and $\sigma_{n,m}$ are the normal stress amplitude and mean stress perpendicular to the critical plane. $\sigma_{n,max}$ and $\sigma_{n,min}$ are the maximum and minimum normal stresses, respectively.

2. In case of Variable Amplitude V.A Cyclic Loading:

$$\gamma_m = \frac{1}{T} \int_0^T \gamma_{MV}(t) dt \quad (3.31a)$$

$$Var [\gamma_{MV}(t)] = \frac{1}{T} \int_0^T [\gamma_{MV}(t) - \gamma_m]^2 dt \quad (3.31b)$$

$$\tau_m = \frac{1}{T} \int_0^T \tau_{MV}(t) dt \quad (3.32a)$$

$$Var [\tau_{MV}(t)] = \frac{1}{T} \int_0^T [\tau_{MV}(t) - \tau_m]^2 dt \quad (3.32b)$$

The equivalent shear strain and shear stress amplitudes can directly be determined by using the above resolved maximum variance terms of the shear stress/strain according to the following definitions:

$$\gamma_a = \sqrt{2 \cdot Var[\gamma_{MV}(t)]_{max}} \quad (3.33)$$

$$\tau_a = \sqrt{2 \cdot Var[\tau_{MV}(t)]_{max}} \quad (3.34)$$

In a similar way, the equivalent normal stress amplitudes and mean stresses perpendicular to the critical plane can be determined by using the following relationship:

$$\sigma_{n,m} = \frac{1}{T} \int_0^T \sigma_n(t) dt \quad (3.35a)$$

$$Var [\sigma_n(t)] = \frac{1}{T} \int_0^T [\sigma_n(t) - \sigma_{n,m}]^2 dt \quad (3.35b)$$

$$\sigma_{n,a} = \sqrt{2 \cdot Var[\sigma_n(t)]_{max}} \quad (3.36)$$

3.6 The Modified Manson-Coffin Curve Method

The last step in the formalisation of the developed method was defining a standard approach to evaluate the fatigue lifetime of metallic notch components under in-service cyclic loading with both constant and variable amplitudes. The pioneering model of the so-called Modified Manson-Coffin Curve Method (MMCCM) that was developed/modified by Susmel (2009) was used. This approach was proposed as the best technique to predict low/medium-cycle fatigue damage of a component when plastic deformation is involved. A proper modification of MMCCM helps the developed model take into account the influence of mean stress and degree of nonproportionality of the cyclic load. The application of the Modified Manson-Coffin Curve in terms of the applied cyclic load can be classified into two forms:

3.6.1 Constant Amplitude C.A Cyclic Loading

Once the orientation of the critical plane was determined and the direction experiencing the maximum variance of the resolved shear strain was calculated (shown in subsection 3.5.1), then all the developed normal and shear stress/strain values on the critical plane can be found by using the following equations:

$$\gamma_{a,max} = \frac{1}{2}(\gamma_{MV,max} - \gamma_{MV,min}) \quad (3.37)$$

$$\gamma_m = \frac{1}{2}(\gamma_{MV,max} + \gamma_{MV,min}) \quad (3.38)$$

Where, γ_a and γ_m are the maximum shear strain amplitude, and mean shear strain on the critical plane, respectively. $\gamma_{MV,max}$ and $\gamma_{MV,min}$ are the maximum and minimum value of shear strain resolved along the direction of maximum variance.

$$\tau_a = \frac{1}{2}(\tau_{MV,max} - \tau_{MV,min}) \quad (3.39)$$

$$\tau_m = \frac{1}{2}(\tau_{MV,max} + \tau_{MV,min}) \quad (3.40)$$

$\tau_{a,max}$ and τ_m can be defined as the maximum shear stress amplitude and mean shear stress relative to the critical plane. $\tau_{MV,max}$ and $\tau_{MV,min}$ are the maximum and minimum resolved shear stresses along the direction of maximum variance, respectively.

$$\sigma_{n,a} = \frac{1}{2}(\sigma_{n,max} - \sigma_{n,min}) \quad (3.41)$$

$$\sigma_{n,m} = \frac{1}{2}(\sigma_{n,max} + \sigma_{n,min}) \quad (3.42)$$

$\sigma_{n,a}$ and $\sigma_{n,m}$ are the normal stress amplitude and mean stress perpendicular to the critical plane. $\sigma_{n,max}$ and $\sigma_{n,min}$ are the maximum and minimum normal stresses, respectively.

According to the Modified Manson-Coffin Curve, the above calculated normal/shear stress quantities allow the stress ratio (stress index) ρ in Eqn.(3.43) to be determined to calibrate the Manson-Coffin Curve (Susmel (2009)).

$$\rho = \frac{\sigma_{n,a} + \sigma_{n,m}}{\tau_a} = \frac{\sigma_{n,max}}{\tau_a} \quad (3.43)$$

Finally, the calculated maximum shear strain amplitude in Eqn.(3.37) on the critical plane, γ_a , with the Modified Manson-Coffin curve MMCCM can be used directly to evaluate the fatigue lifetime and estimate the number of cycles to failure, $N_{f,e}$, should the notch geometry be subjected to a constant amplitude fatigue load. All the processes involved in assessing multiaxial fatigue of notch components under constant amplitude cyclic loading are illustrated in Fig.(3.10).

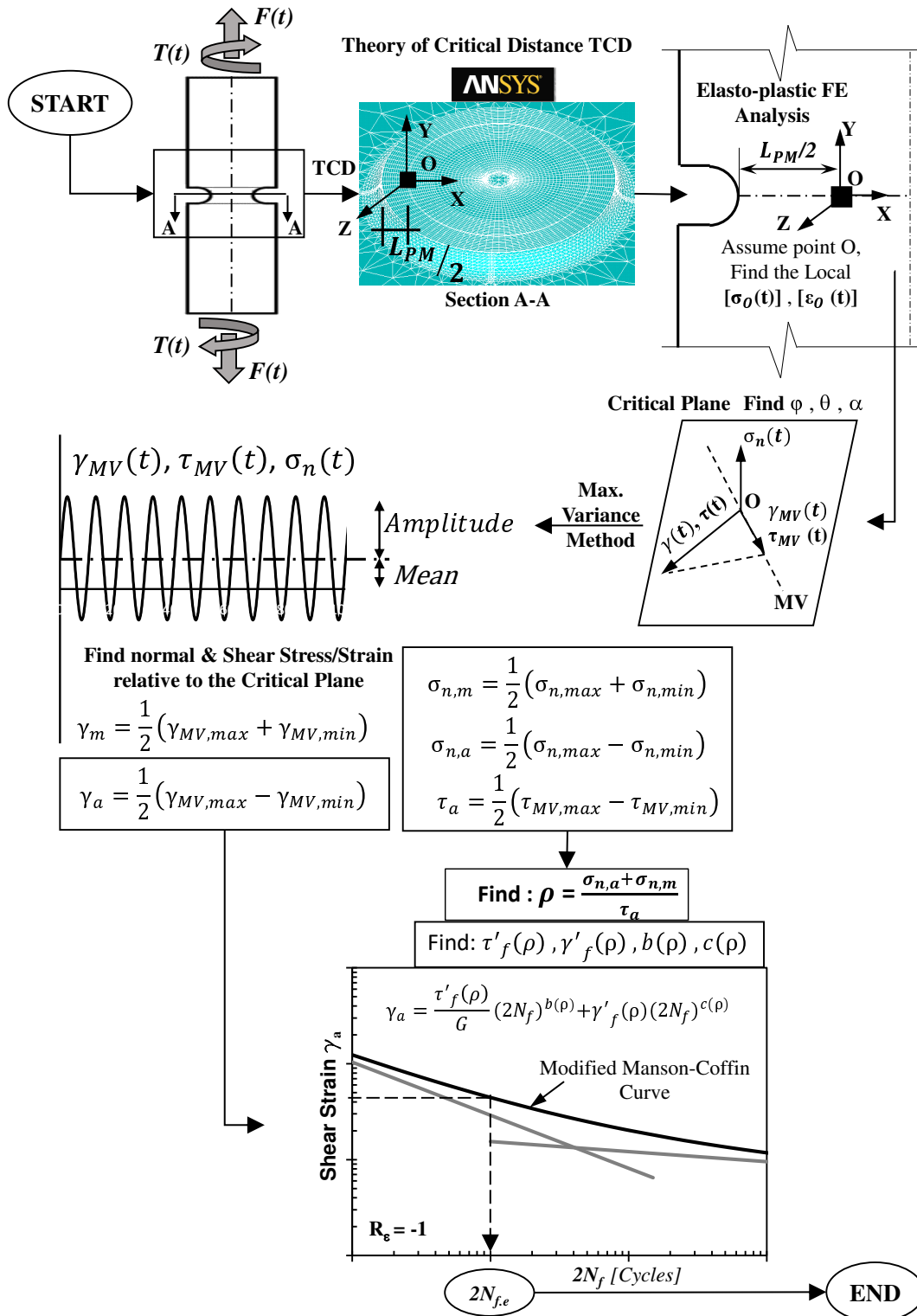


Figure 3.10: Flow Chat: application of the formalised approach under Constant Amplitude C.A. Multiaxial Fatigue Load

3.6.2 Variable Amplitude V.A Cyclic Loading

Fatigue life estimation described in subsection (3.6.1) is applied when the load is constant and its amplitude does not change with time. As mentioned in the last chapter, however, most load-bearing structures and components often undergo a complex variable amplitude multiaxial fatigue load. For this reason, a mathematical form of the developed approach was extended to accommodate variable amplitude loading conditions. Fatigue assessment of random loads is not as easy as that for constant amplitude and not a straightforward action: VA loads need several extra steps/theories that are not required in the CA load cases.

When processing fatigue damage under VA loading, once the local stress/strain states were quantified numerically by using the commercial F.E ANSYS® at a prescribed distance from the notch root. The subsequent step was to determine the corresponding stress/strain magnitudes relative to the critical plane by following the equations below:

$$\gamma_m = \frac{1}{T} \int_0^T \gamma_{MV}(t) dt \quad (3.44a)$$

$$Var [\gamma_{MV}(t)] = \frac{1}{T} \int_0^T [\gamma_{MV}(t) - \gamma_m]^2 dt \quad (3.44b)$$

$$\tau_m = \frac{1}{T} \int_0^T \tau_{MV}(t) dt \quad (3.45a)$$

$$Var [\tau_{MV}(t)] = \frac{1}{T} \int_0^T [\tau_{MV}(t) - \tau_m]^2 dt \quad (3.45b)$$

The equivalent shear strain and shear stress amplitudes can be determined directly by using the above resolved maximum variance terms of the shear stress/strain according to the following equations:

$$\gamma_{a,max} = \sqrt{2 \cdot Var[\gamma_{MV}(t)_{max}]} \quad (3.46)$$

$$\tau_a = \sqrt{2 \cdot Var[\tau_{MV}(t)]} \quad (3.47)$$

In a similar procedure, the equivalent normal stress amplitudes and mean stresses perpendicular to the critical plane can be determined by using the following relationships:

$$\sigma_{n,m} = \frac{1}{T} \int_0^T \sigma_n(t) dt \quad (3.48a)$$

$$Var [\sigma_n(t)] = \frac{1}{T} \int_0^T [\sigma_n(t) - \sigma_{n,m}]^2 dt \quad (3.48b)$$

$$\sigma_{n,a} = \sqrt{2 \cdot \text{Var}[\sigma_n(t)]} \quad (3.49)$$

Once all normal and shear stress/strain amplitudes and mean values were post-processed and determined using the above equations: 1. A cycle counting technique was needed to decrease the complex shear strain history into a series of individual constant amplitudes. 2. Fatigue cumulative damage theory was required to accumulate the fatigue damage of each cycle in the history so as then to be able to determine the overall fatigue lifetime of the notch geometry correctly.

Rainflow Cycle Counting

The most tricky problem behind the definition of variable amplitude fatigue load history is reducing the random shear strain amplitudes into a series of simple constant amplitude cycles. As described in section 2.9, the rainflow cycle counting rule was used to form a series of constant cycles from the random variable amplitude by applying the rain flow rules, as shown in Fig.(2.12). In the proposed strain-based approach, the rainflow cycle counting method applies on the corresponding shear strain history relative to the critical plane in order to evaluate fatigue damage.

In this thesis, Matlab code was used as a numerical calculation tool to perform the rainflow cycle counting method. Simply speaking, the calculated $\gamma_{MV}(t)$ history relative to the critical plane were defined in the form of matrix inside the Matlab code to determine the rainflow counted cycles. The Matlab code rearranges the γ_{MV} signals to start and end with the maximum peak or minimum valley (whichever is greater in absolute value). Then rainflow counting was followed through according to the example presented in Fig.(2.12). The counting procedure continued until all cycles were considered, at which point the program stopped.

Cumulative Fatigue Damage

In variable amplitude fatigue loading, once the rainflow method had classified the variable cycles into individual constant events. Then, according to the Modified Manson-Coffin curve, the number of cycles to failure was determined for each individual CA. According to the literature, the linear cumulative damage content of a time-varies load involving n_i cycles ($i=1, 2, \dots$) can be expressed by using Eqn. 3.50. (Susmel & Taylor 2015 & Mitchell 1996).

$$D_{tot} = \sum_{i=1}^j \frac{n_i}{N_{f,i}} \quad (3.50)$$

Where, D_{tot} is the total cumulative fatigue damage. n_i is the number of cycles at the i -th strain amplitude level. $N_{f,i}$ is the number of cycles to failure at the same strain level.

Once the damage content is known for the investigated material, the number of cycles to failure $N_{f,e}$ can be estimated directly through the equation (3.51).

$$N_{f,e} = \frac{D_{cr}}{D_{tot}} \sum_{i=1}^j n_i \quad (3.51)$$

D_{cr} is the critical value of the damage sum, which is considered to be a particularly tricky problem that always needs to be addressed properly. According to the examination of the state of the art, unfortunately, there is not yet an accepted theory capable of estimating a reliable critical value for the damage sum. Further, such a critical value is seen to be sensitive not only to the geometry, but also as the profile of fatigue load change (Susmel & Taylor 2015). In the most general case, the critical damage, D_{cr} is determined by running appropriate experiments seeking to fit the predicted $N_{f,e}$ and experiment N_f . The entire procedure for evaluating the multiaxial lifetime of notch components against variable amplitude cyclic loadings is presented in the flowchart in Fig.(3.11).

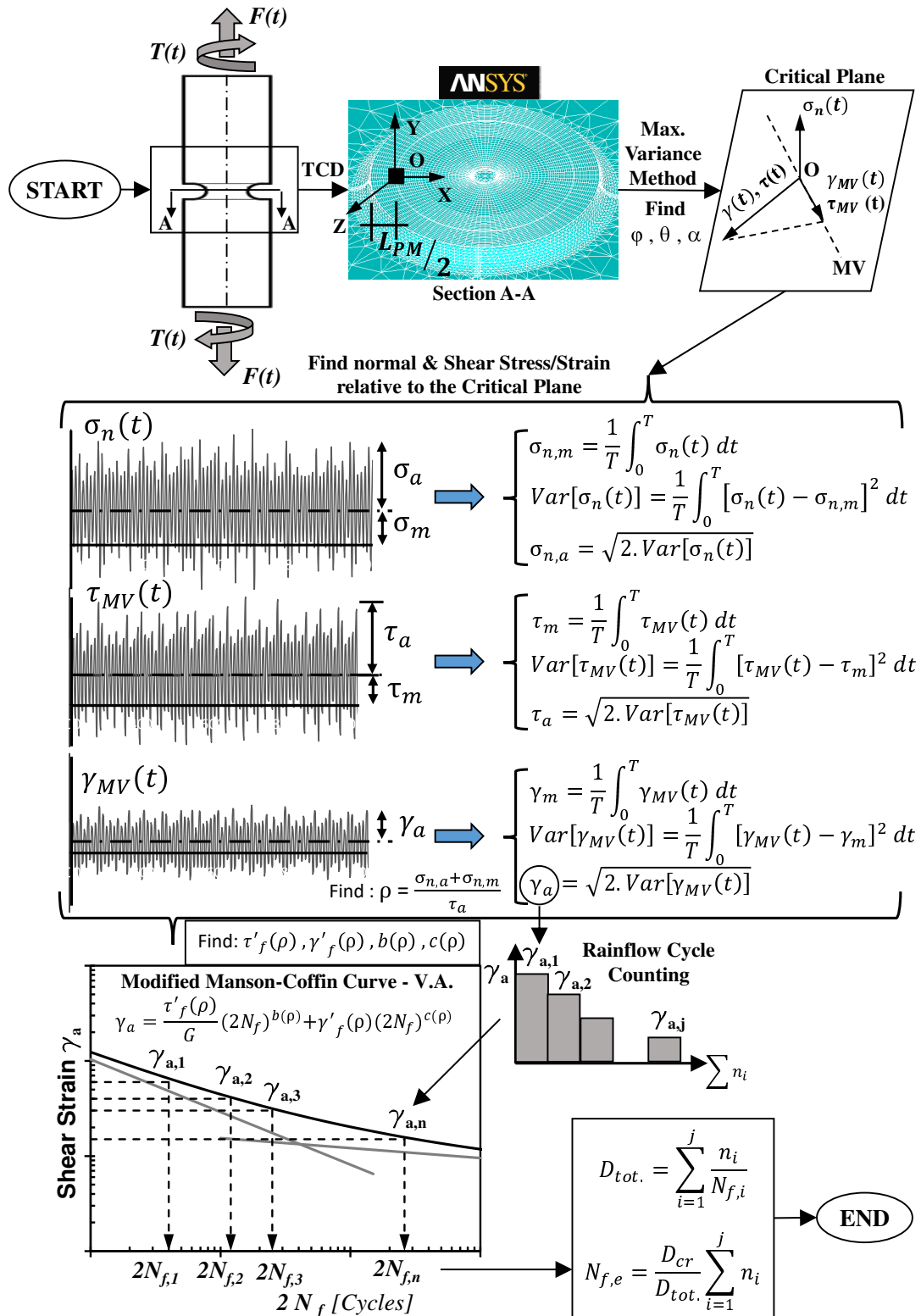


Figure 3.11: Flow Chat: In-field application of the developed approach against Variable Amplitude (VA) Multiaxial Fatigue Load

Chapter 4

Experimental Work

4.1 Introduction

The present chapter describes the experimental part of the research. In order to examine the accuracy and reliability of the model proposed in chapter (3), and to verify its effectiveness. A systematic validation exercise was followed by performing experimental work, and comparing the predicted results with the experimental output. According to the best of the author's knowledge, very limited experimental works have been performed and reported in the field of multiaxial fatigue when notches are involved and the cyclic load is random. The practical work behind this chapter was to apply a set of complex multiaxial fatigue load on notch specimens to validate the developed approach. Specifically, a systematic experimental investigation was performed on the medium carbon steel 080M40 by generating a consistent data sets for testing: 1. cylindrical plane specimens, 2. U-notched samples with three different notch root radii. The notch specimens were classified into Sharp, Intermediate & Blunt notches.

4.2 Multiaxial Fatigue Testing Machine

A multiaxial servo-controlled closed-loop axial-torsion SCHENCK fatigue testing machine was used. The load capacity of the testing rig was 400 kN tension and 1000 N.m torsion. The fatigue testing machine was digitally controlled by a SmarTest ONE MOOG controller system that automatically controlled the output signals to the testing machine and recorded all feedback from machine's actuators by using a data acquisition system at a predefined interval. The digital servo controller was designed for efficient operation utilising between one and four controlled channels. For these experiments, two channels were used for the axial and torsion forces in the force controlled tests, and the other two channels were used to control the extensometer (i.e. the strain controlled test). The testing machine physically applied axial and/or torsion forces to a specimen through an actuator rod. The actuators are a hydraulically-powered device that provides linear forces/displacements and torsion/rotation to a specimen being tested. The operating frequency of the testing machine ranged from low to very high speed. The calibration of the machine was

checked by using external axial and torsional load cells. A complete picture of the testing machine is illustrated in figure 4.1.



(a) Multi-axial Fatigue testing machine with a computerized controller



(b) Axial-Torsional Fatigue Rig

Figure 4.1: Multi-axial (Axial-Torsion) Fatigue Testing Machine

4.3 Multi-axial Hydraulic Collet (End Grips)

Multi-axial MTS 646 Hydraulic Collet Grips Model 646.25S were attached to the fatigue testing machine to hold the specimens properly during the test. The hydraulic collets were designed to perform high and low-cycle fatigue tests and provided a constant and hydraulically actuated gripping force regardless of the applied fatigue test loads. They were mounted in a load unit to secure the specimen under test. The axial capacity of the collet grips was 250 kN and the torsional capacity was 2200 N.m. The grips were controlled by a dedicated external hydraulic supply and the gripping force was adjustable so as to avoid sample damage by the grips or specimen slippage during the test. One of the significant features of the hydraulic collet grips is that, when hydraulic pressure is applied, it pulls the grip housing towards the piston inside the grip, forcing the collet to clamp the specimens in such a way that the applied pressure locks all moving grip parts in a position that eliminates backlash when cycling between tension and compression. A picture of the end grips is illustrated in Fig. (4.2).



(a) Hydraulic Collet Attached to the Actuators of Testing Machine



(b) Axial-Torsional End Grips

Figure 4.2: Multiaxial End Grips of Fatigue testing Machine

4.4 Axial-Torsional Extensometer - Model 3550

In many fatigue tests, strain amplitude measures indirectly from the displacement of loading with a prior calibration on a strain-gauged specimen. Such a measurement of strain subjects to error particularly from the yield, cyclic hardening and at the time of forming fatigue crack.

In this research, a high sensitivity biaxial extensometer with a maximum 25 mm gauge length was used to directly measure and control the strains during the test. The extensometer is often used on round samples tested in biaxial test machines capable of measuring both axial displacements and rotations simultaneously. The Axial-Torsional extensometer was an Epsilon brand, model 3550-025M, as shown in Fig. (4.3). It was designed in such a way that it could be easily attached to the specimens. The extensometer frame was formed to attach to round samples from 9.5 mm diameter to a maximum of 25 mm.

Furthermore, an Epsilon Axial-Torsional digital Electronic calibrator, model 3590AT, was used to calibrate and define the extensometer to the testing machine. The resolution of the calibrator was 0.001mm, and the axial measuring capacity was 50 mm with a rotation equal to 1.27 mm of linear motion, which equates to a 1° angle twist. The digital display and auto-zero button greatly simplified the process of calibrating the extensometer.



Figure 4.3: Axial-Torsional Extensometer - Epsilon MODEL: 3550-025M

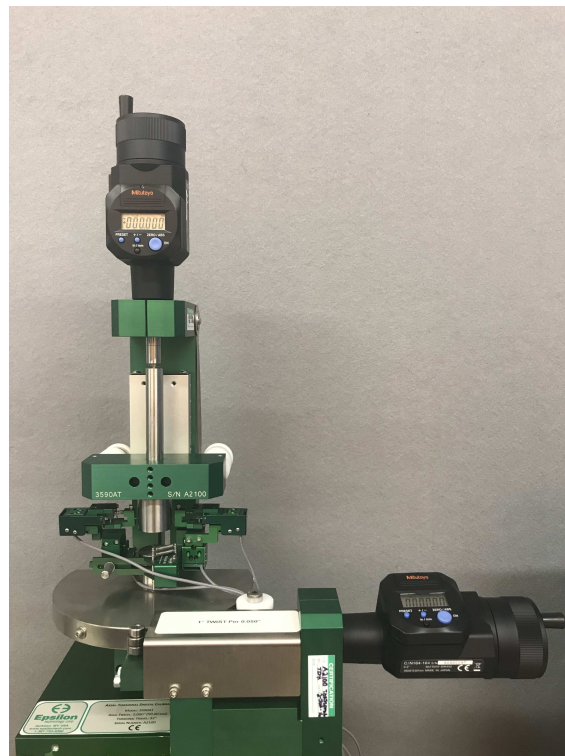


Figure 4.4: Axial-Torsional Digital Calibrator of Extensometer - Epsilon MODEL: 3590AT

4.5 Plane and Notch Specimens

A solid shaft is considered to be the most versatile shape and is preferred by most researchers who study the fatigue behaviour of materials. Such a specimen shape allows the biaxial extensometer

to attach to and measure directly from the sample by controlling the crack initiation region. A solid circular shaft with a diameter of 40 mm of medium carbon steel 080M40 was machined to solid plane samples with a gross diameter of $\phi 38$ mm and a length of 208 mm. An hourglass shape was used for plane specimens to maximise stresses at the centre of the plane sample, with the net diameter at the centre being 18 mm. The same solid circular shaft was also machined to create specimens with U-notches of three different root radii, each with an overall length equalling 180 mm. The gross diameter of all notch specimens were, $\phi 38$ mm and the net diameter was $\phi 18$ mm. The notch geometries were classified as Sharp, Intermediate and Blunt notches with notch root radii of 1.5, 3 & 6 mm, respectively. The notch root radius resulted in linear-elastic net stress concentration factors, K_t , equal to 2.56, 1.93 and 1.53, respectively (Pilkey 2005). The configuration and dimension of the specimens are shown in Fig. (4.6). The material has an ultimate tensile stress, σ_{UTS} of 700 MPa, yield stress, σ_y of 450 MPa, and a Young's modulus of 210 GPa, as listed in the Table (4.1). Overall, 132 specimens were tested as part of this research. 1. Plain samples were tested to: a. determine the axial and torsional fatigue constants, b. find the critical damage D_{cr} , c. quantify ρ_{lim} , d. and validate the formalised Matlab code. While, 2. Notch specimens were tested to validate the developed approach under different multiaxial fatigue load conditions. A summary of the tested specimens and the reasons for the test is provided in Table (4.2).

The following abbreviation are used in the tables to define the specimens:

1. Plain Sample (PS), Sharp Notch (SN), Intermediate Notch (IN), Blunt Notch (BN).
2. Uniaxial (U), Torsional (T), Biaxial (B).
3. Constant Amplitude (CA), Variable Amplitude (VA).
4. In-phase (Iph), Out-of-phase (OoPh).
5. Zero Mean Stress (ZMS), Non-zero Mean Stress (NZMS).
6. Different Frequencies (D.F).

Table 4.1: Mechanical properties of the tested material

Ultimate tensile strength, σ_{UTS}	700 MPa
Yield strength, σ_y	450 MPa
Young's modulus, E	210 GPa
Poisson ratio, ν_e	0.30

4.6 The Test Controlling Parameters

Generally, all the fatigue tests in this research were constructed by accurately arranging the fatigue load profile to ensure that the load sequences were correctly applied in the testing machine, and the tests were performed under two different controlling parameters:

1. **Strain Controlled test:** All plane specimens were tested under strain controlled test. The axial and shear strain amplitudes were calculated by using the Eqns. (4.1) and considered



Figure 4.5: Picture of the Tested Samples

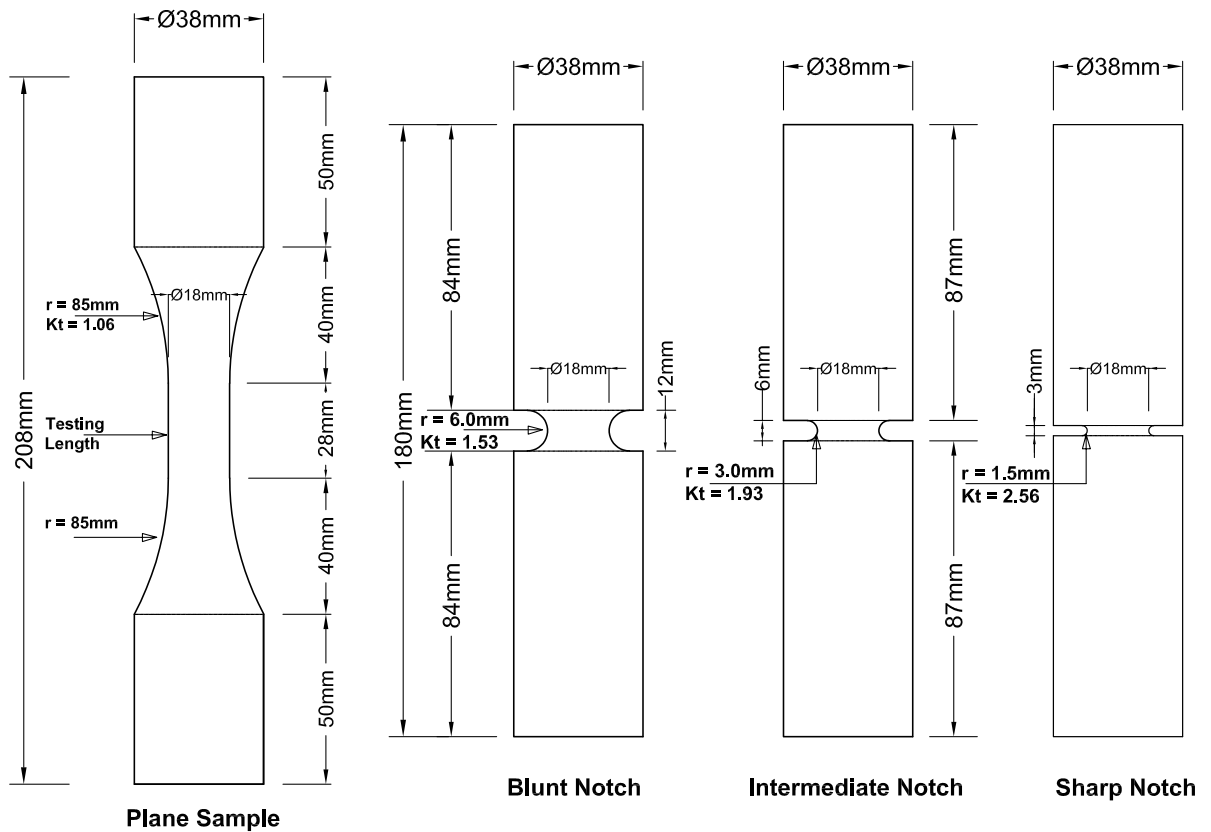


Figure 4.6: Details & Dimensions of the Specimens

Table 4.2: Summary of the tested specimens, type of loading, and purpose of the test

Specimens Type	No. of Specimens	Type of Loading	Reason of the Test
Plane Specimens	8	U, C.A, ZMS	To find Uniaxial and Torsional Fatigue Constants of the material
	8	T, C.A, ZMS	
	1	B, C.A, Iph, ZMS	To Validate the Matlab Code
	1	B, C.A, OoPh, ZMS	
	1	B, C.A, Iph, NZMS	
	1	B, C.A, OoPh, NZMS	To find the ρ_{limit}
4	B, V.A, OoPh, NZMS	To find the D_{cr}	
Sharp Notch Specimens	6	U, C.A, ZMS	To find the Critical Distance
	3	B, C.A, Iph, ZMS	To Validate the Proposed Approach with Sharp Notch
	3	B, C.A, OoPh, ZMS	
	5	B, V.A, Iph, ZMS	
	5	B, V.A, OoPh, ZMS	
	5	B, V.A, IPh, NZMS	
	5	B, V.A, OoPh, NZMS	
	8	B, V.A, D.F, ZMS	
8	B, V.A, D.F, ZMS		
Intermediate Notch Specimens	3	B, C.A, Iph, ZMS	To Validate the Proposed Approach with Intermediate Notch
	3	B, C.A, OoPh, ZMS	
	5	B, V.A, Iph, ZMS	
	5	B, V.A, OoPh, ZMS	
	5	B, V.A, Iph, NZMS	
	5	B, V.A, OoPh, NZMS	
Blunt Notch Specimens	8	B, V.A, D.F, ZMS	To Validate the Proposed Approach with Blunt Notch
	3	B, C.A, Iph, ZMS	
	3	B, C.A, OoPh, ZMS	
	5	B, V.A, Iph, ZMS	
	5	B, V.A, OoPh, ZMS	
	5	B, V.A, Iph, NZMS	
5	B, V.A, OoPh, NZMS		
8	B, V.A, D.F, ZMS		
Total Number of Specimens =	132		

as a controlling parameter that measured directly from the biaxial extensometer.

$$\varepsilon_x = \varepsilon_{x,m} + \varepsilon_a \sin wt \quad (4.1a)$$

$$\gamma_{xy} = \gamma_{xy,m} + \gamma_a \sin (wt - \delta) \quad (4.1b)$$

Where, ε_x & γ_{xy} are the axial and shear strain values, respectively. $\varepsilon_{x,m}$ & $\gamma_{xy,m}$ are the mean axial and shear strain magnitudes. ε_a & γ_a are the axial and shear strain amplitudes. t is time interval, and (δ°) is the degree of non-proportionality of the applied nominal strains.

2. **Force/Stress Controlled test:** All notch specimens were tested under force controlled parameters. Axial force and torsion loading histories were constructed by using the Eqns. (4.2):

$$F_x = F_{x,m} + F_a \sin wt \quad (4.2a)$$

$$T_{xy} = T_{xy,m} + T_a \sin (wt - \delta) \quad (4.2b)$$

Where, σ_x & τ_{xy} are the axial and shear stresses, respectively. $\sigma_{x,m}$ & $\tau_{xy,m}$ are the mean axial and shear stresses. σ_a & τ_a are the axial and shear stress amplitudes.

The multiaxial loading condition was employed by rearranging the uniaxial loading and determining the torsional loading based on the von Mises equivalent stress/strain equations and according to the definition (4.3):

$$\varepsilon_{equivalent} = \varepsilon_a = \sqrt{\varepsilon_{x,a}^2 + \frac{(\gamma_{xy,a})^2}{3}} \quad (4.3a)$$

$$\sigma_{equivalent} = \sigma_a = \sqrt{\sigma_{x,a}^2 + 3(\tau_{xy,a})^2} \quad (4.3b)$$

Where, $\varepsilon_{equivalent}$ & $\sigma_{equivalent}$ are the equivalent strain and stress amplitudes, respectively. ε_a & σ_a are the axial strain and stress amplitudes. $\varepsilon_{x,a}$ & $\sigma_{x,a}$ are the axial strain and stress amplitudes on the direction of x-axis, and $\gamma_{xy,a}$ & $\tau_{xy,a}$ are the shear strain and stress amplitudes on the xy-plane.

4.7 Testing Procedure

A series of fatigue tests were carried out on the solid circular shaft of plane and notch specimens using a closed-loop servo-hydraulic MTS Axial-Torsional fatigue testing machine, shown in Fig. (4.1). The samples were machined from a steel 080M40 material to the geometries sketched in Fig. (4.6). In order to consider zero and non-zero mean stresses, nominal load ratios R_ε equal to -1 & 0 were considered. A sinusoidal signal was used as a waveform for all tests. The mechanical properties of the material are given in Table (4.1). Fatigue tests were performed with an accurate controlling system and correct calibration. The calibration of the testing machine was checked using axial and torque cells prior to the test, and the calibration of the extensometer was also confirmed by using an electronic calibrator, model 3590AT. The specimen was simply fixed between two MTS 646 Hydraulic Collet Grips, as shown in Fig. (4.2). All tests were performed at room temperature. In spite of the high speed capability of the testing machine, low frequencies were used, particularly in the variable amplitude loading conditions, so as to allow the testing machine actuators to accelerate and decelerate properly for each loading cycles, and thus to obtain the desired nominal stress or strain amplitudes. In this research, the operating frequency ranged between (0.5 - 2.0)Hz. A lower frequency was used for variable amplitude tests, equal 1.0 Hz, whereas 2.0 Hz was used in the constant amplitude load cases. The specimens were tested using a low/medium-cycle fatigue regime.

During the tests, the deformation behaviour of the specimens was monitored throughout the life of each sample. All data were counted through the signals gathered from the multiaxial actuators controlled by a computerised system attached to the testing machine. Sufficient stress and strain data points per cycle were recorded in order to provide an adequate description of the stress/strain

versus times. As mentioned elsewhere, two types of controlling load were conducted: a strain-controlled test for the plane samples and stress-controlled test for the notch specimens. Fatigue failure was assumed to occur at the number of cycles at which stiffness instability was evident. That means that crack initiation was considered to have occurred at the point at which the stiffness of the material began to decrease. In more detail, the failure of the specimens under uniaxial and biaxial fatigue tests was recorded when there was a drop in axial stiffness of the material by 5%. While, in the pure torsion tests, fatigue failure was defined when the torque stiffness dropped by 5%. In order to compare the fracture surface of the specimens under different loading conditions, all samples were cycled to a complete fracture. Compared to the fatigue lifetime at 5% stiffness drop, complete fracture was found to occur at around a 10-13% drop in stiffness. The Tables (6.7, 4.7 & 4.8) list the specimen loading conditions and test results that served to validate the proposed approach. Most of the major loading conditions used in real in-service loading of components were conducted in this experiments. Theoretical analysis was performed at the completion of each test and parallel to the experimental work.

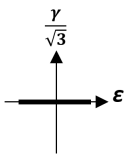
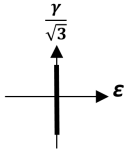
4.8 Mechanical Properties and Fatigue Parameters of the Material

As mentioned in chapter (3), in the formalised approach, not only fatigue damage is considered in the elastic region, but also controlled by elasto-plastic deformation. Correct estimation of the mechanical and fatigue properties of the considered material (steel 080M40) provide an accurate representation of the material response. This section is intended to describe experimentally the behaviour of the tested material in terms of mechanical and fatigue properties.

4.8.1 Determination of the Material Fatigue Constants by Running Fully-reversed Axial and Torsional Cyclic Loading of Plane Specimens

In order to obtain the uniaxial and torsional fatigue properties of the material relevant to the strain-based lifetime relationship, eight systematic fully-reversed tension-compression fatigue tests and eight completely-reversed torsion strain-controlled cyclic tests were conducted separately on plane hourglass-shaped specimens, with zero mean stress. A tension-torsion Epsilon extensometer was used to control the strain. The strain-controlled tests were conducted to determine both the stabilised uniaxial and torsional stress/strain curve (Fig. 4.7 & Fig. 4.8), and the corresponding fully-reversed axial and torsional Manson-Coffin curve (Fig. 4.9 & Fig. 4.10). The fatigue tests were run according to the recommendations of the ASTM standard (Norma (1998)). All tested specimens and experimental results were listed in Table (4.3). The material fatigue constants of (σ'_f , ϵ'_f , τ'_f , γ'_f , b , & c) were determined from the experimental results and are reported in Table (4.4).

Table 4.3: Summary of the experimental results generated by testing Sharply notched specimens $r_n=1.5\text{mm}$ under uniaxial constant amplitude cyclic load

Specimen symbols	Load Ratio [†]	$\varepsilon_{a,max}(t)$ (mm/mm)	$\gamma_{a,max}(t)$	N_f^\ddagger (Cycles)	Loading Path
PSUCAZMS1 [†]	R = -1	0.0018	—	85,408	
PSUCAZMS2		0.0019	—	71,336	
PSUCAZMS3		0.0019	—	40,132	
PSUCAZMS4		0.0020	—	57,039	
PSUCAZMS5		0.0030	—	15,040	
PSUCAZMS6		0.0040	—	7,338	
PSUCAZMS7		0.0050	—	4,059	
PSUCAZMS8		0.0060	—	2,251	
PSTCAZMS1 [†]	R = -1	—	0.0022	673,052	
PSTCAZMS2		—	0.0035	54,255	
PSTCAZMS3		—	0.0044	20,705	
PSTCAZMS4		—	0.0046	14,012	
PSTCAZMS5		—	0.0058	8,247	
PSTCAZMS6		—	0.0068	6,285	
PSTCAZMS7		—	0.0079	4,003	
PSTCAZMS8		—	0.0094	3,142	

[†] PSU/TCAZMS1: Plane Sample, Uniaxial / Torsional, Constant Amplitude, Zero Mean Strain 1

[†] Load Ratio, $R = \frac{\varepsilon_{a,min}}{\varepsilon_{a,max}}$ or $\frac{\gamma_{a,min}}{\gamma_{a,max}}$, [‡] N_f : Number of Cycles to failure at 5% axial/torsional stiffness drop

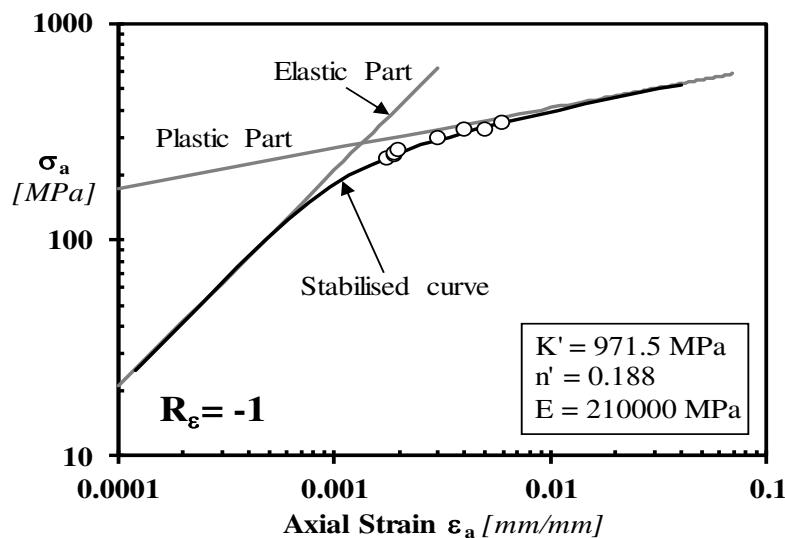


Figure 4.7: Stabilized Uniaxial Stress-Strain Curve

4.9 Uniaxial Fatigue Test to Find the Critical Distance

As discussed in the last chapters, previous studies have confirmed that directly considering notch-root stresses in order to evaluate the fatigue lifetime of notch components increases the level of conservatism of the fatigue assessment. In order to design an optimised notch component, the Theory of Critical Distance recommends the use of corresponding stress/strain states at a specific distance from the notch root. This distance is known as the Critical Distance. According to the entire procedure sketched in the flowchart of Fig. (3.4), six sharply notched specimens having a root radius equal to 1.5 mm were machined and tested under monotonic fully-reversed

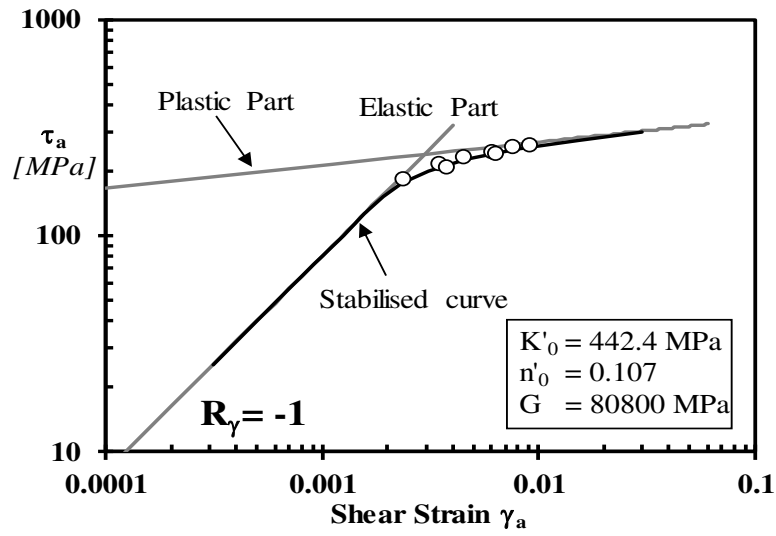


Figure 4.8: Stabilized Torsional Stress-Strain Curve

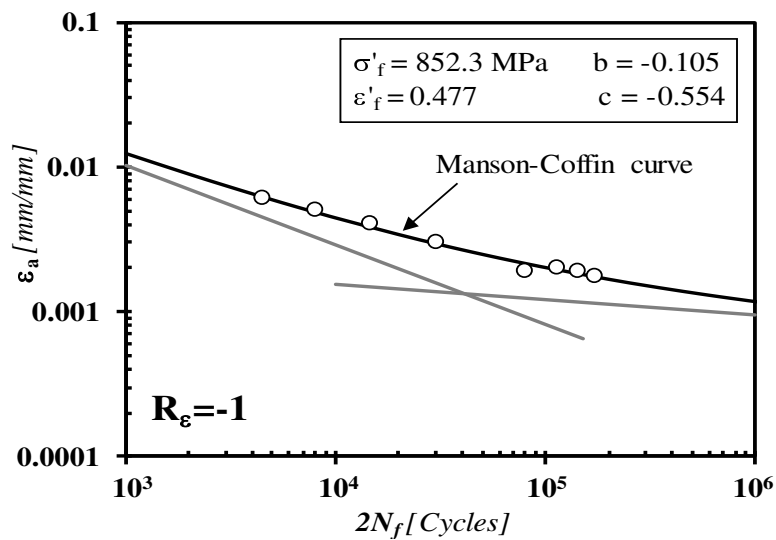


Figure 4.9: Fully-reversed Tension-Compression Manson-Coffin Curve of the Plane material (080M40 Steel)

nominal tension-compression fatigue force $F(t)$ with a constant amplitude loading condition. The specimens were failed at N_f cycles. Summary of the experiments were presented in Table (4.5).

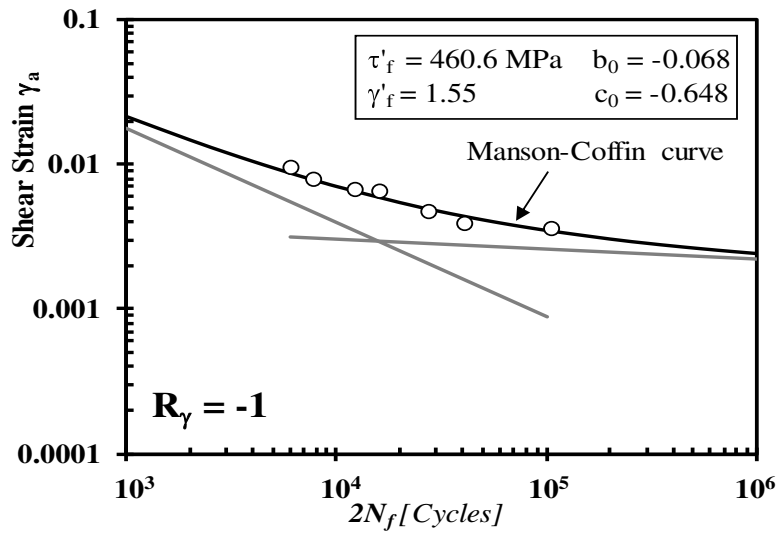


Figure 4.10: Fully-reversed Torsion Manson-Coffin Curve of the plane material (080M49 Steel)

Table 4.4: Uniaxial and Torsional Fatigue Properties of the investigated material

Uniaxial Fatigue Properties		Torsional Fatigue Properties	
K'_f	971.5 MPa	K'_o	442.4 MPa
n'_f	0.188	n'_o	0.107
σ'_f	852.3 MPa	τ'_f	460.6 MPa
ϵ'_f	0.477	γ'_f	1.55
b	-0.105	b_o	-0.068
c	-0.554	c_o	-0.648

† All the fatigue properties was found by running experiments

Table 4.5: Experimental test of Sharp Notch Specimens under Uniaxial Constant Amplitude Fatigue Load to Find the Critical Distance

Specimens	Load Ratio†	$F_a(t)$ (kN)	Experimental N_f^\dagger (Cycles)	Loading Path
SNUCAZMS1†		78.7	6,164	
SNUCAZMS2		58.3	35,247	
SNUCAZMS3	R = -1	52.0	41,229	
SNUCAZMS4		69.8	13,469	
SNUCAZMS5		46.8	81,629	
SNUCAZMS6		42.3	145,989	

† SNUCAZMS1: Sharp Notch, Uniaxial, Constant Amplitude, Zero Mean Stress 1
 † Load Ratio, $R = \frac{\sigma_{a,min}}{\sigma_{a,max}}$, † N_f : Number of Cycles to failure at 5% axial stiffness drop

4.10 Experimental Multiaxial Fatigue Life Evaluation of Notched Components

Multiaxial fatigue damage is a critical fatigue concern for materials and in structural elements. A combination of in-service proportional/non-proportional, constant/variable amplitude, in-phase/out-of-phase fatigue loading conditions make the multiaxial fatigue mechanism more

complex and, sometimes, physical evaluation is beyond the capability of experiments, particularly in complex geometries and notches. In this thesis, a multiaxial fatigue evaluation technique was devised and the methodology was discussed in the last chapter. The current section presents the multiaxial fatigue tests that the author performed in the "Lea Laboratory" of the University of Sheffield, Faculty of Engineering, using three different notched geometries against different multiaxial cyclic loadings. The results were used to validate the proposed approach. In order to validate the formalised method's applicability for a wider range of multiaxial loading conditions, the applied cyclic loads were classified into three main forms: 1. Constant amplitude cyclic loading, 2. Variable amplitude cyclic loading, 3. Variable amplitude fatigue loading at different frequencies. The above-mentioned load combinations were applied on all geometries. All fatigue tests were conducted under load-controlled mode and at room temperature. The applied multiaxial loading paths are presented in the Tables (6.7, 4.7, & 4.8).

4.10.1 Constant Amplitude Fatigue Test

In real-life service operations, engineering structures and components are sometimes subjected to constant amplitude multiaxial cyclic loading. For cases that exhibit constant amplitude, both applied loadings can be undergone proportionally (In-phase) or non-proportionally (out-of-Phase). In this research, overall, 18 notch specimens in Fig. 4.6 (6 for each notch geometry) were tested under in-phase and 90° out-of-phase loadings. The tests were run under force-controlled fully reversed tension-compression and fully reversed torsion constant amplitude cyclic loading. The load signals were applied at a frequency of 2 Hz. The results are summarised in Tables (6.7, 4.7, & 4.8).

4.10.2 Variable Amplitude Fatigue Test

This section schematically illustrates the principal defined of cyclic loading when the profile of signals is variable. Selection of loads for variable amplitude testing and scripting the fatigue testing machine to run variable amplitude loads was not a straightforward procedure. A specific load spectra, as shown in Fig.(4.11a), was designed to investigate VA fatigue based on the characteristics of the biaxial testing machine. In order to control the loading better, and achieve the desired load amplitudes, a profile of the investigated loads was applied at a low level of frequency, equal to 1 Hz. $\frac{\sum_{a-i}}{\sum_{a-max}}$ is the ratio between a load amplitude (Force or Torque) of i^{th} cycle to the maximum amplitude in the spectrum. This ratio was different from cycle to cycle during the test. The sequence length, S_L , was equal to 50 cycles and the designed cycles are shown in Fig. 4.11b. Fifty cycles were considered as one unit block of loading. $F_{a,max}(t)$ & $T_{a,max}(t)$ are the nominal axial & torsional time-variable load. $F_{m,max}$ and $T_{m,max}$ are the mean of nominal force and moment. A combination of zero/non-zero, in-phase/out-of-phase loadings was used in the tests. A total of 60 samples were tested (20 specimens for each notch shape) according to the detail summarised in Tables (6.7, 4.7, & 4.8).

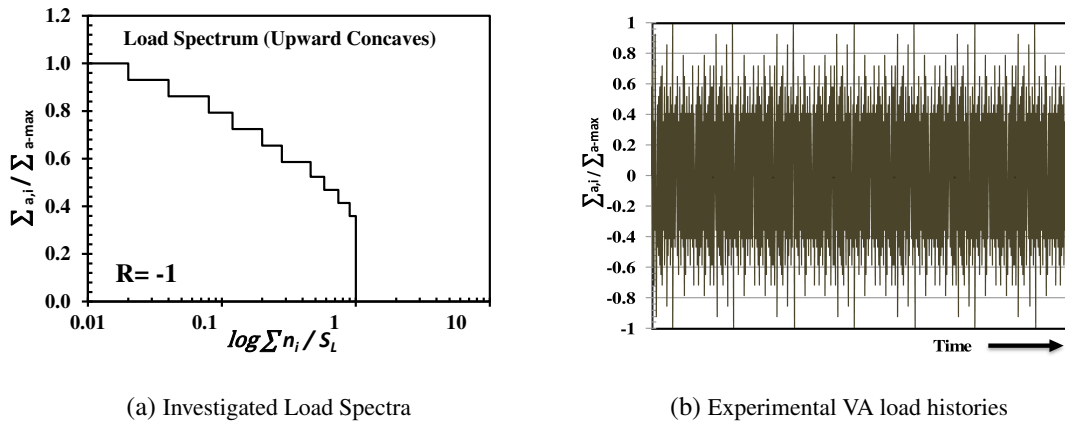


Figure 4.11: Investigated Load employed to test the notched samples 080M40Steel

Table 4.6: Summary of the Experimental Results Generated by Testing the Sharp Notch Specimens $r_n=1.5\text{mm}$

Specimen symbols [†]	Load Ratio [†]	$F_{a,max}(t)$ (kN)	$F_{m,max}$ (kN)	$T_{a,max}(t)$ (N.m)	$T_{m,max}$ (N.m)	$\delta^{\circ\ddagger}$	N_f^{\ddagger} (Cycles)	Loading Path
SNBCAZMSIph1	R = -1	39.1	—	101.8	—	0	63,012	$\sqrt{3} \tau$
SNBCAZMSIph2		44.1	—	120.5	—	0	22,974	
SNBCAZMSIph3		55.1	—	153.7	—	0	7,156	
SNBCAZMSOoPh1	R = -1	41.3	—	110.6	—	90	31,594	$\sqrt{3} \tau$
SNBCAZMSOoPh2		45.1	—	125.6	—	90	11,989	
SNBCAZMSOoPh3		55.8	—	158.1	—	90	6,229	
SNBVAZMSIph1	R = -1	64.6	—	160.4	—	0	39,428	$\sqrt{3} \tau$
SNBVAZMSIph2		67.2	—	174.6	—	0	19,510	
SNBVAZMSIph3		71.8	—	154.1	—	0	22,811	
SNBVAZMSIph4		57.3	—	114.5	—	0	54,296	
SNBVAZMSIph5		58.4	—	86.3	—	0	82,054	
SNBVAZMSOut1	R = -1	65.6	—	117.9	—	90	50,764	$\sqrt{3} \tau$
SNBVAZMSIph2		67.7	—	130.3	—	90	35,338	
SNBVAZMSOut3		72.9	—	128.9	—	90	22,436	
SNBVAZMSOut4		56.4	—	132.1	—	90	67,704	
SNBVAZMSOut5		55.2	—	99.4	—	90	78,078	
SNBVANZMIph1	R = 0	57	57	148.1	148.1	0	34,677	
SNBVANZMIph2		60.5	60.5	157.2	157.2	0	25,220	
SNBVANZMIph3		48.6	48.6	126.3	126.3	0	47,235	
SNBVANZMIph4		68.4	68.4	177.7	177.7	0	12,857	
SNBVANZMIph5		45.6	45.6	118.5	118.5	0	45,245	
SNBVANZMOut1	R = 0	48.6	48.6	126.3	126.3	90	62,310	$\sqrt{3} \tau$
SNBVANZMIph2		60.5	60.5	157.2	157.2	90	30,665	
SNBVANZMOut3		57	57	148.1	148.1	90	58,580	
SNBVANZMOut4		68.4	68.4	177.7	177.7	90	13,755	
SNBVANZMOut5		45.6	45.6	118.5	118.5	90	70,019	

[†]SN: Sharp Notch, B: Biaxial, C.A: Constant Ampl., VA: Variable Ampl., ZMS: Zero Mean Stress, NZMS: Non-Zero Mean Stress

[†]Load Ratio, $R = \frac{\sigma_{a,min}}{\sigma_{a,max}}$, [†] δ° : Degree of Non-proportionality of the applied loads.

[†] N_f : Number of Cycles to failure at 5% axial stiffness drop

4.10.3 Variable Amplitude Fatigue Tests - Different Frequency

In light of the encouraging accuracy obtained by applying the constant/variable amplitude fatigue loading under constant operating frequency, the author subsequently decided to investigate the

Table 4.7: Summary of the Experimental Results Generated by Testing the Intermediate Notch Specimens $r_n=3\text{mm}$

Specimen symbols [†]	Load Ratio [†]	$F_{a,max}(t)$ (kN)	$F_{m,max}$ (kN)	$T_{a,max}(t)$ (N.m)	$T_{m,max}$ (N.m)	δ° [†]	N_f^\dagger (Cycles)	Loading Path
INBCAZMSIph1		40.4	—	102.72	—	0	156,422	
INBCAZMSIph2		49.0	—	123.0	—	0	47,739	
INBCAZMSIph3		60.6	—	178.8	—	0	9,725	
	R = -1							
INBCAZMSOoPh1		46.0	—	140.0	—	90	46,428	
INBCAZMSOoPh2		51.0	—	132.5	—	90	33,269	
INBCAZMSOoPh3		63.6	—	181.7	—	90	8,428	
	R = -1							
INBVAZMSIph1		66.7	—	153.1	—	0	39,837	
INBVAZMSIph2		56.9	—	124.5	—	0	70,645	
INBVAZMSIph3		71.8	—	163.1	—	0	30,919	
INBVAZMSIph4		79.5	—	184.7	—	0	24,372	
INBVAZMSIph5		54.0	—	129.1	—	0	70,879	
	R = -1							
INBVAZMSOut1		64.5	—	176.4	—	90	32,549	
INBVAZMSIph2		56.7	—	135.8	—	90	59,743	
INBVAZMSOut3		72.9	—	177.0	—	90	24,930	
INBVAZMSOut4		77.2	—	197.9	—	90	19,385	
INBVAZMSOut5		54.3	—	132.9	—	90	65,910	
	R = 0							
INBVANZMIph1		55.1	55.1	143.2	143.2	0	77,310	
INBVANZMIph2		60.6	60.6	157.4	157.4	0	39,124	
INBVANZMIph3		66.7	66.7	173.3	173.3	0	37,870	
INBVANZMIph4		73.4	73.4	190.7	190.7	0	25,609	
INBVANZMIph5		80.8	80.8	209.9	209.9	0	9,559	
	R = 0							
INBVANZMOut1		55.1	55.1	143.2	143.2	90	99,157	
INBVANZMIph2		60.6	60.6	157.4	157.4	90	45,491	
INBVANZMOut3		66.7	66.7	173.3	173.3	90	28,616	
INBVANZMOut4		73.4	73.4	190.7	190.7	90	20,810	
INBVANZMOut5		80.8	80.8	209.9	209.9	90	10,386	

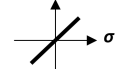
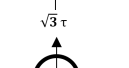

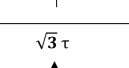
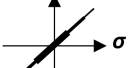
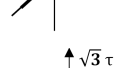




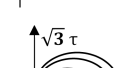


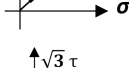


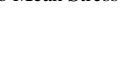



[†]IN: Intermediate Notch, B: Biaxial, C/V.A: Constant/Variable Ampl., ZMS: Zero Mean Stress, NZMS: Non-Zero Mean Stress

[†]Load Ratio, $R = \frac{\sigma_{a,min}}{\sigma_{a,max}}$, [†] δ° : Degree of Non-proportionality of the applied loads.

[†] N_f : Number of Cycles to failure at 5% axial stiffness drop

accuracy of the developed approach further in a situation involving a different operating frequency for the applied multiaxial load. Twenty-four tests of notched specimens with different root radii were also performed under different frequencies (eight tests for each notch geometry). The first four specimens of each notch geometry were tested under axial to torsional frequencies equal to 0.5 Hz and 1.0 Hz, respectively. While, the other four samples were tested with the opposite parameters, i.e. where the axial frequency was 1.0 and the torsional 0.5. Zero mean stress was considered in these tests. The results of these tests are reported in Table (4.9).

Table 4.8: Summary of the Experimental Results Generated by Testing the Blunt Notch Specimens $r_n=6\text{mm}$

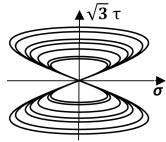
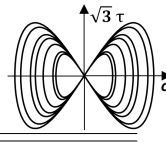
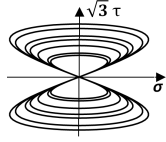
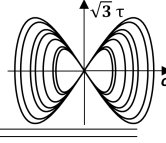
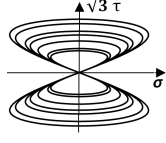
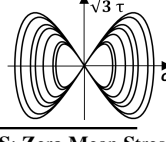
Specimen symbols [†]	Load Ratio [‡]	$F_{a,max}(t)$ (kN)	$F_{m,max}$ (kN)	$T_{a,max}(t)$ (N.m)	$T_{m,max}$ (N.m)	$\delta\circ^{\dagger}$	N_f^{\ddagger} (Cycles)	Loading Path
BNBCAZMSIph1		39.3	—	114.8	—	0	225,655	$\sqrt{3}\tau$
BNBCAZMSIph2		49.8	—	126.3	—	0	58,662	
BNBCAZMSIph3		67.2	—	170.7	—	0	12,423	
	R = -1							
BNBCAZMSOoPh1		49.6	—	114.2	—	90	131,784	$\sqrt{3}\tau$
BNBCAZMSOoPh2		61.8	—	148.4	—	90	35,127	
BNBCAZMSOoPh3		69.5	—	186.5	—	90	14,146	
BNBVAZMSIph1		80.6	—	209.5	—	0	33,765	$\sqrt{3}\tau$
BNBVAZMSIph2		88.7	—	230.4	—	0	15,386	
BNBVAZMSIph3		72.6	—	188.6	—	0	52,223	
BNBVAZMSIph4		65.3	—	169.8	—	0	97,300	
BNBVAZMSIph5		95.0	—	246.8	—	0	14,169	
	R = -1							
BNBVAZMSOut1		80.6	—	209.5	—	90	36,032	$\sqrt{3}\tau$
BNBVAZMSIph2		88.7	—	230.4	—	90	15,681	
BNBVAZMSOut3		72.6	—	188.6	—	90	51,710	
BNBVAZMSOut4		65.3	—	169.8	—	90	75,650	
BNBVAZMSOut5		95.0	—	246.8	—	90	12,223	
BNBVANZMIph1		65.0	65.0	168.9	168.9	0	39,870	$\sqrt{3}\tau$
BNBVANZMIph2		71.5	71.5	185.8	185.8	0	29,100	
BNBVANZMIph3		78.7	78.7	204.5	204.5	0	10,486	
BNBVANZMIph4		59.8	59.8	155.4	155.4	0	62,620	
BNBVANZMIph5		67.9	67.9	176.4	176.4	0	35,225	
	R = 0							
BNBVANZMOut1		67.9	67.9	176.4	176.4	90	50,072	$\sqrt{3}\tau$
BNBVANZMIph2		78.7	78.7	204.5	204.5	90	27,149	
BNBVANZMOut3		71.5	71.5	185.8	185.8	90	28,250	
BNBVANZMOut4		59.8	59.8	155.4	155.4	90	61,250	
BNBVANZMOut5		65	65	168.9	168.9	90	46,328	

[†]BN: Blunt Notch, B: Biaxial, C/V.A: Constant/Variable Ampl., ZMS: Zero Mean Stress, NZMS: Non-Zero Mean Stress

[‡]Load Ratio, $R = \frac{\sigma_{a,min}}{\sigma_{a,max}}$, [†] $\delta\circ$: Degree of Non-proportionality of the applied loads.

[‡] N_f : Number of Cycles to failure at 5% axial stiffness drop

Table 4.9: Summary of the Experimental Results of the Notches Generated by Testing under Different Frequencies

Specimen Symbols [†]	Loading Type & Operating Frequency [†]	$F_{a,max}(t)$ (kN)	$T_{a,max}(t)$ (N.m)	N_f^{\dagger} (Block)	Loading Path
Sharp Noth $r_n = 1.5mm$					
SNBVAZMSDF1	Axial Frequency = 0.5 Torsional Frequency = 1.0 R = -1	70.0	181.9	52.54	
SNBVAZMSDF2		57.96	150.6	75.99	
SNBVAZMSDF3		64.40	167.3	69.44	
SNBVAZMSDF4		52.1	135.4	179.02	
SNBVAZMSDF5	Axial Frequency = 1.0	70.0	181.9	216.58	
SNBVAZMSDF6	Torsional Frequency = 0.5	64.4	167.3	344.19	
SNBVAZMSDF7	R = -1	57.96	150.6	646.65	
SNBVAZMSDF8		77.0	200.1	147.6	
Intermediate Noth $r_n = 3.0mm$					
INBVAZMSDF1	Axial Frequency = 0.5 Torsional Frequency = 1.0 R = -1	70.0	181.9	95.78	
INBVAZMSDF2		64.4	167.3	131.88	
INBVAZMSDF3		57.96	150.6	162.94	
INBVAZMSDF4		52.1	135.4	280.26	
INBVAZMSDF5	Axial Frequency = 1.0	70.0	181.9	277.82	
INBVAZMSDF6	Torsional Frequency = 0.5	64.4	167.3	510.15	
INBVAZMSDF7	R = -1	57.96	150.6	785.52	
INBVAZMSDF8		77.0	200.1	252.4	
Blunt Noth $r_n = 6.0mm$					
BNBVAZMSDF1	Axial Frequency = 0.5 Torsional Frequency = 1.0 R = -1	70	181.9	162.38	
BNBVAZMSDF2		64.4	167.3	163.06	
BNBVAZMSDF3		57.96	150.6	290.9	
BNBVAZMSDF4		77.0	200.1	72.22	
BNBVAZMSDF5	Axial Frequency = 1.0	70.0	181.9	780	
BNBVAZMSDF6	Torsional Frequency = 0.5	64.4	167.3	813.16	
BNBVAZMSDF7	R = -1	77.0	200.1	564.56	
BNBVAZMSDF8		84.7	220.1	240.18	

[†]SN: Sharp Notch, IN: Intermediate Notch., BN: Blunt Notch., B: Biaxial., V.A: Variable Ampl., ZMS: Zero Mean Stress, DF: Different Frequency, [†]Load Ratio, $R = \frac{\sigma_{a,min}}{\sigma_{a,max}}$, [†] N_f : Number of Blocks to failure at 5% axial stiffness drop

Chapter 5

An Elasto-plastic Finite Element model Validation to Determine Local Stress-strain Sequences under Complex Fatigue Loading ^[i]

5.1 Introduction

In any component with a geometrical feature under fatigue loading, the corresponding local stress/strain states vary along the cross-section of the geometry. For further development of a reliable and theoretically accepted fatigue criteria, it is important to understand the local stress-strain response and to have deep insight into the damage mechanisms during multiaxial fatigue. In order to apply the strain-based approach (MMCCM) that has been primarily used in the proposed approach, and to obtain good estimates of the fatigue lifetime of materials, there is obviously a need to describe the accurate elasto-plastic infield stress-strain states developed on the material being assessed. For a measurement point of view, researcher came to believe that running a convenient experiments is the best choice to determine the corresponding stress-strain states of a material. However, engineering designers have argued that time and monitoring involved in experimental investigation, in addition access to an appropriate testing machine is not always an easy task. Also, physical investigation (experimental measurement) of sub-surface stress/strain at notches under fatigue loading are not yet applicable. Consequently, the development of a computer software have increased the emphasis on the use of numerical calculation rather experiments. There are a good number of theoretical solutions that were proposed to determine the local stresses and strains in the notch components (Hoffmann & Seeger 1985, Hoffmann & Seeger 1985, Kötting et al. 1995,

^[i]The Content of this Chapter has been published as follow:

An Elasto-plastic model Simulation to Calculate Local Stress-strain Sequences under Uniaxial/multiaxial Constant/Variable Amplitude Cyclic Loading, The Annual Postgraduate Research Student Conference - United Kingdom

Author: N. Zuhair Faruq & L. Susmel ISBN 978-88-95940-50-2, P25-31: April 2015

<http://www.gruppofrattura.it/pdf/Sheffield2015/files/assets/basic-html/page-29.html>

and Ince & Glinka 2016). However, such a solutions apply to determine sub-surface stress/strain states only at notch tips (i.e estimating stress/strain states solely at the notch root). Owing to the fact that according to the Critical Distance that used in the developed approach of this research work, fatigue damage can be estimated by the local elasto-plastic stress/strain states developed in the vicinity of the notch tip inside materials rather root stresses/strains. Infield measurement of such a developed triaxial stress-stain states inside notch materials under fatigue loading is indeed experimentally and numerically impractical. This highlights the need for a validated and confidence numerical method to describe the developed local stress-strain histories inside materials. According to the best of the author's knowledge, the only standard procedure to determine the local elasto-plastic stress-strain states at any location in notch components is solving the problem by using elasto-plastic finite element FE method. The FE model is not only capable of analyse a component when the cyclic stress/strain is involved, but also considers plastic hardening/softening of materials. In light of the above well-known facts, this chapter summarises an attempt to formalise and validate an accurate three dimensional finite element model (3D FE model) capable of estimating the local elasto-plastic stress-strain response of materials at a certain point on defined geometries. In order to build up a confidence finite element code and perform a reliable validation, as a starting point, an elasto-plastic plain tube and solid cylinder were modelled and analysed. The scientific goal behind studying un-notched materials in this chapter is, the determined stresses/strains of plain geometries under fatigue loading by using FE model can accurately be validated either by running experiments or using the available theoretical tools, for instance Jiang & Sehitoglu (1996) approach, but validating the estimated stress/strain values inside materials by using FE model is impractical.

In this chapter, two types of plain geometries (tube and solid cylinder) were modelled and numerically analysed by using a 3D finite element FE ANSYS-Mechanical APDL®, the local elasto-plastic cyclic stress and strain states were determined and presented as a hysteresis loop graphs. The hysteresis loop characteristically shows both a linear elastic region of materials followed by a non-linear plastic regime, recognising that there are periods of time when a material experiences elasto-plastic deformation. Such a hysteresis loop allows to compare the numerical and experimental results easily and simplify the process of validation.

5.2 Type of Geometries Used in the FE Model Validation

According to the strategy formulated in this chapter, and to built up a confidence in using the developed FE model to determine the local elasto-plastic stresses and strains, two groups of plain geometries of tubes & solid circular shafts were considered. All material properties and experimental results of plain tubes were taken from other literature. But, the solid un-notched specimens were machined and tested by the author in the Lea lab. of Sheffield University. All the considered materials responded plastically. According to the author's information, however, very limited experimental works have been reported in respect to complex multiaxial random loads, but to perform a comprehensive and wider investigation, attempt has been made to consider a variety of Constant and Variable Amplitude loading cases, paths and amplitudes in this validation exercise, as shown in Fig.(5.1).

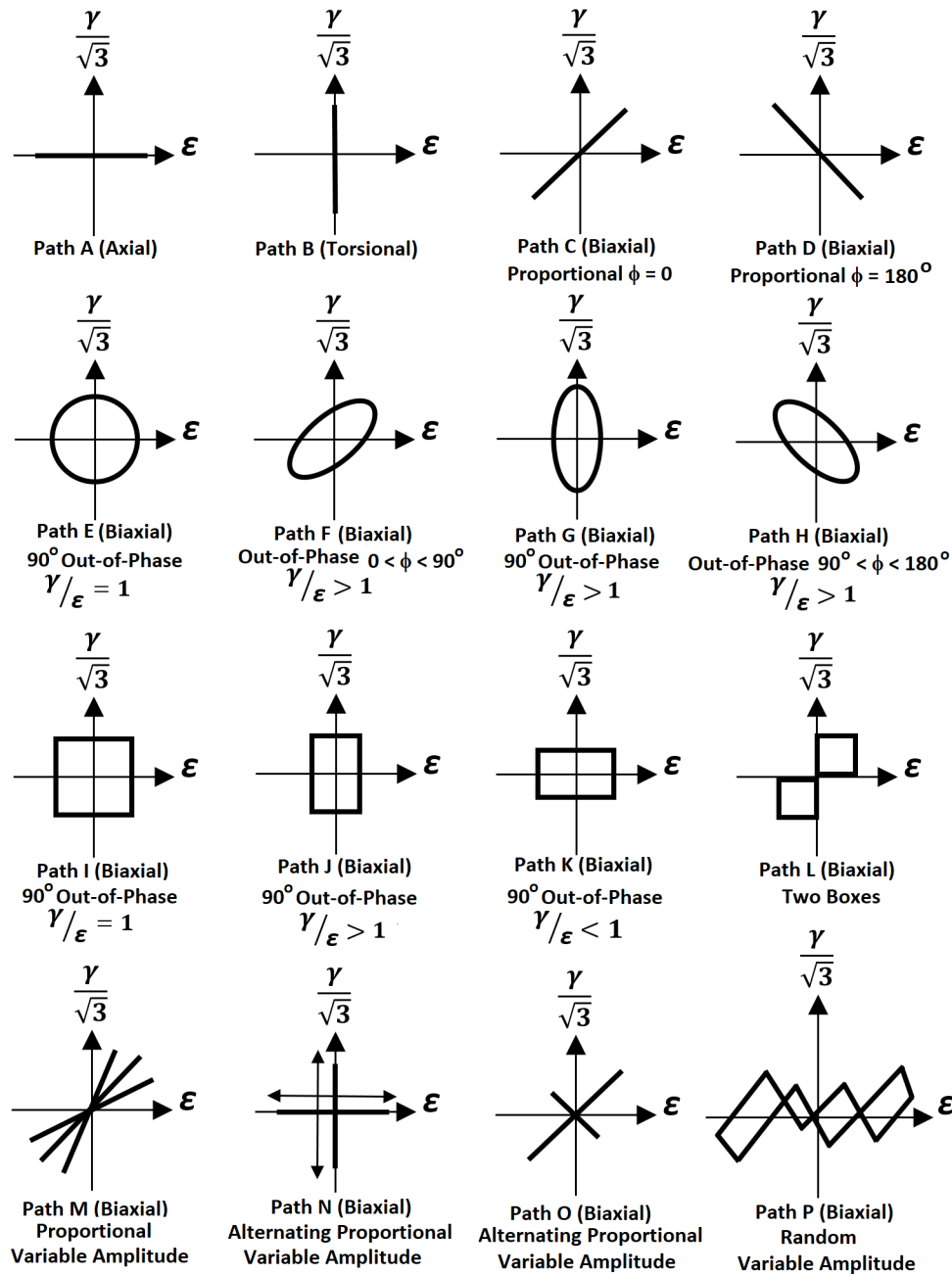


Figure 5.1: All the applied Loading paths

5.2.1 Tubular Geometries - Datasets Taken From Other Literature

Twenty circular tubes made with different metallic materials were chosen from various technical literature. Almost all the elasto-plastic mechanical properties and fatigue constants of the materials were taken from the original sources (Socie 1987, Hoffmeyer et al. 2006, Han et al. 2002, Kanazawa et al. 1979, Shang et al. 2007, Kim et al. 1999). A few torsional fatigue data were not listed in the original literature, and in these cases the corresponding uniaxial fatigue constants were used to estimate the torsional data by using von Mises definition and according to the Eqns.(5.1) (Socie & Marquis 2000, Kim et al. 2002 & Susmel 2009). Typical geometry of the tubular specimens were illustrated in Fig.(5.2). All the mechanical properties, fatigue constants of the materials

and outer/inner diameter of the tube specimens were listed in Table (5.1). Profile of the applied constant amplitude CA load signals was summarised in Table (5.2), and variable amplitude cyclic loadings were listed in Table (5.3).

$$\tau'_f = \frac{\sigma'_f}{\sqrt{3}} \quad (5.1a)$$

$$\gamma'_f = \sqrt{3} \varepsilon'_f \quad (5.1b)$$

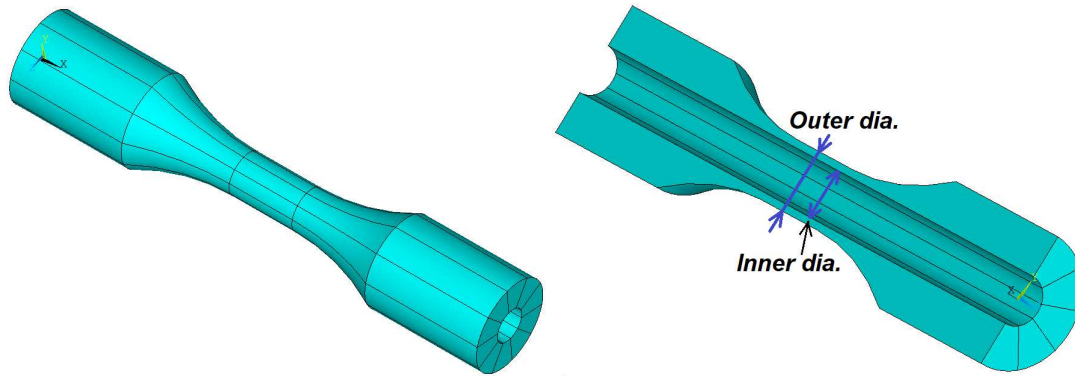
$$b_o = b \quad (5.1c)$$

$$c_o = c \quad (5.1d)$$

Where, σ'_f and ε'_f represent the fatigue strength and ductility coefficient, respectively. τ'_f and γ'_f are the shear fatigue strength coefficient and shear fatigue ductility coefficient. b and b_o are the axial and shear fatigue strength exponent. c and c_o represent the axial and shear fatigue ductility exponent, respectively.

Table 5.1: Fatigue constant of materials from other technical literatures

Mechanical properties	304 Stainless Steel (Socie 1987)	Stainless Steel (Hoffmeyer et al. 2006)	SNCM630 (Han et al. 2002)	%1 Cr-Mo-V (Kanazawa et al. 1979)	45 Steel (Shang et al. 2007)	S45C (Kim et al. 1999)
<i>Tube (mm):</i>						
<i>Outer/inner dia.</i>	16/15	41/36	12.5/10	22/16	25/21	12.5/10
<i>E (GPa)</i>	183	200	196	200	190	186
<i>G (GPa)</i>	82.8	77	77	76.9	79	70.6
<i>ν</i>	0.3	0.3	0.273	0.3	0.202	0.28
<i>σ_y (MPa)</i>	325	365	951	707	370	496
<i>σ_u (MPa)</i>	650	—	1103	805	610	770
Uniaxial Fatigue properties:						
<i>σ'_f (MPa)</i>	1000	865	1272	987	843	923
<i>b</i>	-0.114	-0.097	-0.073	-0.071	-0.1047	-0.099
<i>ε'_f</i>	0.171	0.119	1.54	1.369	0.3269	0.359
<i>c</i>	-0.402	-0.359	-0.823	-0.802	-0.5458	-0.519
<i>K' (MPa)</i>	1660	1329	1056	1113	1258	1215
<i>n'</i>	0.287	0.244	0.054	0.11	0.208	0.217
Torsional Fatigue properties:						
<i>τ'_f (MPa)</i>	709	500	858	570	559	685
<i>b_o</i>	-0.121	-0.097	-0.061	-0.071	-0.1078	-0.12
<i>γ'_f</i>	0.413	0.206	1.51	2.371	0.496	0.198
<i>c_o</i>	-0.353	-0.359	-0.706	-0.802	-0.469	-0.36
<i>K'_o (MPa)</i>	785	—	592	—	—	—
<i>n'_o</i>	0.296	—	0.05	—	—	—
Coefficient of Non-proportionality (Out of Phase):						
<i>K'_{NP} (MPa)</i>	2075	1661	1320	1391	1573	1519
<i>n'_{NP}</i>	0.287	0.244	0.054	0.11	0.208	0.217



(a) Isometric of the Tubular Specimen

(b) Longitudinal Cross Section of the Tube

Figure 5.2: Tubular Geometry

Table 5.2: Type of materials, Loading paths with Stress and Strain value (Constant Amplitude)

References	Materials	Strain Path	Phase angle δ (degree)	$\lambda = \left(\frac{\gamma_a}{\varepsilon_a}\right)$	$\varepsilon_a = \frac{\Delta\varepsilon}{2}$ (%)	$\gamma_a = \frac{\Delta\gamma}{2}$ (%)	$\sigma_a = \frac{\Delta\sigma}{2}$ (Mpa)	$\tau_a = \frac{\Delta\tau}{2}$ (Mpa)
(Socie 1987)	304 Stainless Steel	Path A	—	—	0.25	—	184	—
		Path B	—	—	—	0.476	—	109
		Path C	0	2.0	0.25	0.476	184	109
		Path L	—	1.7	0.25	0.43	365	199
(Hoffmeyer et al. 2006)	347 Stainless Steel	Path E	90	1.7	0.577	1.0	—	—
(Han et al. 2002)	SNCM630	Path G	90	1.5	0.6	0.9	—	—
		Path K	90	0.45	0.576	0.262	—	—
(Kanazawa et al. 1979)	%1 Cr-Mo-V	Path C	0	4.0	0.51	2.05	288	314
		Path D	180	1.5	0.99	1.54	528	230
		Path F	45	1.5	1.01	1.55	634	360
		Path G	90	1.5	1.02	1.54	669	366
		Path G	90	4.0	0.51	2.07	625	366
		Path H	135	1.5	1.01	1.52	674	349

5.2.2 Plain Cylinder Geometries - Datasets Taken by Running Experiments

A number of un-notched solid shaft is made with 40mm diameter of medium carbon steel 080M40. Plain specimens were machined with a versatile shape that allows the biaxial extensometer to attach and easily measure biaxial strains directly from the sample as shown in Fig.(5.4a). A gross diameter of solid specimens were $\phi 38$ mm and a length of 208 mm. An hourglass shape was used for plane specimens to maximise stresses at the centre of the plane sample, with a net diameter at the centre equals 18 mm, detail of the geometry were illustrated in Fig.(5.4b). The mechanical properties of the material was summarised in Table (5.4). An axial stabilised stress-strain curve were used to define the mechanical behaviour of the material as shown in Fig.(5.3)

Table 5.3: Type of materials, Loading paths with Stress and Strain value (Variable Amplitude)

Reference	Materials	Strain Path	Strain History							
(Shang et al. 2007)	45 Steel	Path C	$\varepsilon_a = \frac{\Delta\varepsilon}{2}$ (%)	0	±0.2	±0.4	±0.6	±0.8	±1	0
			$\gamma_a = \frac{\Delta\gamma}{2}$ (%)	0	±0.346	±0.693	±1.039	±1.386	±1.732	0
		Path E	$\varepsilon_a = \frac{\Delta\varepsilon}{2}$ (%)	0	±0.2	±0.4	±0.6	±0.8	±1	0
			$\gamma_a = \frac{\Delta\gamma}{2}$ (%)	0	±0.346	±0.693	±1.039	±1.386	±1.732	0
		Path F	$\varepsilon_a = \frac{\Delta\varepsilon}{2}$ (%)	0	±0.2	±0.4	±0.6	±0.8	±1	0
			$\gamma_a = \frac{\Delta\gamma}{2}$ (%)	0	±0.346	±0.693	±1.039	±1.386	±1.732	0
(Kim et al. 1999)	S45C	Path M	$\varepsilon_a = \frac{\Delta\varepsilon}{2}$ (%)	-0.068	±0.11	-0.15	0.15	-0.11	0.068	-0.068
			$\gamma_a = \frac{\Delta\gamma}{2}$ (%)	-0.8	0.61	-0.41	0.41	-0.61	0.80	-0.80
		Path N	$\varepsilon_a = \frac{\Delta\varepsilon}{2}$ (%)	0	0.41	-0.41	0	0	0	0
			$\gamma_a = \frac{\Delta\gamma}{2}$ (%)	0	0	0	0	-1.26	1.26	0
		Path O	$\varepsilon_a = \frac{\Delta\varepsilon}{2}$ (%)	0	0.68	-0.68	0	0.28	-0.24	0
			$\gamma_a = \frac{\Delta\gamma}{2}$ (%)	0	1.48	-1.38	0	-0.57	0.63	0
		Path P	$\varepsilon_a = \frac{\Delta\varepsilon}{2}$ (%)	0	0.10	0.30	0.43	0.32	0.06	-0.12 [†]
			$\gamma_a = \frac{\Delta\gamma}{2}$ (%)	0	0.66	-0.66	0.27	1.0	-0.66	0.49 [†]
			$\varepsilon_a = \frac{\Delta\varepsilon}{2}$ (%)	-0.35	-0.43	-0.23	-0.05	0	—	—
			$\gamma_a = \frac{\Delta\gamma}{2}$ (%)	-1.0	-0.47	0.84	-0.33	0	—	—

[†]Continued in the following ε_a or γ_a line.

Table 5.4: Mechanical properties of the tested material

Ultimate tensile strength, σ_{UTS}	700 MPa
Yield strength, σ_y	450 MPa
Young's modulus, E	210 GPa
Poisson ratio, ν_e	0.30

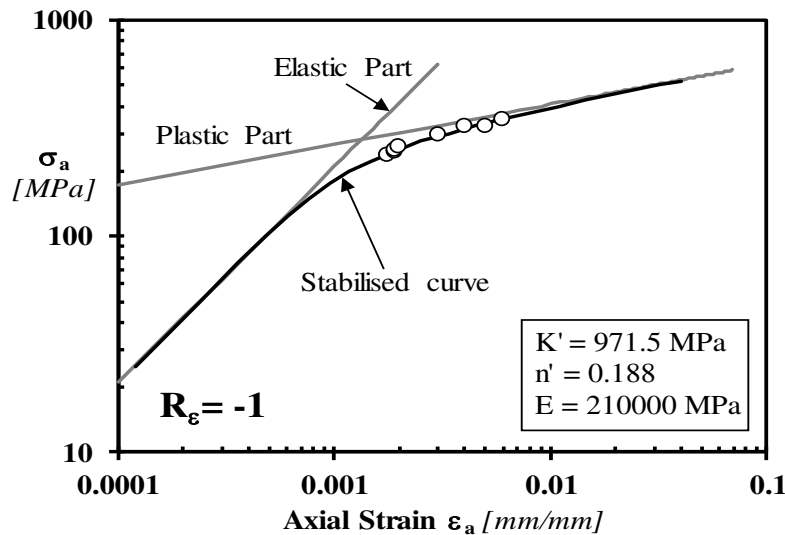
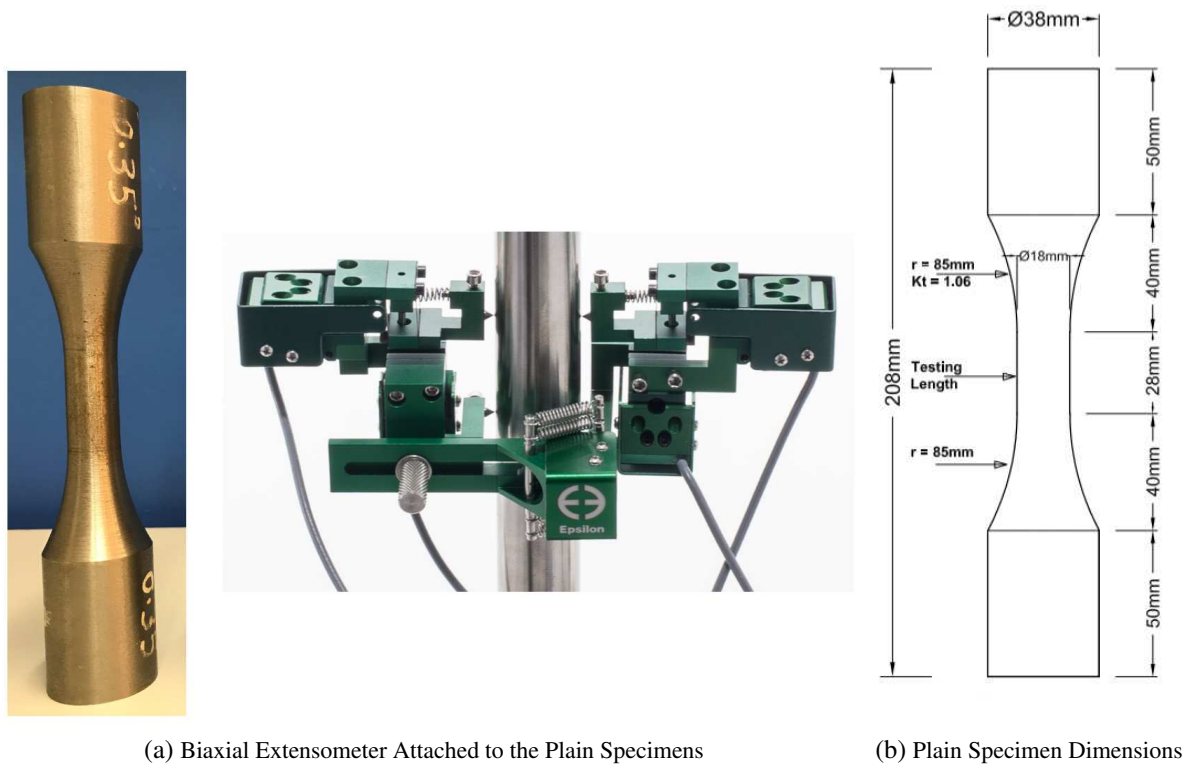


Figure 5.3: Stabilized Uniaxial Stress-Strain Curve



(a) Biaxial Extensometer Attached to the Plain Specimens

(b) Plain Specimen Dimensions

Figure 5.4: Dimensions of the Specimen

5.3 Testing Procedure

Fatigue tests were performed on all specimens by using a closed-loop servo-hydraulic MTS axial-torsional testing machine. All specimen groups were tested under strain controlled system. A biaxial extensometer was used to control the test. A sine signal was used as a testing waveform. In order to consider mean strain effect, various ratio of minimum strain amplitude to the maximum amplitudes (R) were used. As a boundary condition, the specimens were fixed between two Collet Grips and fatigue loads were applied at one end and the other end keep fixed. All tests were performed at room temperature. All data were counted through the signals received from the multi-axial actuators connected to a computer system. Enough stress and strain points were recorded per each cycle to plot a hysteresis loops. Fatigue failure was assumed to be happened when stiffness of materials drop by 5%. The Tables (5.2, 5.3 & 5.5) summarises the specimen loading conditions.

5.4 Formulating the Finite Element Model

In order to implement a computational process, a tubular and cylindrical specimens were modelled by using a three dimensional finite element ANSYS-Mechanical design language APDL®, a SOLID185 cubic with 8-node structural element being employed to define the geometry as shown in Fig.(5.5). A multi-linear kinematic hardening rule was used to define the elasto-plastic

Table 5.5: Summary of the applied Stress and Strain on the Plain Specimens

Specimen Symbols	Load Ratio	Out of Phase degree	$\varepsilon_{x,a}$	$\varepsilon_{x,m}$	$\gamma_{xy,a}$	$\gamma_{xy,m}$	Loading Path
PSUCAZMS7	-1	0	0.005	0	0	0	
PSTCAZMS7	-1	0	0	0.0079	0	0	
PSBCAZMSIph1	-1	0	0.00274	0	0.00457	0	
PSBCAZMSOoPh2	-1	90	0.00258	0	0.00448	0	
PSBCANZMSIph1	0	0	0.003	0.003	0.0046	0.0046	
PSBCANZMSOoPh2	0	90	0.00245	0.00245	0.0039	0.0039	

cyclic deformation of the materials, and the mechanical properties of the materials were described via the axial stabilised stress versus strain curve (Lee et al. 2005). To check the element meshing size, density of the mesh was gradually re-fined to a level at which linear-elastic field stresses were not influenced by the mesh density. To simulate a boundary condition similar to the experiments, one end of the specimens were fixed with zero displacement and rotation, and the cyclic loads were applied to the other end and expressed in terms of axial displacements in (mm) and/or rotations in (angle) as illustrated in Fig.(5.6). In more detail, the simulations were performed by considering the applied load histories in terms of strains, and the corresponding elasto-plastic stresses were determined numerically and physically. To model the results under constant amplitude load history, six complete cycles were run in the FE model so as to ensure that the numerical solution of the materials had reached a stabilised configuration level for the stress-strain response. For the variable amplitude loading conditions, the local elasto-plastic stresses/strains were estimated by simulating two blocks of loading (each loading block equals 50 cycles). The uniaxial elasto-plastic stress-strain curves were plotted using the Ramberg-Osgood equation Eqn.(5.2) and these curves were then used to define the elasto-plastic properties of the materials (Lee et al. 2005).

$$\frac{\Delta\varepsilon}{2} = \frac{\Delta\sigma}{2E} + \left(\frac{\Delta\sigma}{2K'} \right)^{\frac{1}{n'}} \quad (5.2)$$

K' , n' are the cyclic strength coefficient and the cyclic strength exponent, respectively.

The corresponding elasto-plastic stress histories were estimated by using the model developed by Jiang & Sehitoglu (1996). In case of non-proportional cyclic loading, the cyclic strength coefficient K'_{NP} , and cyclic strain hardening exponent n'_{NP} were determined using the following equations (Socie & Marquis 2000):

$$K'_{NP} = 1.25.K_{NP} \quad (5.3a)$$

$$n'_{NP} = n' \quad (5.3b)$$

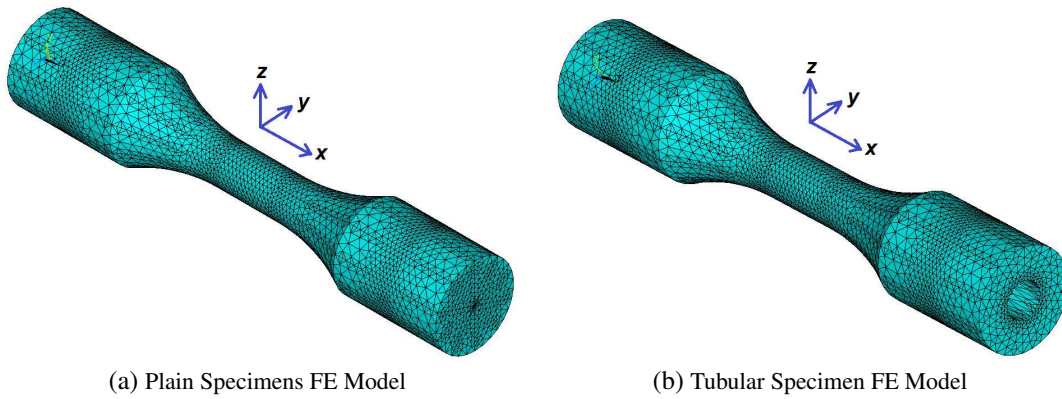


Figure 5.5: Three Dimensional Finite Element Model of Plain Specimens by Using ANSYS

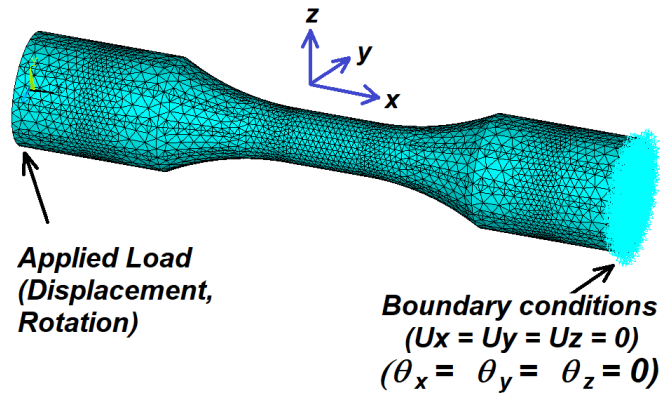


Figure 5.6: Boundary conditions and applied loads (Displacement and Rotation)

5.5 Results and Comparison

As summarised in section (5.1), calculating the local elasto-plastic stress-strain histories with sufficient accuracy can result in a reliable fatigue assessment. From a validation point of view, this chapter has described a novel application of the formalised elasto-plastic FE model to estimate the local elasto-plastic stress-strain state of a material under cyclic loading obtained from stress/strain-controlled tests performed using different loading values, paths and amplitudes. The diagrams reported in subsections (5.5.1, and 5.5.2) summarise the accuracy of the developed ANSYS® model

in estimating the cyclic stress versus strain history. According to the validation exercise, and based on the well-documented hysteresis loop, the following results were concluded:

5.5.1 Validation by Using Tubular Specimens

Since the results taken from the technical literature, hysteresis loop graphs presented in Figs.(5.7, 5.8, 5.9, 5.10, 5.11, & 5.12) was drawn to compare the experiment results, numerical simulations ran by using FE code ANSYS® and Jiang & Sehitoglu (1996) analytical method under CA and VA fatigue loading. All the sequences illustrated that the predicted curves agreed very well with the experimentally reported stress-strain responses and hysteresis loops from the Jiang model. The maximum error in terms of stress amplitude can be seen in the order of 15%. That mean, the maximum values of the corresponding stress amplitudes in the CA and VA cycles well within a scatter band (error factor) of two, Figs.(5.13, & 5.14).

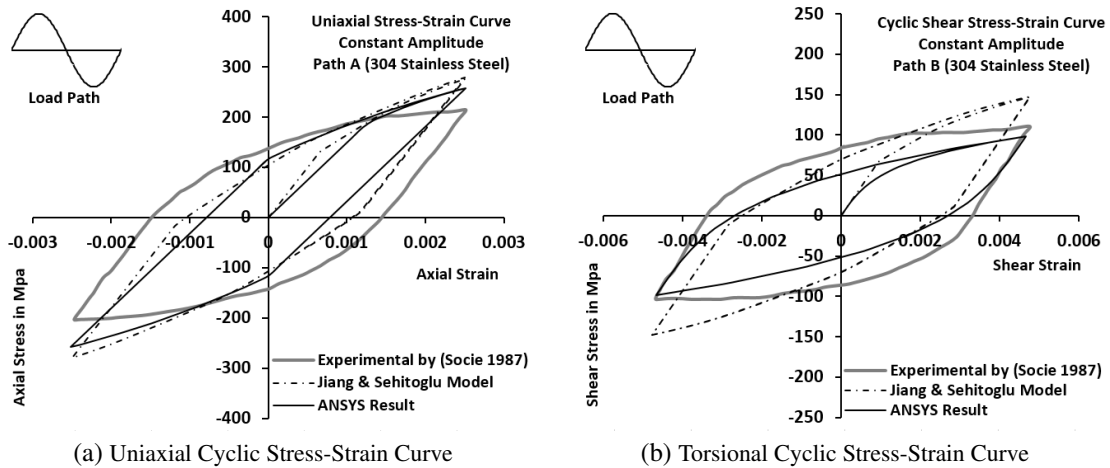


Figure 5.7: Uniaxial and Pure Torsion Hysteresis loop

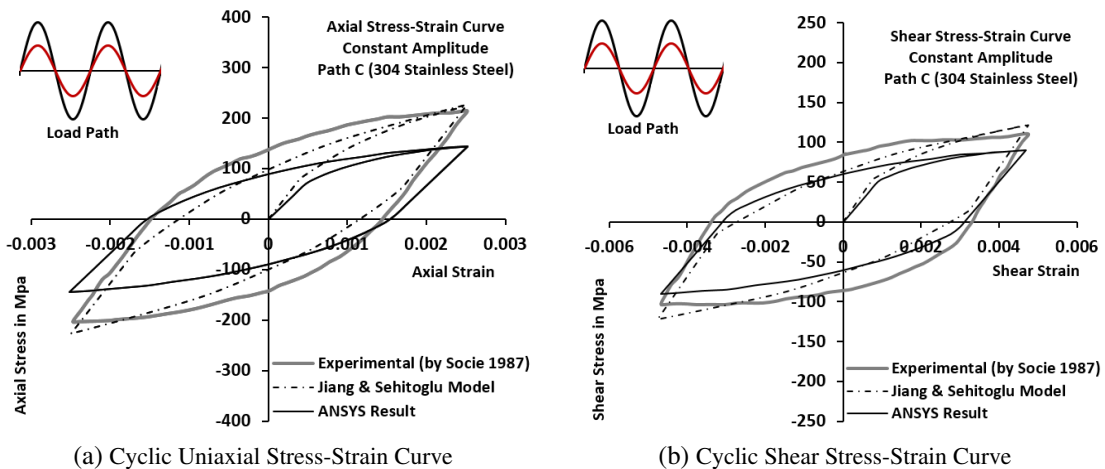


Figure 5.8: Axial and Shear Stress-strain Hysteresis loop - Loading Path C

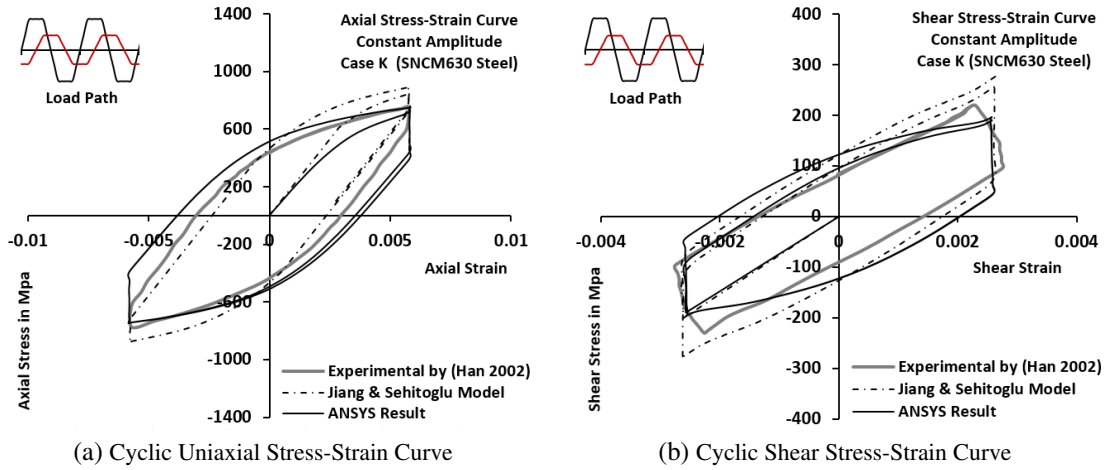


Figure 5.9: Axial and Shear Stress-strain Hysteresis loop - Loading Path K

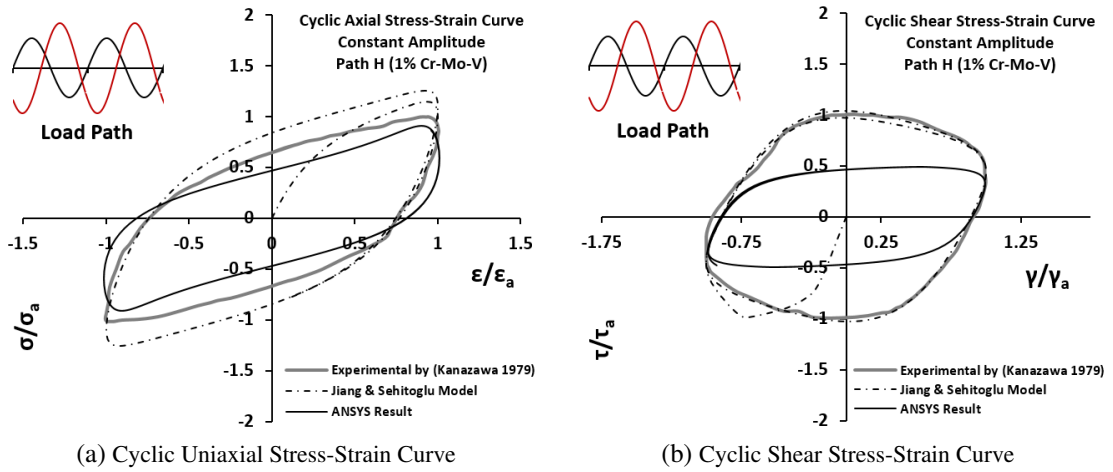


Figure 5.10: Axial and Shear Stress-strain Hysteresis loop - Loading Path H

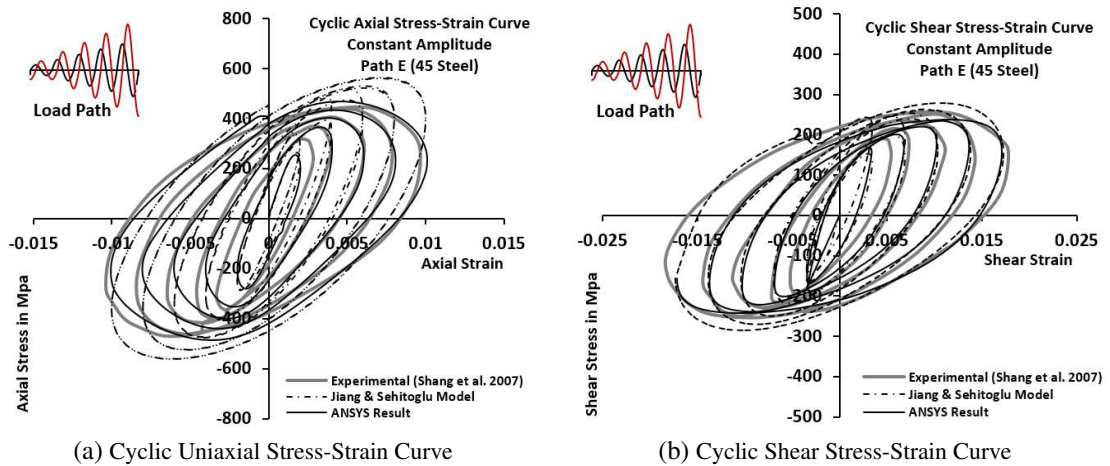


Figure 5.11: Axial and Shear Stress-strain Hysteresis loop - Loading Path E

5.5.2 Validation by Using Plain Specimens

For the sake of validity, Ten plain specimens were tested experimentally and also analysed theoretically under different loading conditions reported in Table. Hysteresis loops were built based on 6

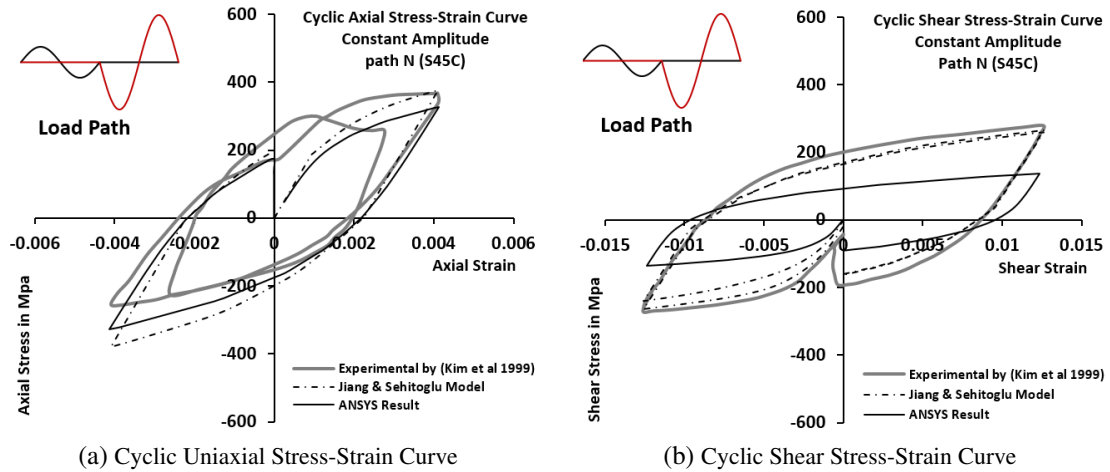


Figure 5.12: Axial and Shear Stress-strain Hysteresis loop - Loading Path N

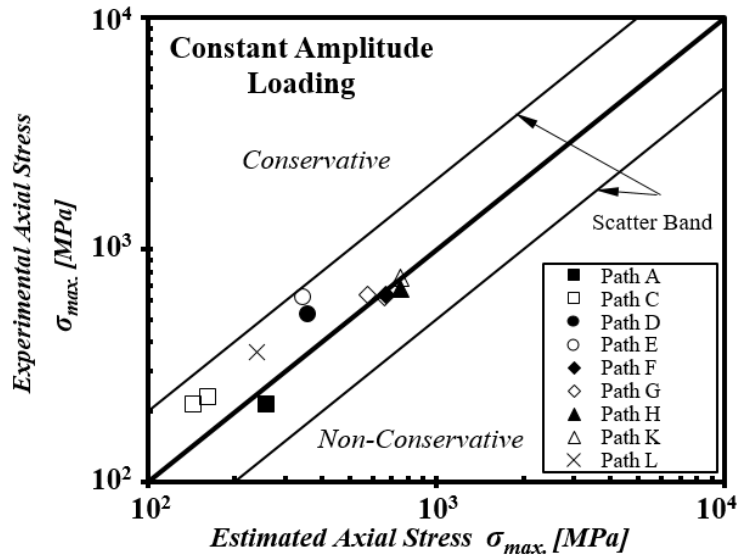


Figure 5.13: The Predicted versus Experiment Elasto-plastic Stresses - Constant Amplitude Loading

virtual cycles for CA loading and by plotting 50 cycles (one block of loading) for the VA. The hysteresis loops were illustrated in Figs.(5.15, 5.16, 5.17, 5.18, 5.19, 5.20, 5.21, 5.22, & 5.23). The charts make it evident that the predicted local elasto-plastic cyclic σ - ϵ and τ - γ are fully support and are in very remarkable agreement with the experimental results.

5.6 Conclusions

The Finite Element model was analysed using ANSYS® software to find the corresponding stress-strain state at any point on the geometry. Since no significant difference was found when the predicted results were compared with the experimental outcome, that proved the developed FE model is robust and computationally efficient to estimate the local elasto-plastic stress-strain of a component. Further, the developed model gave an excellent correlation when plotting the elasto-plastic hysteresis loop by using both the numerical and analytical approach. The present chapter

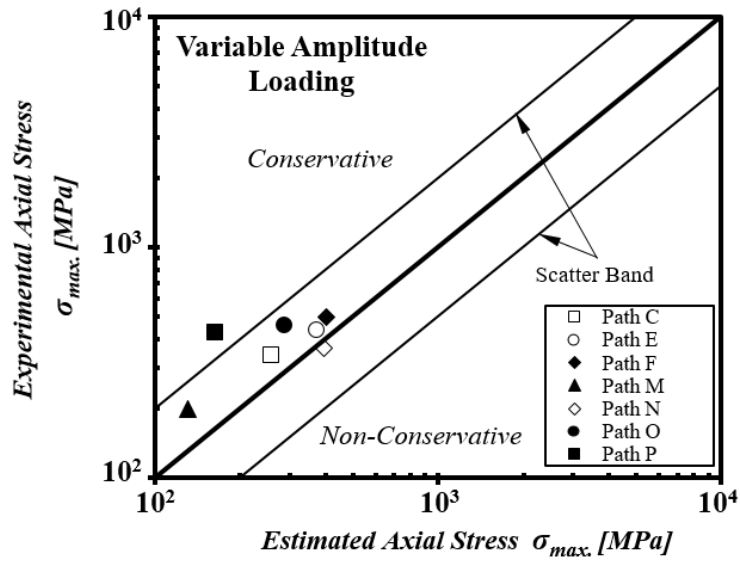


Figure 5.14: The Predicted versus Experiment Elasto-plastic Stresses - Variable Amplitude Loading

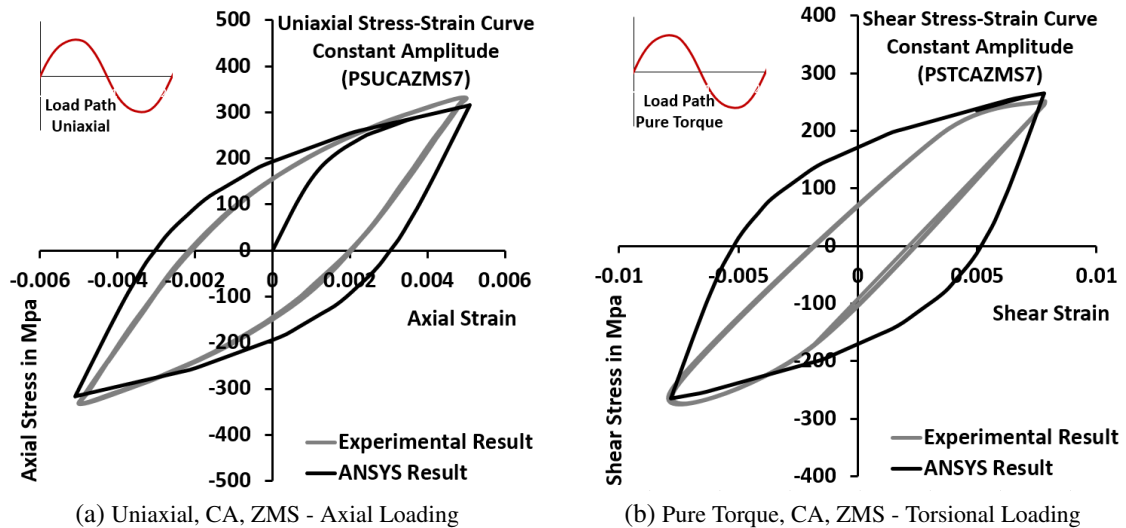


Figure 5.15: Hysteresis Loop - Uniaxial, Constant Amplitude, Zero Mean Stress Fatigue Loading

has therefore demonstrated that ANSYS® is capable to correctly estimate the elasto-plastic stress-strain histories of metallic materials for a wide variety of problems and loading conditions. For all the example problems considered in this chapter, solutions have been found that are more accurate than those obtained using previously proposed numerical analysis techniques. This result is surprising while only the stabilised uniaxial stress/strain curve is used in ANSYS® to model the elasto-plastic behaviour of materials. However, the best available numerical method of Jiang & Sehitoglu (1996) need both uniaxial and torsional stabilised stress-strain curve to model elasto-plastic response of materials.

To conclude, the predicted elasto-plastic hysteresis loops were compared with their experimentally determined counterparts and the results from the model proposed by Jiang & Sehitoglu (1996) so as to verify the proposed FE model. This extensive exercise showed that the proposed FE model has the ability to describe the local elasto-plastic deformation features of materials under different

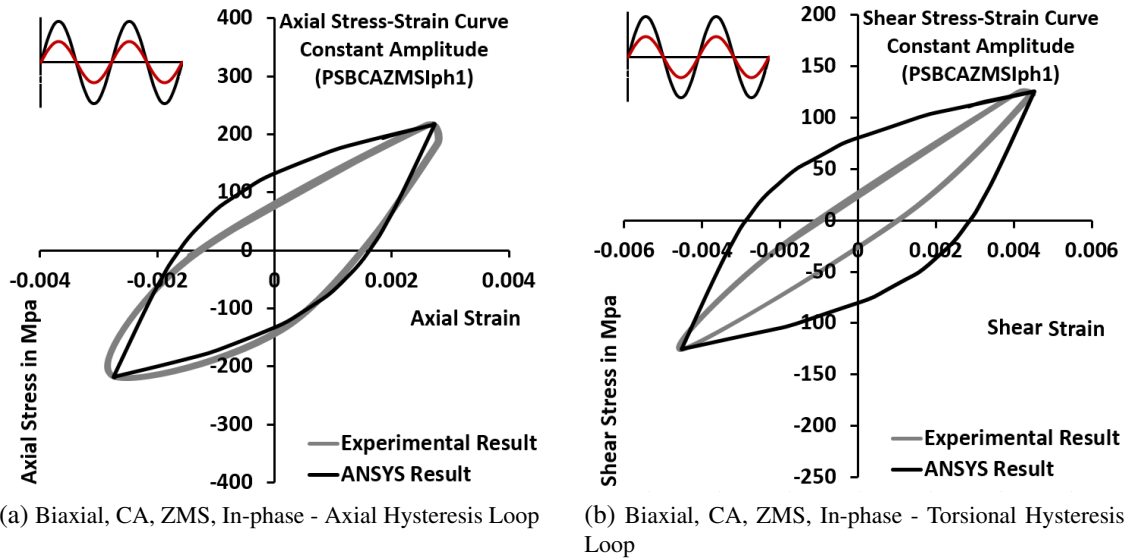


Figure 5.16: Hysteresis Loop - Biaxial, Constant Amplitude, Zero Mean Stress, In-phase Fatigue Loading

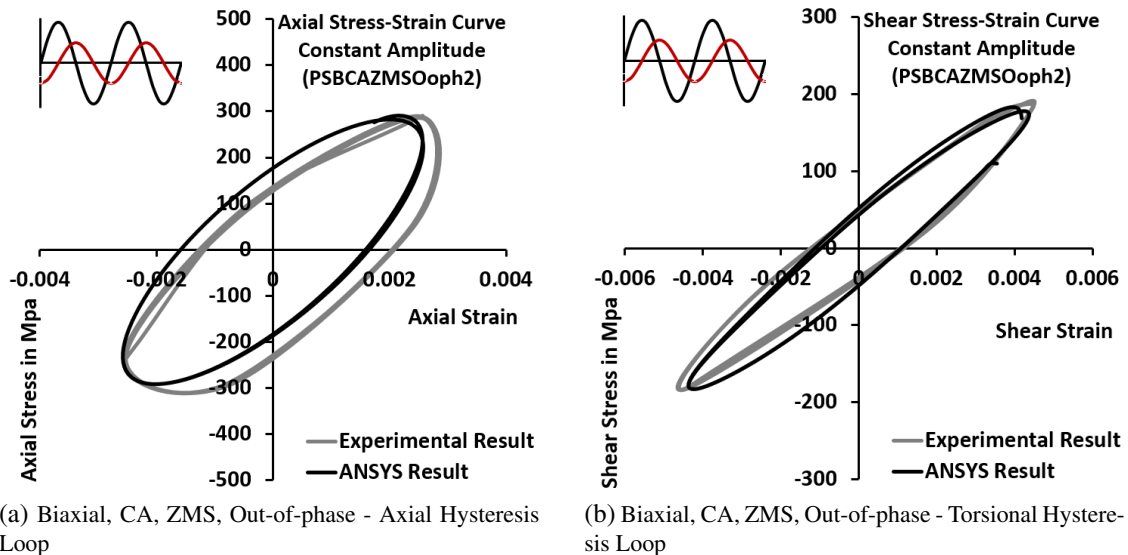
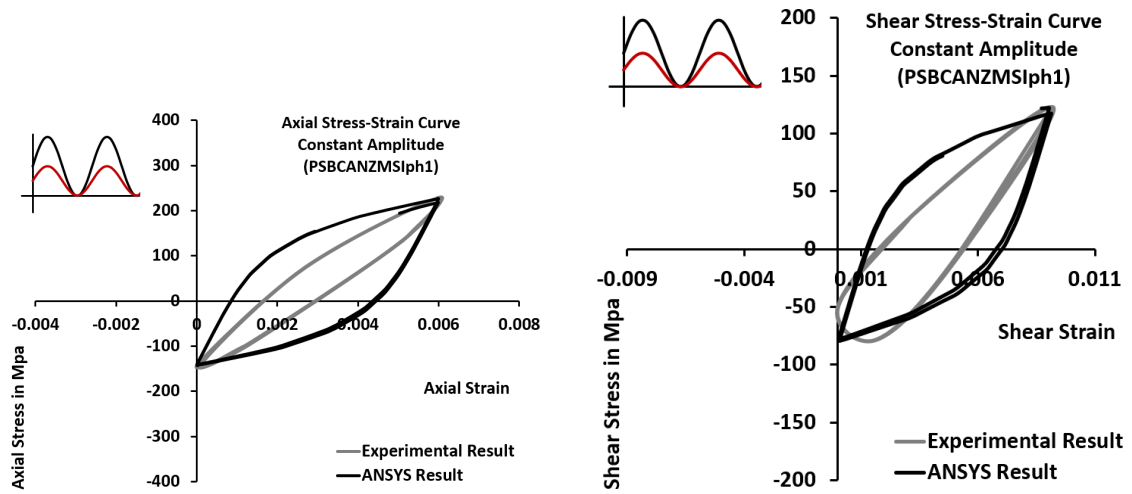


Figure 5.17: Hysteresis Loop - Biaxial, Constant Amplitude, Zero Mean Stress, Out-of-phase Fatigue Loading

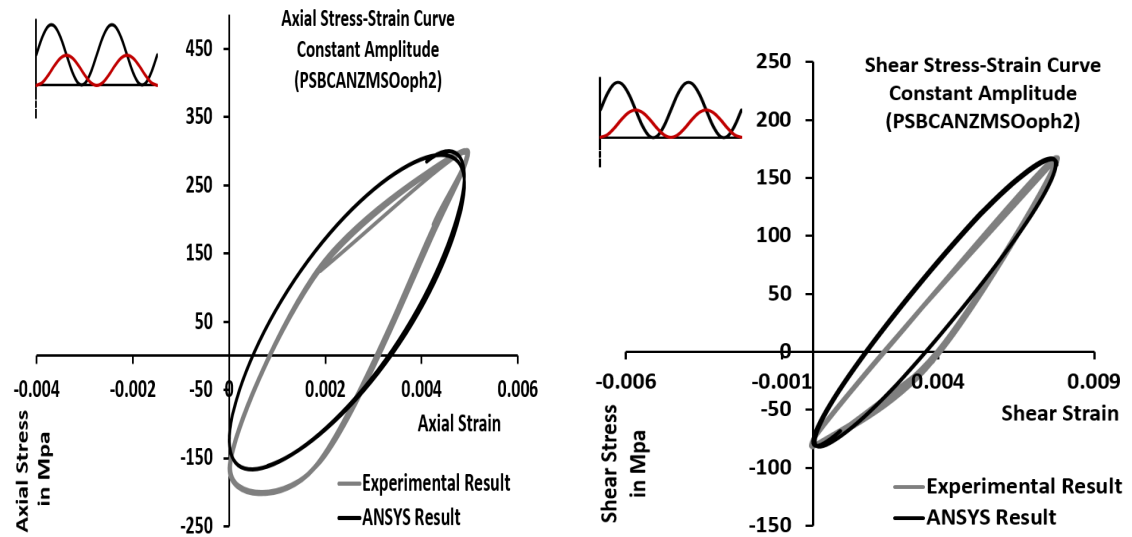
cyclic loading conditions. The last point that deserves to mention is different material properties lead to different behaviours and responses under fatigue loadings. Consequently, a slight discrepancy can be observed between the predicted stress-strain sequences and their experimental counterparts. These differences are due to inconsistencies in the micro-structure features of the material and theoretical background/mathematical formulation of the finite element solution (Socie 1987).



(a) Biaxial, CA, NZMS, In-phase - Axial Hysteresis Loop

(b) Biaxial, CA, NZMS, In-phase - Torsional Hysteresis Loop

Figure 5.18: Hysteresis Loop - Biaxial, Constant Amplitude, Non-Zero Mean Stress, In-phase Fatigue Loading



(a) Biaxial, CA, NZMS, Out-of-phase - Axial Hysteresis Loop

(b) Biaxial, CA, NZMS, Out-of-phase - Torsional Hysteresis Loop

Figure 5.19: Hysteresis Loop - Biaxial, Constant Amplitude, Non-Zero Mean Stress, Out-of-phase Fatigue Loading

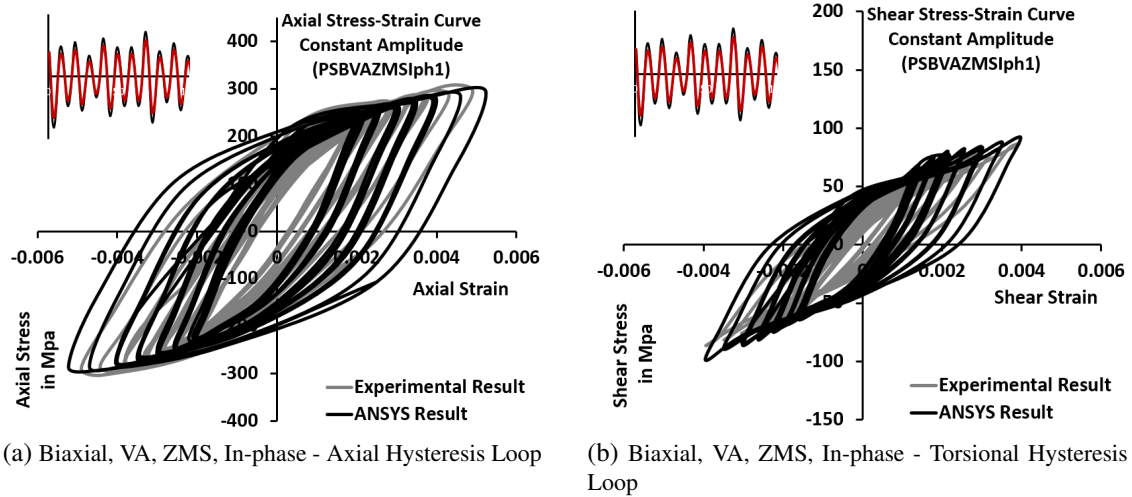


Figure 5.20: Hysteresis Loop - Biaxial, Variable Amplitude, Zero Mean Stress, In-phase Fatigue Loading

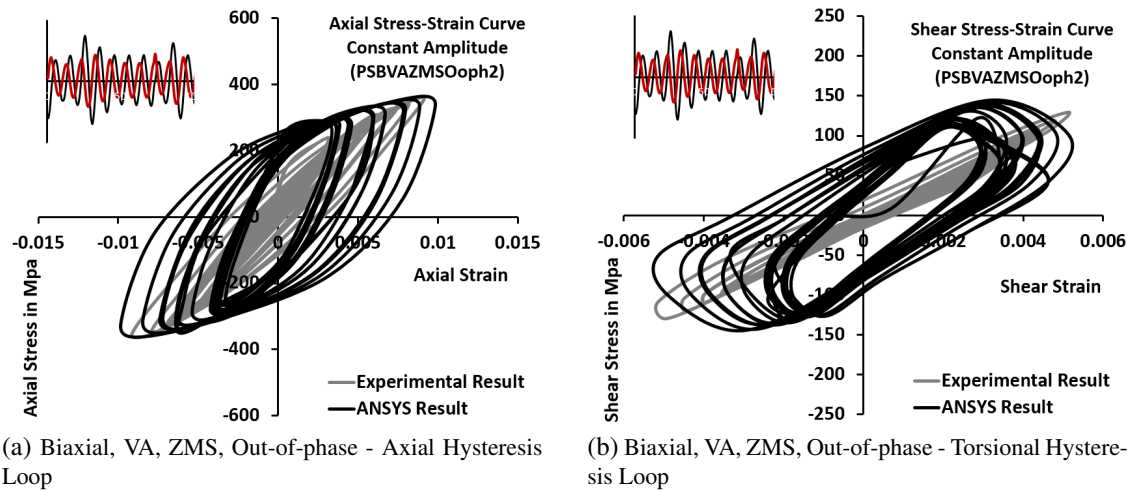


Figure 5.21: Hysteresis Loop - Biaxial, Variable Amplitude, Zero Mean Stress, Out-of-phase Fatigue Loading

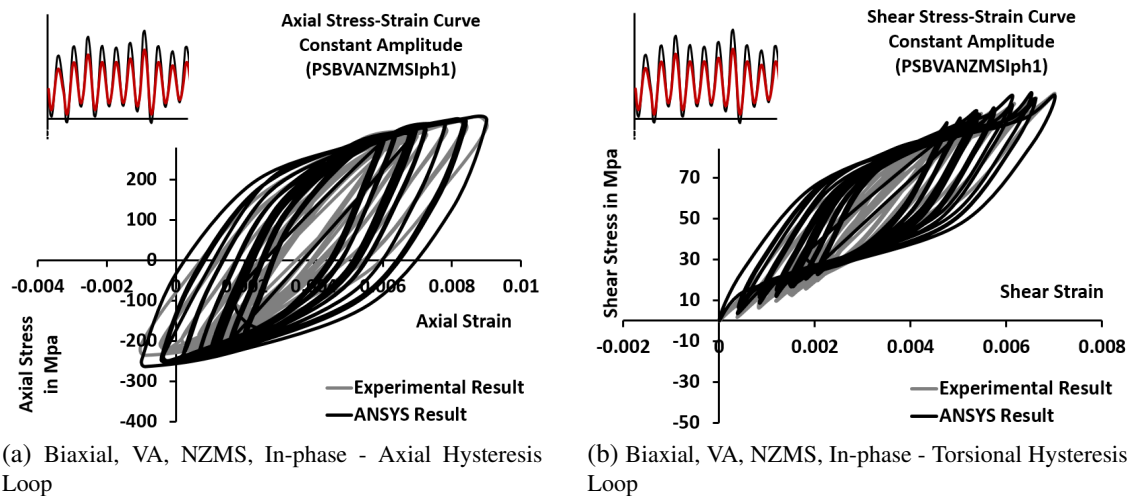
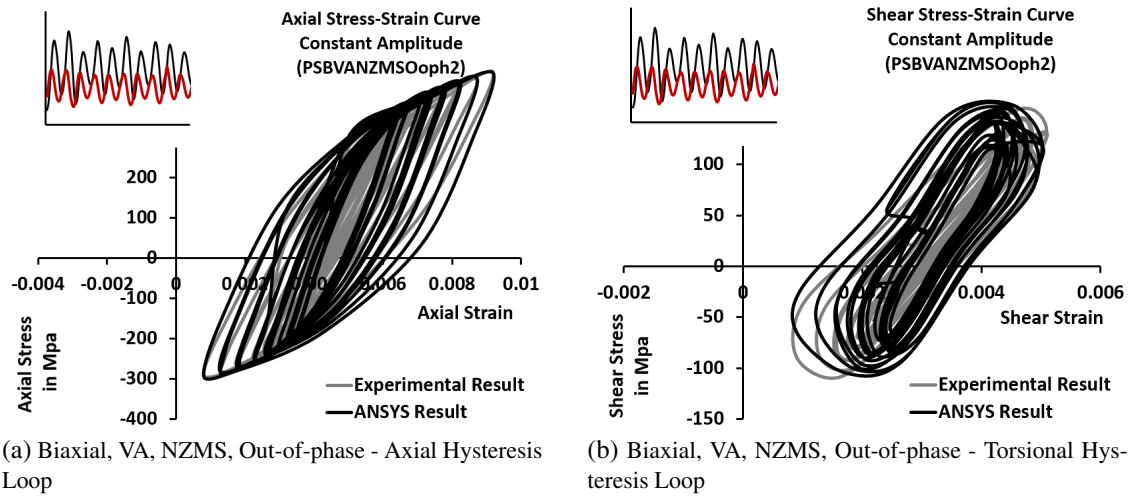


Figure 5.22: Hysteresis Loop - Biaxial, Variable Amplitude, Non-Zero Mean Stress, In-phase Fatigue Loading



(a) Biaxial, VA, NZMS, Out-of-phase - Axial Hysteresis Loop

(b) Biaxial, VA, NZMS, Out-of-phase - Torsional Hysteresis Loop

Figure 5.23: Hysteresis Loop - Biaxial, Variable Amplitude, Non-Zero Mean Stress, Out-of-phase Fatigue Loading

Chapter 6

Results and Discussion

6.1 Introduction

According to the overview provided by our state of knowledge of fatigue control, in many applications, components or structural elements subject to a cyclic load that fail even at stress amplitudes below the yield strength of the materials. In addition, developments in industry have increased the focus on investigating multiaxial fatigue in complex geometries. Recent evidence agrees that an accurate model of the complex behaviour of notch geometries against uniaxial/multiaxial fatigue load and involving mean stress/strain and a degree of nonproportionality of the applied load requires the introduction of a large number of parameters. This creates a barrier for practitioners and engineers who have no background in such approaches. More importantly, incorrect programming of even one of these parameters can cause unexpected results and erroneous solutions, leading to unsafe analysis and design. Despite the great effort made by many researchers, and the considerable practical importance for the scientific community, to the best of the author's knowledge, the area of complex multiaxial fatigue of notches combining all the above-mentioned parameters and complexities in one model has not yet resulted in a universally accepted definition. In this research, much effort has been expended to determine the nature of the multiaxial fatigue damage problem with notch geometries and to propose a relatively simple theory encompassing an algorithm that utilises few fatigue parameters. This work is an attempt to integrate cyclic plasticity into the fatigue damage modelling. A key element in the proposed model is the assumption that both cyclic elasticity and plasticity are the cause of fatigue damage. This hypothesis assumes that fatigue cracks initiate on the plane where the shear strain amplitude reaches its maximum value, known as the critical plane (Jiang et al. 2007). The proposed approach and methodology were discussed in chapter (3).

In order to validate the formalised method in this research, multiaxial fatigue tests were conducted in chapter (4) on 132 specimens made from an unalloyed medium-carbon steel EN8 (080E40) steel shaft under complex cyclic loading at room temperature and covering both constant and variable amplitude loading conditions. Fatigue failure was defined to occur when there was a drop in the stiffness range of the material by 5%. Various loading paths and amplitudes were examined, including push-pull, torsion, in-phase and out-of-phase, with different multiaxiality and phase angles.

The validation process physically confirmed that the formalised approach described the multi-axial fatigue damage of complex geometries well. According to the comparison presented in the subsequent sections, the proposed approach provided fatigue life predictions that are in very reasonable agreement with the experimental observation. The developed model is generally accurate for the design of notch geometries against uniaxial/multi-axial proportional/nonproportional, constant/variable amplitude cyclic loading. One of the most attractive features of the formalised technique is that it is based on the description of local stress-strain states inside the material. This means that the proposed approach remains accurate, no matter how complex the external applied loads, because the model is backed up by the internally-developed stress-strain state inside the geometry being assessed. The work of this research has been restricted to low-cycle and/or mid-range fatigue regions. Accordingly, the force levels used in the experiments were taken fairly high in order to keep the fatigue lives in the range of low to intermediate cycle fatigue.

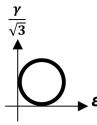
6.2 The Index Factor (Stress Ratio ρ) and (ρ_{limit})

As mentioned in section (2.5.2), the Manson-Coffin Curve was modified to consider the influence of mean stress and degree of nonproportionality of the applied load (Susmel 2009). The modification is based on a factor called Index Factor (*stress ratio* ρ). According to the modification principle, the Manson-Coffin Curve is moved upward and downward to consider the detrimental effect of mean stress and phase shift of the applied multi-axial load by considering the index factor ρ . Such a stress ratio is defined by the Equ.(2.3). Basically, there is a direct relation between fatigue damage and ρ value, when fatigue damage increases, stress ratio ρ increases and number of cycles to failure decrease. According to the proposed approach in this research work and experimental validation, each material has a maximum index factor called index limit ρ_{limit} that is used in fatigue evaluation if the numerically determined ρ value greater than the ρ_{limit} . In more detail, any material under cyclic loading, the calculated stress ratio ρ need to be lower than the stress-ratio limit ρ_{limit} , otherwise the ρ_{limit} should be considered in the numerical fatigue estimation. In this research, the results of the numerical simulation indicate that using any ρ value greater than the ρ_{limit} can cause an inverse in the Modified Manson-Coffin Curve as shown in Fig.(6.1) and the fatigue evaluation by using any ρ value beyond the ρ_{limit} is not correlates with the test data satisfactorily.

According to the state of the art explained in section (2.5.2),the index factor limit (ρ_{limit}) is determined by running an appropriate experiments. In order to find the index factor limit ρ_{limit} of the evaluated material in this research, a plain specimen was tested under biaxial CA tension-torsion complex fatigue load with 90° phase shift in the loadings and involving the mean stress. Results of the experiment presented in Table (6.1).

Then, an index factor was assumed and by using the modified Manson Coffin Equation (Eqn.2.3), numerical number of cycles to failure was determined. According to the trail and error calculation, a value of ρ_{limit} was determined by fitting the estimated number of cycles to failure $N_{f.e}$ equals the experiments N_f .

Table 6.1: Experimental Test to Find the Material Index Factor Limit ρ_{limit}

Specimen Symbols	Load Ratio [†]	$\varepsilon_{x,a}$	$\varepsilon_{x,m}$	$\gamma_{xy,a}$	$\gamma_{xy,m}$	N_f^\dagger (Cycles)	ρ_{limit}^\dagger	$N_{f.e.\rho_{limit}}^\dagger$ (Cycles)	Loading Path
PSBCANZMSOoPh2 [†]	0	0.00245	0.00245	0.0039	0.0039	1,356	1.70	1,356	

[†] PSBCANZMSOoPh: Plane Sample, Biaxial / Constant Amplitude, None Zero Mean Strain, OoPh: Out of Phase
[†] Load Ratio, $R = \frac{\varepsilon_{a,min}}{\varepsilon_{a,max}}$, [†] N_f : Number of Cycles to failure at 5% axial stiffness drop, [†] ρ_{limit} : Estimated index factor limit
[†] $N_{f.e.}$: Estimated Number of Cycles to failure by Using ρ_{limit}

6.2.1 Numerical Calculation to Find the Index Factor Limit (ρ_{limit}) by Using Experiments:

In order to find the stress ratio limit ρ_{limit} , a plain specimen with symbol (PSBCANZMSOoPh2) was tested in the laboratory under fatigue loading, experimental number of cycles to failure N_f was recorded at 5% drop in the axial stiffness of the specimen, and equals 1,356 cycles. Alongside experiments, the same specimen was modelled by using the validated finite element FE method. The FE model was post-proceeded with ANSYS® software to find the corresponding elasto-plastic stress $\sigma(t)$ and strain $\varepsilon(t)$ histories on the outer surface of the plain specimen by using the same experimental applied fatigue load presented in Table (6.1). As soon as the infield stress/strain states were known, then by using the re-formulated Maximum Variance Method MVM presented in section (3.5.1), orientation of the critical plane and shear strain amplitude γ_a on the critical plain were determined. The orientation angles and shear strain amplitude relative to the critical plane were found and equals:

$$\phi = 0, \quad \theta = 45, \quad \alpha = 0, \quad \text{and} \quad \gamma_a = 0.00393.$$

Then, the experimental number of cycles to failure $N_f=1356$ cycles and the determined maximum shear strain amplitude γ_a relative to the critical plane was used to estimate the ρ_{limit} by using the Modified Manson-Coffin equation ($\gamma_a = \frac{\tau_f'(\rho)}{G}(2N_f)^{b(\rho)} + \gamma_f'(\rho).(2N_f)^{c(\rho)}$). Based on the numerical calculations, and for the tested material in this research, the index factor limit equals $\rho_{limit} = 1.70$.

6.3 Determining the Critical Damage by Using Experimental Results

As pointed out in chapter (3), D_{cr} was found by testing four plane specimens under variable amplitude fatigue loading with in-phase/out-of-phase and zero/non-zero mean stresses. According to the outcome of the experiments performed in this research, the material failed under fatigue when the critical damage D_{cr} was nearly equal unity, as shown in Table 6.2. Consequently, based

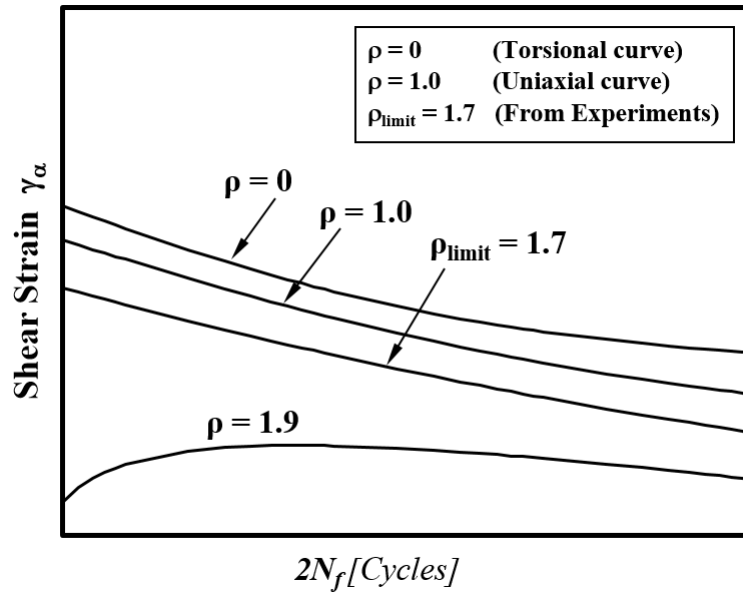


Figure 6.1: The Modified Manson-Coffin Curve for Different ρ values and ρ_{limit}

on the experimental result and the previous literature (Hua & Socie 1985), the critical damage was assumed to be constant for all specimens under different loading levels and equals one.

Table 6.2: Experimental fatigue test of plain samples under VA to determine the experimental critical damage D_{cr}

No.	Specimens	$R = \frac{\sigma_{a,min}}{\sigma_{a,max}}$	$\varepsilon_{x,a-max}$ mm/mm	$\varepsilon_{x,m}$ mm/mm	$\gamma_{xy,a-max}$	$\gamma_{xy,m}$	$N_{f,e}$	$D_{cr,exp}$
1	PSBVAZMSIph1 [†]	-1	0.005	0	0.0037	0	14,936	1.12
2	PSBVAZMSOoph2	-1	0.0037	0	0.0021	0	9,986	0.778
3	PSBVANZMSIph1	0	0.0045	0.0045	0.0035	0.0035	10,806	1.15
4	PSBVANZMSOoph2 [†]	0	0.0046	0.0046	0.0025	0.0025	8,926	1.11
Average $D_{cr,exp} =$								1.04

[†]PSBVAZMSIph1 : Plain Sample Biaxial Variable Amplitude Zero Mean Stress In-phase 1

[†]PSBVANZMSOoph2 : Plain Sample Biaxial Variable Amplitude Non-Zero Mean Stress Out of phase 2

6.4 Validating the Strain-Based Algorithm and Matlab Code

In the strain-based approach, one of the key steps is finding the orientation of the critical plane. This can sometimes be extremely time-consuming, particularly when complex load histories are involved. The current capability of computers and software, however, has improved the efficiency and accuracy of solving complex equations within a limited time. In this research, a Matlab script was created to evaluate the multiaxial fatigue damage of materials under complex uniaxial/multiaxial fatigue load. The proposed Matlab code is capable of solving the most complex load histories within a short period of time.

The proposed Finite Element ANSYS model that was validated in chapter (5), in conjunction with the developed Matlab code presented in Appendix-A can be safely used to analyse and evaluate fatigue damage in complex geometries subject to multiaxial sequential load histories. In more

detail, once the local stress-strain state at a critical location inside the material is quantified by taking advantage of the validated FE model, the Matlab code can be used to find the orientation of the most damaging plane (the critical plane) experiencing the maximum shear strain amplitude, and thence to determine the magnitude of the normal/shear stress/strain amplitudes relative to the critical plane. The developed computer code (Matlab script) was validated by testing three plane specimens against multiaxial complex fatigue load. The validation presented in Table (6.3) and Fig.(6.2) makes it clear that there is good consistency between the estimated number of cycles to failure $N_{f,e}$ calculated by the formalised Matlab script and the results from both experiments N_f and Socie & Marquis (2000) criterion $N_{f,Socie}$. The Socie & Marquis (2000) concluded that by using a static equilibrium, a stresses/strains value on a plane with angle equals θ can be determined by the definition presented in Eqns.(6.1).

$$\sigma_\theta = \frac{\sigma_x + \sigma_y}{2} + \frac{\sigma_x - \sigma_y}{2} \cos(2\theta) + \tau_{xy} \sin(2\theta) \quad (6.1a)$$

$$\tau_\theta = \frac{\sigma_x - \sigma_y}{2} \sin(2\theta) - \tau_{xy} \cos(2\theta) \quad (6.1b)$$

$$\varepsilon_\theta = \frac{\varepsilon_x + \varepsilon_y}{2} + \frac{\varepsilon_x - \varepsilon_y}{2} \cos(2\theta) + \frac{\gamma_{xy}}{2} \sin(2\theta) \quad (6.1c)$$

$$\frac{\gamma_\theta}{2} = \frac{\varepsilon_x - \varepsilon_y}{2} \sin(2\theta) - \frac{\gamma_{xy}}{2} \cos(2\theta) \quad (6.1d)$$

According to the validation exercise, the statistical Matlab code is highly capable in solving uni-axial/multiaxial cyclic loads while also taking into account mean stress and degree of nonproportionality.

Table 6.3: Summary of the experimental N_f generated by testing Plane specimens under multiaxial constant amplitude cyclic load and estimated $N_{f,e}$ & $N_{f,Socie}$

Specimen Symbols	Load Ratio [†]	$\varepsilon_{x,a}$	$\varepsilon_{x,m}$	$\gamma_{xy,a}$	$\gamma_{xy,m}$	N_f^\dagger (Cycles)	$N_{f,e}^\dagger$ (Cycles)	$N_{f,Socie}^\dagger$ (Cycles) Socie & Marquis 2000)	Loading Path
PSBCAZMSIph1 [†]	-1	0.00274	0	0.00457	0	8,050	8,105	8,000	
PSBCAZMSOoPh2	-1	0.00258	0	0.00448	0	1,779	1,763	1,904	
PSBCANZMSIph1	0	0.003	0.003	0.0046	0.0046	5,711	6,408	6,486	

[†] PSBCA: Plane Sample, Biaxial / Constant Amplitude, None Zero Mean Strain, [†] Load Ratio, $R = \frac{\varepsilon_{a,min}}{\varepsilon_{a,max}}$

[†] N_f : Number of Cycles to failure at 5% axial stiffness drop, [†] $N_{f,e}$: Estimated Number of Cycles to failure by Using Matlab Code [†] $N_{f,Socie}$: Estimated Number of Cycles to failure by Using Socie criterion (Socie & Marquis 2000)

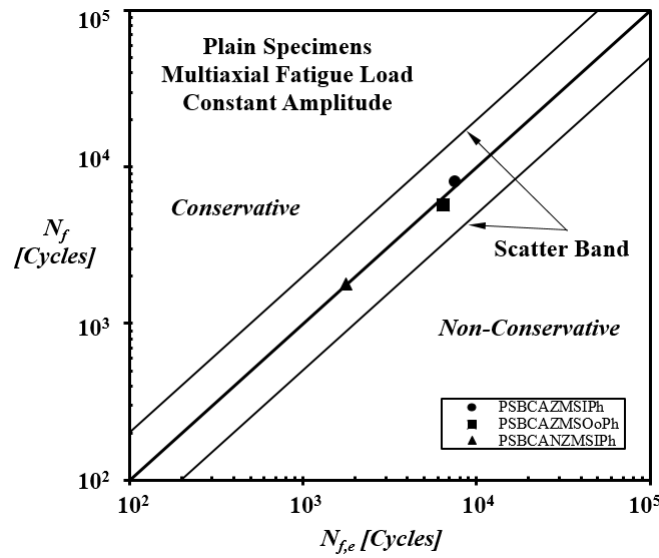


Figure 6.2: The Predicted Number of Cycles to Failure $N_{f,e}$ versus Experimental Number of Cycles N_f under Multiaxial Constant Amplitude Cyclic Loading

6.5 Numerical Calculation to find the Critical Distance by Using the TCD Theory

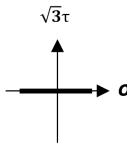
In order to find an appropriate critical distance, as presented in section (4.9), six plain specimens were tested in the lab. under uniaxial CA fatigue load. Then, through an appropriate numerical analysis formalised in section (3.3), the experimental number of cycles to failure was best fitted to the predicted $N_{f,e}$ found from the Modified Manson-Coffin Curve by post-processing the in-field stress/strain states along the focus path that damaging the investigated material at an assumed distance from the notch tip of the stress raiser. The theory of critical distance (TCD) was applied in terms of the point method (PM). The average value of the Critical Distances derived from the experiments were equal to $\frac{L_{PM}}{2} = 0.78mm$, as shown in Table (6.4). The TCD philosophy hypothesises that the critical distance is a property of a material whose value does not change in the same material. Consequently, the determined CDs were used to find the location of effective local stress/strain states of all the other notches under different loading conditions so as to evaluate the fatigue damage.

An average value for $\frac{L_{PM}}{2}$ is calculated from the aforementioned six experimental results. In this research, the systematic use of the numerical strategy to find the critical distance resulted in an average value for $\frac{L_{PM}}{2} = 0.78mm$.

6.6 Validation of the Proposed Approach for Different Notch Geometries

Real mechanical components and structural elements contain a wide range of geometrical features that favour the initiation of fatigue cracks. The presence of stress raisers, for instance notches in

Table 6.4: Summary of determining a critical distance C.D by testing Sharply notch specimens $r_n=1.5\text{mm}$ under uniaxial constant amplitude cyclic loading

Specimens	Load Ratio [†]	$F_a(t)$ (kN)	Experimental N_f^\ddagger (Cycles)	Calculated Critical Distances (mm)	Estimated $N_{f,e}$ (Cycles)	Loading Path
SNUCAZMS1 [†]		78.7	6,164	0.80	6,162	
SNUCAZMS2		58.3	35,247	0.84	35,550	
SNUCAZMS3	R = -1	52.0	41,229	0.76	44,400	
SNUCAZMS4		69.8	13,469	0.78	13,070	
SNUCAZMS5		46.8	81,629	0.76	82,050	
SNUCAZMS6		42.3	145,989	0.76	145,250	
Average Critical Distance $\frac{L_{FM}}{2} =$				0.78mm		

[†] SNUCAZMS1: Sharp Notch, Uniaxial, Constant Amplitude, Zero Mean Stress 1
[†] Load Ratio, $R = \frac{\sigma_{a,min}}{\sigma_{a,max}}$, [†] N_f : Number of Cycles to failure at 5% axial stiffness drop

a component, has a serious detrimental effect on the fatigue strength of materials and complicates the stress/strain distribution along the material due to the stress concentration phenomenon. In more detail, in any notch component subjected to a uniaxial/multiaxial fatigue load, the corresponding stress/strain value at the stress concentration zone is relatively higher than the average net stress. As mentioned in section (2.2.1), although an early study used the root stress at the notch tip to predict the fatigue lifetime of notched geometries, according to the recent literature, using the notch root stress is not appropriate in fatigue evaluation since it leads to conservative results (Susmel & Taylor 2007). In the present research, the fatigue estimation for notched geometries was obtained by using the stress/strain field within a certain distance from the notch tip. In order to investigate the accuracy of the proposed approach in evaluating the notch fatigue limit, a systematic validation exercise was followed involving the testing of three different types of notched geometry (Sharp, Intermediate & Blunt notches with root radii equal to 1.5 mm, 3 mm & 6 mm, respectively) as shown in Fig.(4.6)) against a range of fatigue loadings. According to the validation review, the error diagram of Figures (6.3, 6.4 & 6.5) fully supports the idea that our novel multiaxial formalisation of the elasto-plastic fatigue assessment methodology reflects the mechanism of fatigue damage and correctly identifies the critical damage to the material. Eventually, the estimated number of cycles to failures $N_{f,e}$ was found to fall largely within an error factor of two (scatter band 2) compared to the experimental N_f . This good correlation between $N_{f,e}$ and N_f was satisfactory for all of the notch geometries.

6.7 Validation of the Proposed Approach against Different Loading Conditions

Real components and structural elements are often subject to a complex multiaxial fatigue load. In order to evaluate such components against multiaxial fatigue, it is often required to combine the uniaxial and shear stress amplitudes with a specific degree of nonproportionality and to take account of mean stresses, all applied in a variable amplitude loading profile so as to get the most damaging and largest magnitude of normal and shear stress/strain. Despite much research in the field of multiaxial fatigue, no single theory has been able to combine all the above loading

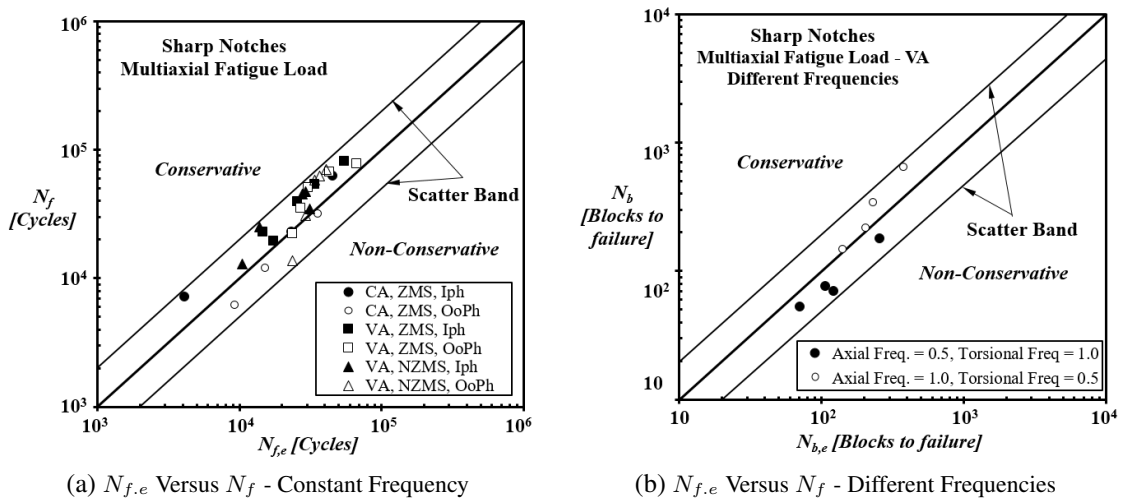


Figure 6.3: The Predicted Number of Cycles to Failure $N_{f,e}$ versus Experimental Number of Cycles to Failure - Sharp Notch

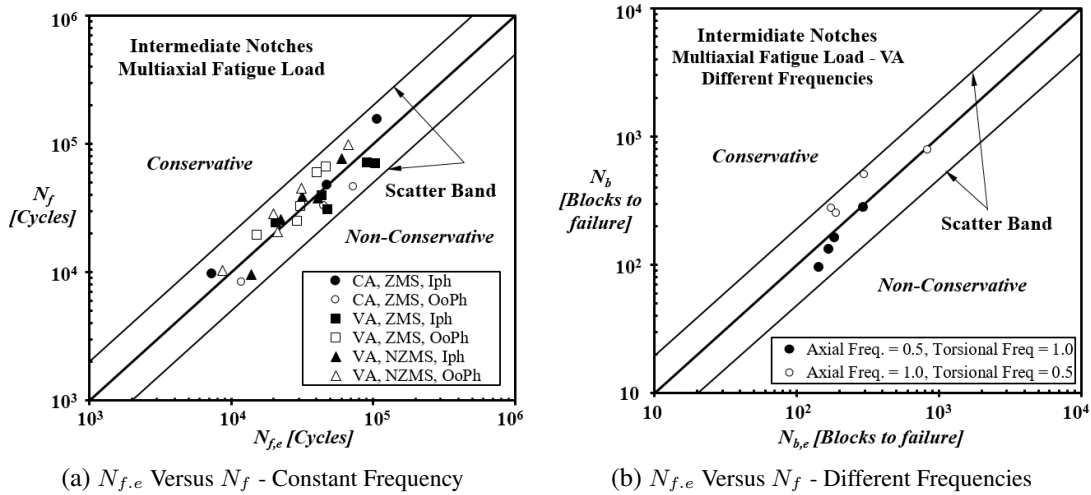


Figure 6.4: The Predicted Number of Cycles to Failure $N_{f,e}$ versus Experimental Number of Cycles to Failure - Intermediate Notch

complexities and scenarios. The approach devised in this research attempted to cover all the forms of load application and paths. To examine the proposed technique, a large number of complex uniaxial/multiaxial fatigue loads were considered as follows:

6.7.1 Constant Amplitude Fatigue Loading

The first group of tests were followed for those fatigue loads where the amplitudes did not change with time (Constant Amplitude). Eighteen specimens were tested under a variety of constant amplitude cyclic loading conditions. The experimental number of cycles to failure N_f were plotted against the estimated number of cycles $N_{f,e}$, as shown in Fig.(6.6). The validation result showed that the proposed approach is able to estimate the fatigue lifetime of a component accurately, with all data points falling within an error factor of two. This confirms the good correlation between the predicted and experimental cycles to failure and validate that the proposed approach can accurately

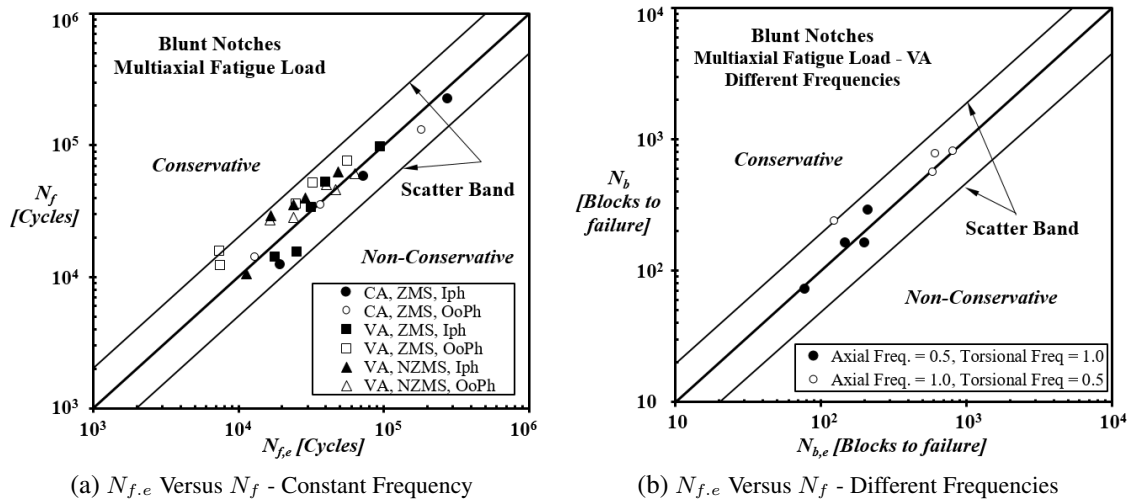


Figure 6.5: The Predicted Number of Cycles to Failure $N_{f,e}$ versus Experimental Number of Cycles to Failure - Blunt Notch

Table 6.5: Summary of the Numerical Results of the Sharp Notch Specimens $r_n=1.5\text{mm}$

Specimen Symbols [†]	ϕ°	θ°	α°	γ_a	τ_a (MPa)	$\sigma_{n,max}$ (MPa)	ρ	$N_{f,e}$ (Cycles)
SNBCAZMSIph1	45	20	60	0.00149	98.4	157.3	1.60	45,286
SNBCAZMSIph2	10	105	85	0.00189	111.5	176.9	1.60	23,200
SNBCAZMSIph3	90	35	45	0.00293	132.4	218.9	1.65	4,105
SNBCAZMSOoPh1	45	20	60	0.00167	104.5	165	1.58	35,810
SNBCAZMSOoPh2	45	20	60	0.0018	110.1	178.2	1.62	15,245
SNBCAZMSOoPh3	45	20	60	0.0028	128.2	218.5	1.70	9,256
SNBVAZMSIph1	65	130	60	0.00131	88.7	163	1.70	25,456
SNBVAZMSIph2	65	130	55	0.0016	100.9	182.3	1.70	17,372
SNBVAZMSIph3	65	130	55	0.00183	108.3	193.2	1.70	14,576
SNBVAZMSIph4	65	130	60	0.00105	76.4	145.1	1.70	33,775
SNBVAZMSIph5	100	45	75	0.00087	69.4	133.3	1.70	55,072
SNBVAZMSOut1	65	130	60	0.00106	75.7	148.6	1.70	30,344
SNBVAZMSIph2	65	130	60	0.00123	82.9	160.9	1.70	27,116
SNBVAZMSOut3	65	130	60	0.00138	88.1	169.1	1.70	23,616
SNBVAZMSOut4	65	130	60	0.00086	64.5	127.3	1.70	43,244
SNBVAZMSOut5	95	45	80	0.00077	60.5	121.1	1.70	67,175
SNBVANZMIph1	55	125	60	0.00134	65.9	294.7	1.70	31,275
SNBVANZMIph2	55	20	50	0.00156	89.4	314.6	1.70	13,791
SNBVANZMIph3	45	20	60	0.00095	67.6	273.3	1.70	29,461
SNBVANZMIph4	55	125	55	0.00257	94.1	348.1	1.70	10,517
SNBVANZMIph5	50	20	55	0.00101	63.7	240.6	1.70	27,564
SNBVANZMOut1	100	45	60	0.00081	61.2	303.4	1.70	36,787
SNBVANZMIph2	5	10	85	0.00112	80.8	391.8	1.70	29,304
SNBVANZMOut3	10	10	80	0.00088	65.8	329.4	1.70	34,024
SNBVANZMOut4	30	15	65	0.00149	81.6	393.8	1.70	23,661
SNBVANZMOut5	5	10	85	0.00077	59.5	309.9	1.70	40,981

[†]SN: Sharp Notch, B: Biaxial, C.A: Constant Ampl., V.A: Variable Ampl., ZMS: Zero Mean Stress, NZMS: Non-Zero Mean Stress
 $\phi^\circ, \theta^\circ, \alpha^\circ$: Orientation of the Critical Plane in degree, $\gamma_a, \tau_a, \sigma_{n,max}$: Shear Strain, Shear Stress Amplitude and Normal Stress relative to the Critical Plane. [†] ρ : Index Factor (Stress Ratio), $N_{f,e}$: Estimated Number of Cycles to Failure

be used to evaluate fatigue damage under constant amplitude cyclic loadings.

Table 6.6: Summary of the Numerical Results of the Intermediate Notch Specimens $r_n=3.0\text{mm}$

Specimen Symbols [†]	ϕ°	θ°	α°	γ_a	τ_a (MPa)	$\sigma_{n,max}$ (MPa)	ρ	$N_{f,e}$ (Cycles)
INBCAZMSIph1	110	50	60	0.0018	109.3	141.7	1.30	106,390
INBCAZMSIph2	90	25	90	0.00274	138.4	147.7	1.07	47,105
INBCAZMSIph3	65	130	55	0.00445	151.3	195	1.30	7,330
INBCAZMSOoPh1	85	45	95	0.00183	103.4	143	1.38	72,356
INBCAZMSOoPh2	90	45	90	0.00213	113.2	156.1	1.38	45,085
INBCAZMSOoPh3	90	135	95	0.00345	130.6	177.6	1.36	11,740
INBVAZMSIph1	30	20	70	0.00173	122.6	197.8	1.61	43,509
INBVAZMSIph2	15	20	80	0.0013	89.1	141.1	1.59	104,230
INBVAZMSIph3	45	120	60	0.00211	79.3	128.3	1.62	48,038
INBVAZMSIph4	0	10	90	0.00249	125.2	203.5	1.63	20,678
INBVAZMSIph5	0	15	80	0.00144	100.8	157.3	1.56	91,206
INBVAZMSOut1	180	170	90	0.00167	101.8	165.3	1.62	30,765
INBVAZMSIph2	5	15	85	0.00127	81.8	134.2	1.64	40,417
INBVAZMSOut3	0	10	90	0.00194	110.8	177.2	1.60	29,167
INBVAZMSOut4	5	10	85	0.00207	112	185.8	1.66	15,182
INBVAZMSOut5	0	15	90	0.00115	76.1	125.2	1.64	46,899
INBVANZMIph1	95	50	85	0.00156	73.6	199.2	1.70	60,308
INBVANZMIph2	90	20	95	0.00286	94.1	211.7	1.70	31,633
INBVANZMIph3	140	70	70	0.00294	99	259.2	1.70	41,106
INBVANZMIph4	85	140	80	0.00327	98	260	1.70	22,417
INBVANZMIph5	90	20	100	0.0075	130.8	276.8	1.70	13,876
INBVANZMOut1	85	135	85	0.00101	73.8	211.1	1.70	67,331
INBVANZMIph2	120	55	60	0.00146	83.9	276.4	1.70	31,220
INBVANZMOut3	155	165	75	0.00191	96.1	333.1	1.70	19,813
INBVANZMOut4	120	55	60	0.00195	102.7	315.3	1.70	21,274
INBVANZMOut5	100	150	50	0.00251	106.7	333.3	1.70	8,708

[†]IN: Intermed. Notch, B: Biaxial, C.A: Cons. Ampl., V.A: Variable Ampl., ZMS: Zero Mean Stress, NZMS: Non-Zero Mean Stress
 $\phi^\circ, \theta^\circ, \alpha^\circ$: Orientation of the Critical Plane in degree, $\gamma_a, \tau_a, \sigma_{n,max}$: Shear Strain, Shear Stress Amplitude and Normal Stress relative to the Critical Plane. [†] ρ : Index Factor (Stress Ratio), $N_{f,e}$: Estimated Number of Cycles to Failure

6.7.2 Variable Amplitude Fatigue Loading

Another step in the validation exercise was considering variable amplitude loading conditions. Many loading cases with variable amplitude were applied, for instance, proportional, phase shifted and butterfly-path/different frequencies, and the experimental outcomes were reported in Tables (6.7, 4.7, 4.8, & 4.9). The physical datasets and error diagram illustrated in Fig.(6.7 & 6.8) summarise the accuracy of the developed approach in estimating the fatigue lifetime of a component under variable amplitude loading conditions. The formalised approach involved building up the accumulated fatigue damage from each cycle by taking advantage of a rainflow cycle counting scheme so as to describe the overall multiaxial fatigue damage of a component (Shamsaei et al. 2011).

Furthermore, with respect to the out-of-phase loading, according to the theoretical analysis, during a nonproportional cyclic load, the principal stresses and strains continuously rotate, meaning that a crack can be expected in any direction depending on the magnitude of the applied uniaxial and torsional loads. Multiaxial out-of-phase fatigue loading, meanwhile, results in a difficult lifetime estimation task for a component, because in this case the fatigue damage depends on the cyclic change in the direction of the maximum principal stress (Susmel & Taylor 2011). Fatigue damage accumulates with each rotation of the principal axes, resulting in a shorter fatigue life (Döring et al. 2003). The experimental observation also predicted much more fatigue damage under out-of-phase loading compare to the in-phase cases under the same axial and torsional stresses/strains.

Table 6.7: Summary of the Numerical Results of the Blunt Notch Specimens $r_n=6.0\text{mm}$

Specimen Symbols [†]	ϕ°	θ°	α°	γ_a	τ_a (MPa)	$\sigma_{n,max}$ (MPa)	ρ	$N_{f,e}$ (Cycles)
BNBCAZMSIph1	25	20	75	0.0016	102.1	117.7	1.20	274,390
BNBCAZMSIph2	105	45	55	0.00215	118	143.9	1.20	72,873
BNBCAZMSIph3	110	50	55	0.0040	145.9	169	1.20	19,329
BNBCAZMSOoPh1	85	135	85	0.00168	102.9	135.3	1.30	182,470
BNBCAZMSOoPh2	65	135	75	0.0024	116.7	155.7	1.40	36,693
BNBCAZMSOoPh3	80	135	80	0.0032	127.6	164.8	1.20	13,037
BNBVAZMSIph1	30	20	70	0.00215	155.6	248.2	1.60	31,597
BNBVAZMSIph2	0	5	85	0.0025	122.2	194	1.59	25,405
BNBVAZMSIph3	30	20	70	0.00178	144.4	231.9	1.61	39,766
BNBVAZMSIph4	0	10	90	0.00139	93.8	145.8	1.55	94,078
BNBVAZMSIph5	0	5	90	0.00253	124	203.3	1.64	17,864
BNBVAZMSOut1	0	15	90	0.00167	98.4	162	1.65	24,815
BNBVAZMSIph2	0	5	90	0.00251	128.3	219.6	1.71	7,364
BNBVAZMSOut3	0	10	90	0.00162	102.9	167.6	1.63	32,706
BNBVAZMSOut4	0	15	90	0.00124	82.9	134.1	1.62	56,082
BNBVAZMSOut5	0	10	90	0.00265	130.6	224.8	1.72	7,501
BNBVANZMIph1	75	35	50	0.0023	68.7	111.4	1.62	28,936
BNBVANZMIph2	55	130	60	0.0025	100	203.5	1.70	16,797
BNBVANZMIph3	55	135	60	0.00373	102	220.3	1.70	11,413
BNBVANZMIph4	45	25	60	0.0017	74.3	120.3	1.62	48,555
BNBVANZMIph5	85	40	50	0.0024	83.2	133.1	1.60	23,953
BNBVANZMOut1	5	10	85	0.00149	92.3	151.6	1.64	40,063
BNBVANZMIph2	10	15	80	0.00193	109.6	285	1.70	16,480
BNBVANZMOut3	5	15	85	0.00172	100.7	167.6	1.67	23,989
BNBVANZMOut4	5	15	85	0.00131	79.1	127.7	1.62	63,046
BNBVANZMOut5	30	20	70	0.00146	81.2	132.5	1.63	46,593

[†]BN: Blunt Notch, B: Biaxial, C.A: Constant Ampl., V.A: Variable Ampl., ZMS: Zero Mean Stress, NZMS: Non-Zero Mean Stress
 $\phi^\circ, \theta^\circ, \alpha^\circ$: Orientation of the Critical Plane in degree, $\gamma_a, \tau_a, \sigma_{n,max}$: Shear Strain, Shear Stress Amplitude and Normal Stress relative to the Critical Plane. [†] ρ : Index Factor (Stress Ratio), $N_{f,e}$: Estimated Number of Cycles to Failure

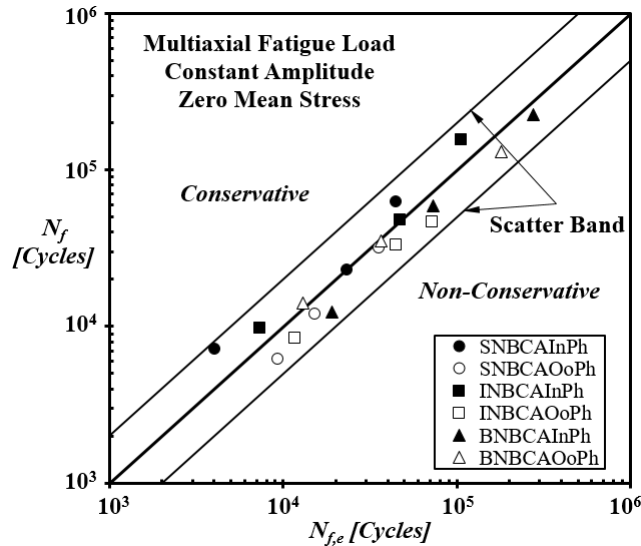


Figure 6.6: The Predicted Number of Cycles to Failure $N_{f,e}$ versus Experimental Number of Cycles under Constant Amplitude Fatigue Loadings

To sum up, a comparison of the observed fatigue lives N_f with the predicted lives $N_{f,e}$ using the proposed technique revealed a reasonable level of correlation, reflecting the efficacy of using critical plane theory.

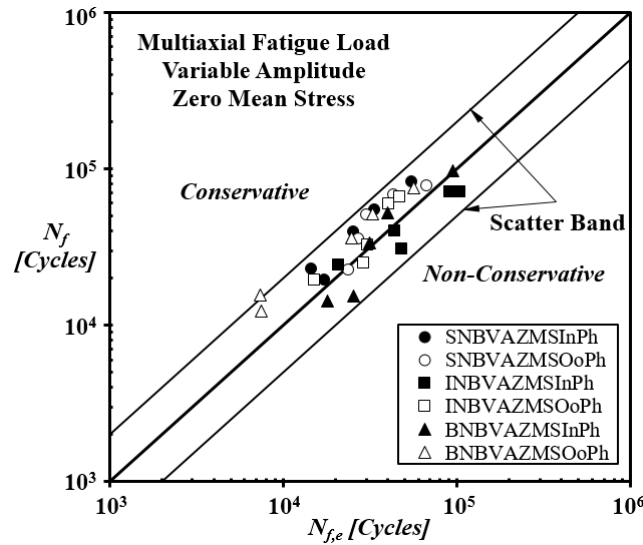


Figure 6.7: The Predicted Number of Cycles to Failure $N_{f,e}$ versus Experimental Number of Cycles under Variable Amplitude Fatigue Loadings

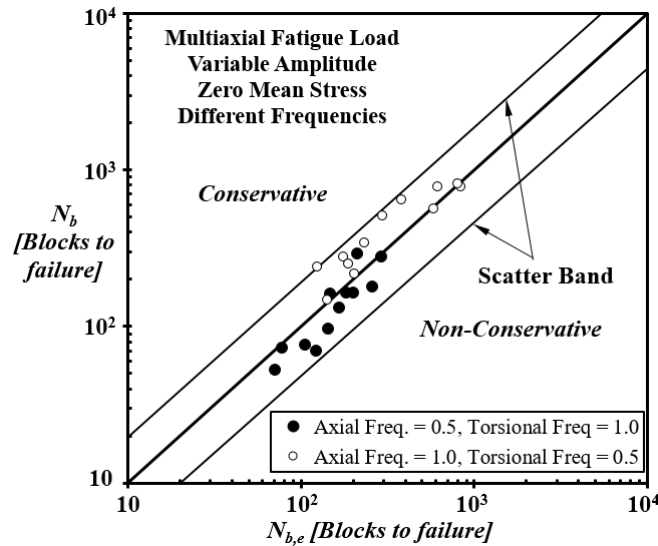


Figure 6.8: The Predicted Number of Cycles to Failure $N_{f,e}$ versus Experimental Number of Cycles under Variable Amplitude Fatigue Loadings - Different Frequencies

6.7.3 Multiaxial Fatigue Loading Taking Account of Mean Stress/Strain

As discussed in chapter (2), mean stress/strain has a significant effect on the overall fatigue strength of materials. Superimposed static stress is one of the simplest examples of mean stress. In notch geometries, however, the issue of modelling mean stress is rather more complicated because the local corresponding stress/strain in the vicinity of notch tip depends not only on the external applied cyclic forces and/or moments but also on the elasto-plastic behaviour of the material and the features of the notch geometry. In the low-cycle fatigue regime, mean stress increases fatigue damage and reduces material resistance. To further support the validity of the formalised approach for situations involving mean stresses, different fatigue loadings were considered with the presence of mean stress/strain on different notch geometries. The experimental and predicted

fatigue lives are compared in Fig.(6.9) and the data points are seen to lie within the band of factor 2. This simply means that the proposed technique correlates test data satisfactorily and thus is capable of simultaneously consider not only the notch, but also the influence of mean stress. In more detail, the diagram fully confirms that the proposed concept is highly accurate in evaluating fatigue lifetime in the presence of mean stress.

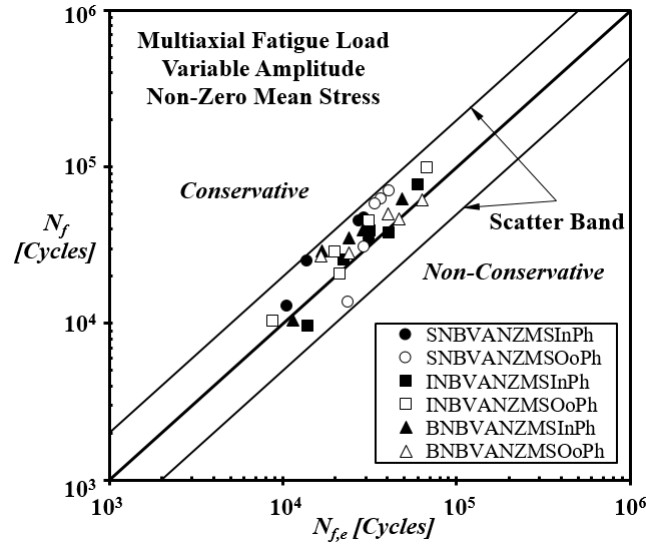
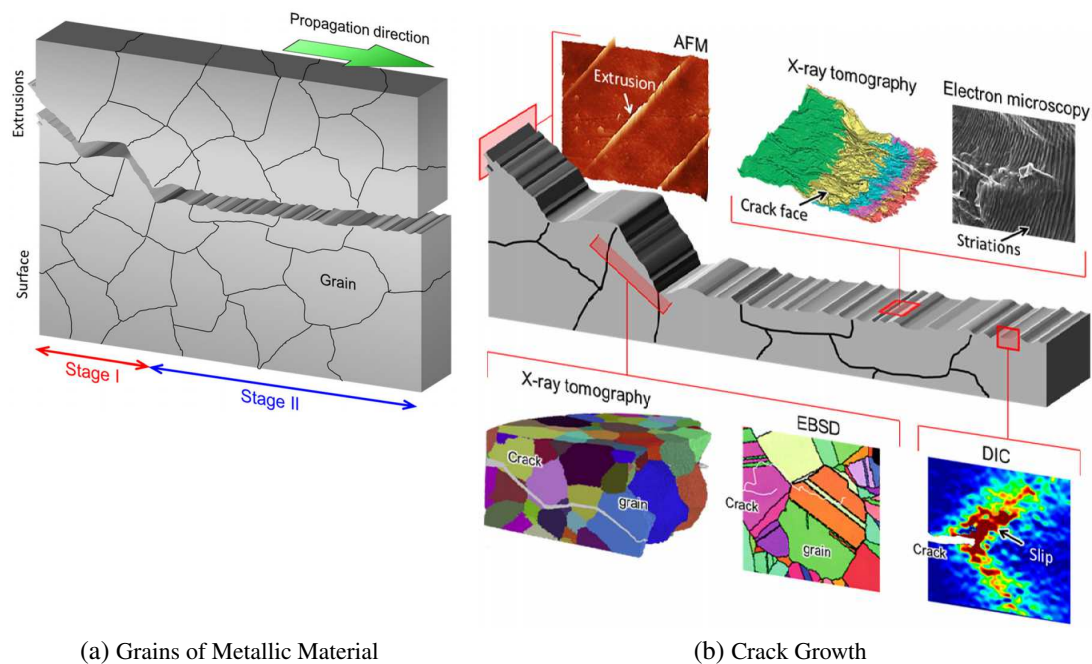


Figure 6.9: The Predicted Number of Cycles to Failure $N_{f,e}$ versus Experimental Number of Cycles under Variable Amplitude Loading and involving mean stresses

6.8 Observed Cracking Behaviour and Surface Failure

Fatigue crack is considered as one of the complicated process that happens at a stress level much lower than the strength of materials especially in the situation of multiaxial cyclic loadings. Such a crack is defined as a localized mechanisms controlled by a combination of local shear and tensile strain (Hertzberg et al. 1996). According to the most commonly engineering guidelines, fatigue crack has long been treated as two separate problems: (i) crack initiation, and (ii) crack propagation. Distinguish between these two stages is important to investigate fatigue damage of a component. Plumbridge & Ryder (1969) has reviewed the crack initiation and propagation process of metallic materials and stated that fatigue crack influenced by texture and grain orientation of a material (Fig.6.10a). Fatigue loading induces a continuous accumulation of local slip at the microscopic stress concentration field, resulting in material separation. Such a movement and slip at microlevel is considered as a crack nucleation. Chowdhury & Sehitoglu (2016) stated that fatigue crack formed along a slip plane that experiencing a maximum shear stress/strain. After crack nucleation, the developed crack propagate on the maximum shear plane by a slip and decohesion process. The entire crack nucleation and growth undergo two stages. Stage I that is sensitive to the microstructure of a material, following by Stage II. According to the physical observation, stage I crack undergoes fluctuating due to the history of irreversible slip accumulation. Finally, the crack growth reaches stage II that is no longer influenced by interfaces. Stage II of fatigue crack continues until final rapture. All stages of crack initiation and propagation was explained by Chowdhury

& Sehitoglu (2016) and illustrated in Fig.(6.10).



(a) Grains of Metallic Material

(b) Crack Growth

Figure 6.10: Fatigue Crack Initiation and Propagation (Chowdhury & Sehitoglu 2016)

In this research, the fracture surfaces of the tested notch specimens were investigated in detail in order to understand the predominant cracking mechanisms. The fatigue failure matrix reported in Appendix-B, summarised the observed fracture surfaces. For any loading/geometrical configuration, the first and second pictures in the Tables (B.1, B.2 & B.3) show failures in the medium and low-cycle fatigue regime, respectively. To investigate the cracking behaviour of the notch specimens, the number of cycles to failure was defined as occurring when there was a 5% drop in the stiffness of the material. To examine the surface failure, tests were run continuously until complete breakage. Tensile and shear mode of failure crack were observed, depending upon non-proportionality and strain level of fatigue loads. As a general, in the constant amplitude fatigue loading, the developed cracks very small and mainly grow in one direction. However, for those cases that the loading history is variable, cracks changed the paths to propagate faster.

Regarding the orientation of the critical plane and crack initiation of the plane specimens, in the uniaxial tests of the plane specimens, it was observed that the cracks tended to grow into the surface and aligned at nearly 45° to the specimen's axis. The load carrying capacity then dropped quickly as the cracks propagated into the surface. According to the theoretical analysis and due to the developed normal stress on the critical plane, more damage can be seen in the uniaxial loading and the crack propagation stage was rather short (Atzori et al. 2005). In contrast, in the pure torsion cases, cracks initiated and grew along the specimen's axis, and the orientation of the critical planes were 0° and 90° . In the pure torsion loading cases, the crack propagation time was remarkably long and sometimes the specimens did not completely break, because the normal stress that accelerates the propagation stage on the critical plane was zero. Both crack mechanisms are shown in Fig.(6.12).

From a practical point of view, however, the macroscopic identification of the critical plane of the notch specimens during fatigue testing was not a simple task, because the surface fracture of

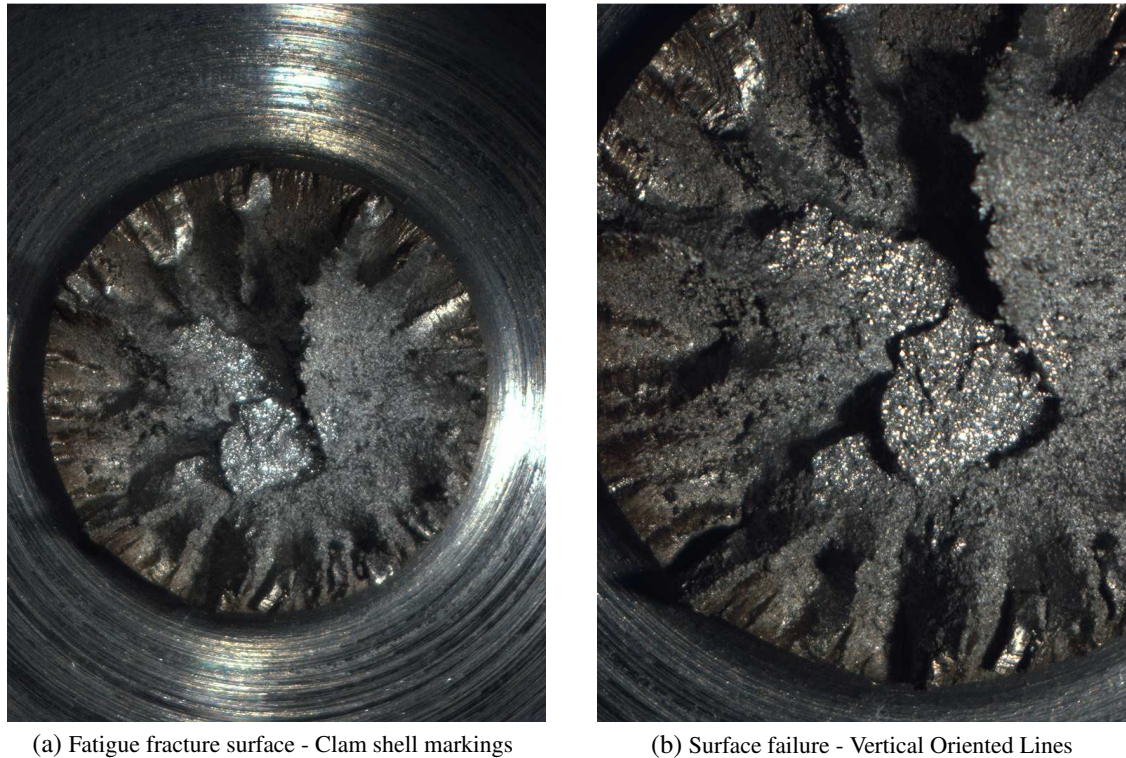


Figure 6.11: Fatigue Fracture Surface Appearance of Notched component

notch geometries is very complex as shown in Fig.(6.13). Nevertheless, the formalised theoretical approach was used through applying the algorithm and Matlab code to determine the orientation of the plane with the greatest damage value, and fatigue life associated with this plane was considered to be the total fatigue life of the geometry (Susmel et al. (2014)).

6.9 Review the Results and Discussion

This research work summarizes an attempt of formalising methodology suitable for estimating fatigue lifetime of real engineering components when damaged by multiaxial cyclic stress/strain states with involving mean stresses. Then, accuracy of the proposed approach was checked by following a physical examination in the laboratory. The formalisation and validation of the developed methodology is based on the assumption that number of cycles to failure N_f of any components under fatigue loading can correctly be estimated only by using the cyclic elasto-plastic behaviour of the material. By considering the above mentioned hypothesis, the proposed approach was mainly devised by modifying the Manson-Coffin Curve method (MCCM) to be sensitive to consider degree of non-proportionality of the infield stress/strain states and mean stresses (Chen et al. 1996). According to the proposed strategy in this thesis, fatigue crack initiate on a plane experiencing the maximum shear strain amplitude and known by a critical plane, whereas the crack propagation influenced by the maximum normal stress on the critical plane. The accurate fatigue estimation by using the modified Manson-Coffin Curve seem to highly support the idea of considering index factor (ρ), because such a factor capable of correctly accounting face shift of the

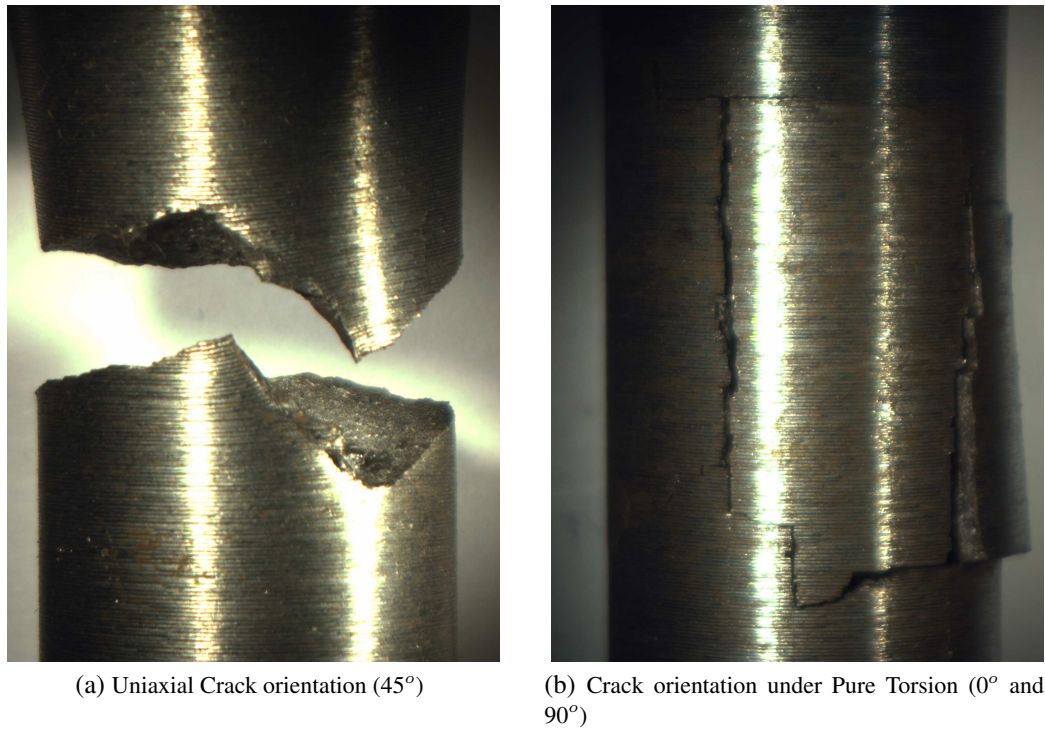


Figure 6.12: Crack Orientation and Fracture Surface from Cyclic Load

stress/strain and the presence of mean stresses. Further, the Maximum Variance Method (MVM) was reformulated in terms of strain to determine orientation of the crack initiation plain and relative stress/strain amplitudes. The proposed criterion is accepted for low/medium-cycle fatigue regime.

Theory of Critical Distances TCD was used to quantify the effective stress/strain states. Such the effective stress/strain states of the material were taken at a critical location inside the material by a distance far from the notch root by $\frac{L_{PM}}{2}$. The Critical Distance was found by taking full advantage of the Theory of Critical Distances, applied in the point method form. The stress/strain history $\sigma(t)/\varepsilon(t)$ at a critical location were taken in all directions that consist of axial stresses and strains on the directions of $(x, y \ \& \ z)$ $\sigma_x(t), \varepsilon_x(t), \sigma_y(t), \varepsilon_y(t), \sigma_z(t), \varepsilon_z(t), \tau_{xy}(t)$, as well as shear stresses and strains in the directions of $(xy, xz \ \& \ yz)$ $\gamma_{xy}(t), \tau_{xz}(t), \gamma_{xz}(t), \tau_{yz}(t), \gamma_{yz}(t)$. These stress/strain states were determined from the validated finite element model solved by using ANSYS software, and represent the entire elasto-plastic deformation history of the component. The Theory of Critical Distance assumes that the $\frac{L_{PM}}{2}$ is a material property whose value does not change with changing notch geometry and the profile of cyclic loading. The critical distance value, meanwhile, $\frac{L_{PM}}{2}$ was determined directly from the physical examination presented in section (4.9). Interestingly, from the experimental examinations of six sharply notched specimens that were used to find the critical distance through the strain-based approach, it was noted that the values of $\frac{L_{PM}}{2}$ presented in Table (6.4) are quite similar and the average equals 0.78mm. This proves the fact that the value of $\frac{L_{PM}}{2}$ is constant and part of the material property, which value not changes with different geometry and different loading profiles. According to the systematic validation procedure, the Theory of Critical Distances is capable of accurately determining the ef-

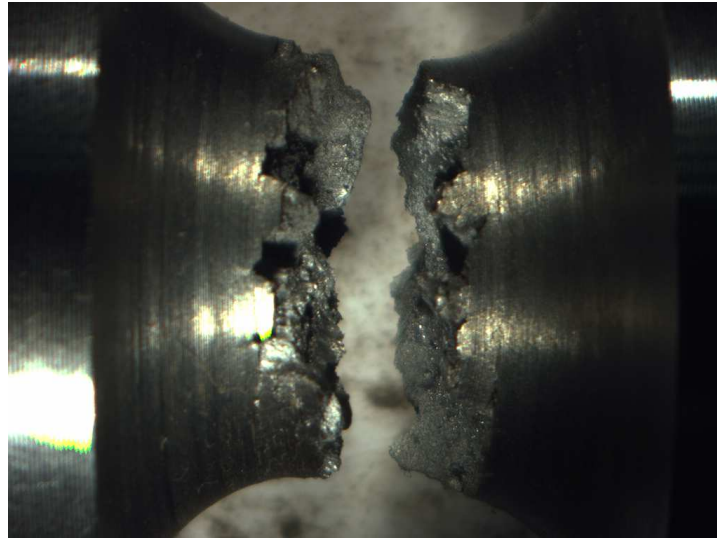


Figure 6.13: Crack Initiation and Fatigue Fracture of Notched Geometry

fective stress/strain states so as accurately evaluate the lifetime of components containing not only notches but also any sort of developed cracks. The determined in-field stress/strain states were used as an input datasets for fatigue life calculation. The numerical Maximum Variance Method was used to find the orientation of the critical plane. A Matlab script was written to solve the complex equations of the Maximum Variance Method MVM. To consider the influence of mean stress and the degree of non-proportionality, the stress ratio (ρ) value was used to find the appropriate Manson-Coffin curve to evaluate fatigue (Wang & Susmel 2016). From the Modified Manson-Coffin Curve, the number of cycles to failure $N_{f,e}$ was determined. Moreover, in the situation of variable amplitude cyclic loadings, the methodology of fatigue evaluation was not a straightforward procedure as of constant amplitudes. The variable amplitude loadings were required to breakdown the variable cycles into a series of constant amplitude events to evaluate fatigue damage of each cycle. Rainflow cycle counting method was used to perform the cycle breakdowns. Then, the overall fatigue damage of a specimens were determined by using a Cumulative Fatigue Damage method as described in section (3.6.2).

In order to verify the effectiveness of the developed approach, research finding by Author of this thesis was also pointed towards experimental validation. A series low/medium-cycle fatigue experiments were conducted on notch geometries manufactured from 080E40 steel. The tests were performed using a computer-controlled multiaxial fatigue testing machine. A wide range of loading conditions were involved, including uniaxial/multiaxial, constant/variable amplitude, in-phase/out-of-phase, same/different frequencies and a combination of cyclic and static loads to represent the mean stresses. To simplify the process of comparison, tests with different frequencies were considered as a block cycles, with each block consisting of 50 variable amplitude cycles. Failure was defined as the number of cycles to failure N_f at which a 5% drop was recorded from the tensile for the uniaxial and multiaxial loading cases, and a 5% drop was recorded from shear amplitude for the pure torsion loading conditions. 132 specimens were tested under different fatigue loads as presented in Table(4.2). The error diagrams reported in this chapter show

the accuracy of the formalised method. According to the experiment results, among all the tested specimens, only four data points were slightly out of the factor-of-two lines, otherwise all the other points exhibited a fair distribution around the perfect correlation line and falling within an error factor of scatter band two, as illustrated in Figs.(6.2, 6.3, 6.4, 6.5, 6.6, 6.7, 6.8, & 6.9) . In light of the encouraging accuracy obtained by using the Modified Manson-Coffin Curve combined with the Theory of Critical Distances applied in the form of point method PM, the validation stage confirmed that the proposed approach gives a satisfactory result in respect to estimating the fatigue lifetime in the low/medium-cycle fatigue regime, despite the differences in the theoretical background and the mathematical formulation.

In conclusion, to the best of the author's knowledge, this research can be considered as a successful attempt to evaluate low/medium-cycle multiaxial fatigue damage of a complex geometry under the most damaging multiaxial cyclic load, for instance considering all potential uniaxial/multiaxial and proportional/nonproportional cyclic loading and taking account of mean stresses. The hypothesis is based on considering elasto-plastic shear strain amplitude rather than elastic stresses. Although the concept of using the Modified Manson-Coffin Curve and the Theory of Critical Distances is not new, but combining all the above-mentioned complexity in terms of geometry and fatigue loading in one model can be considered as a novel methodology to define elasto-plastic multiaxial fatigue. The accuracy of the calculated results compared to the experimental ones is reasonably good. The experimental N_f , versus estimated $N_{f,e}$ diagram confirms the accuracy and reliability of the novel multiaxial formalisation of the elasto-plastic fatigue evaluation. This seems to confirm the level of consistency characterising the proposed methodology.

Another consequences that deserved to be mentioned here: First: its author's opinion that the proposed approach and formalised Matlab code is considered as a validated tools that can be recommended for a designer engineer and industrial use to evaluate multiaxial fatigue at stress concentration features against all complex loading conditions because of its physical basis. Second: in addition to the accuracy, the developed method can be seen very simple and economical. Third: another feature of the proposed method, it can be used to evaluate fatigue damage of not only notched geometry but also cracked components. Because it was already known that the sharp notch behaves much the same as cracks.

Despite the above-mentioned advantage and simplicity, the described research work in this thesis is not a complete solution to the multiaxial fatigue problem of all materials. More investigation needs to check the applicability of the proposed technique on a wide range of materials different than metallic components. Furthermore, for the purpose of simplicity, a multilinear kinematic hardening criteria is chosen in the FE analysis to define the elasto-plastic deformation of the material being investigated. However, based on the numerical calculations and plotted hysteresis loop diagrams presented in Chapter (5), it can be seen that a better choice to describe the plasticity of the material is certainly a combined isotropic and kinematic hardening rule. Application of such a combined model requires more parameter identifications of the material and complicate the numerical analysis of FE model. In this research, only the kinematic hardening rule is used in the

FE model with accepting a level of discrepancy between the predicted and experimental hysteresis loops. For the future investigation, and in order to correctly define the elasto-plastic behaviour of the material, it is recommended to use the combined isotropic and kinematic hardening rule. Another concern point that need to be highlighted here, the developed approach is mainly based on the determination of the stress/strain states at a critical location inside the material. The only method to determine such a stress/strain states is correct modelling the geometry with a finite element method. Analysing three dimensional complex geometry with the current FE software is not an easy task and a time consuming process that sometimes crash the analysis due to limitation in the capacity of the existing finite element software. More work needs to be done in developing novel technological solution software that allow a real engineering components to be modelled and analysed with the formalised methodology.

Chapter 7

Conclusions

In the present research work, a novel multiaxial fatigue lifetime estimation technique of notch geometry was formulated based on the combined use of the Modified Manson-Coffin Curve Method MMCCM, the Maximum Variance Method MVM, and the elasto-plastic critical distance in the form of point method PM. Then, the proposed methodology was validated against a large number of experimental results. The most important conclusions were summarised as follows:

- The developed elasto-plastic three dimensional Finite Element FE model allows multiaxial fatigue lifetime of notched structural components to be designed against complex multiaxial cyclic loadings. The validation process concluded that the proposed FE model is worthy of considerable interest. The effort in this research has been directed towards the cyclic multiaxial plasticity of the local stress/strain states determined by solving the developed elasto-plastic FE model.
- The Maximum Variance Method that reformulated in terms of strain can be used to determine orientation of the critical plane and relative stress/strain amplitudes under complex multiaxial fatigue loadings. When the variance and covariance terms are determined from the input load history, then the required time to determine global maxima not depend on the length of the applied load history.
- The proposed multiaxial fatigue methodology is seen to be successful in evaluating lifetime of metallic notched geometry not only under constant amplitude CA loading conditions but also variable amplitudes VA. That explains the proposed approach reflects the mechanism of fatigue damage very well and correctly identifies the critical plane of materials under cyclic loading. The failure plane was also observed to be consistent with the critical plane predictions.
- According to the validation exercise, using the proposed methodology is seen to result in a remarkable level of accuracy in estimates falling within an error factor of 2. That mean all data points of the validation graph located within a scatter band of wide two.
- The written Matlab Code that used to solve the maximum variance MV can be considered as an efficient computer programming to predict the multiaxial fatigue of a component. Most

importantly, the Matlab script code can be assumed as a rapid design tool for use in the field of industry.

- The proposed method is not only applicable for simple loading paths but can also address general multiaxial random load histories involving mean stress/strain terms.
- The developed approach can be used with complex interactions between different load components because it was developed based on the use of corresponding local stress/strain states instead of nominal externally applied loads/moments.
- In the non-proportional multiaxial loadings, where the axes of principal strain rotate, according to the validation results, a 90 degree out-of-phase rotation resulted in the most damaging case and lowest fatigue lifetime compare to in-phase rotation and a lower degree of non-proportionality.
- The most interesting point in respect to the developed FE model and Matlab code is that it can simply edit the monotonic and fatigue properties of materials being assessed in the Matlab program and determine the in-field stress/strain states at any point inside the material, then evaluate fatigue damage of a component. Than explain, no need for a designer engineer or industrial staff to have a deep understanding of multiaxial fatigue when uses a formalised Matlab code.
- Systematic verification through the data from the literature shows that the proposed method is a precise and computationally efficient tool that lays the foundation for more accurate prediction of low/medium-cycle multiaxial notch fatigue.

Chapter 8

Recommendations for Future Work

Areas for further work are indicated below:

- Extend the developed approach so that it can be applied to welded geometries and investigate a potential cracklike flaw cases under both uniaxial and multiaxial forces, constant/variable amplitude fatigue loading with involving zero/non-zero mean stresses.
- Applying the proposed method on a wide range of materials other than metallic, and validating the results by running experiments.
- Develop a novel numerical solutions to perform an elasto-plastic stress/strain analyses of complex geometries by using Finite Element FE method in a remarkable reduced time.

References

- , D. (2010), *The theory of critical distances: a new perspective in fracture mechanics*, Elsevier.
- Atzori, B., Berto, F., Lazzarin, P. & Quaresimin, M. (2006), 'Multi-axial fatigue behaviour of a severely notched carbon steel', *International Journal of Fatigue* **28**(5-6), 485–493.
- Atzori, B., Meneghetti, G. & Susmel, L. (2005), On the use of the modified manson-coffin curves to predict fatigue lifetime in the low-cycle fatigue regime, in 'Giornata di studio IGF Ferrara 2005'.
- Berto, F., Lazzarin, P. & Yates, J. (2011), 'Multiaxial fatigue of v-notched steel specimens: a non-conventional application of the local energy method', *Fatigue & Fracture of Engineering Materials & Structures* **34**(11), 921–943.
- Branco, R., Costa, J., Berto, F. & Antunes, F. (2018), 'Fatigue life assessment of notched round bars under multiaxial loading based on the total strain energy density approach', *Theoretical and Applied Fracture Mechanics* **97**, 340–348.
- Brown, M. W. & Miller, K. (1973), 'A theory for fatigue failure under multiaxial stress-strain conditions', *Proceedings of the Institution of Mechanical Engineers* **187**(1), 745–755.
- Carpinteri, A., Spagnoli, A., Vantadori, S. & Bagni, C. (2013), 'Structural integrity assessment of metallic components under multiaxial fatigue: the c–s criterion and its evolution', *Fatigue & Fracture of Engineering Materials & Structures* **36**(9), 870–883.
- Chen, X., Gao, Q., Abel, A. & Wu, S. (1996), 'Evaluation of low cycle fatigue under non-proportional loading', *Fatigue & Fracture of Engineering Materials & Structures* **19**(10), 1161–1168.
- Chowdhury, P. & Sehitoglu, H. (2016), 'Mechanisms of fatigue crack growth—a critical digest of theoretical developments', *Fatigue & Fracture of Engineering Materials & Structures* **39**(6), 652–674.
- Coffin, L. F. (1954), 'A study of the effects of cyclic thermal stresses on a ductile metal', *trans. ASME* **76**, 931–950.
- Dang-Van, K. (1993), Macro-micro approach in high-cycle multiaxial fatigue, in 'Advances in multiaxial fatigue', ASTM International.

- Döring, R., Hoffmeyer, J., Seeger, T. & Vormwald, M. (2003), 'A plasticity model for calculating stress-strain sequences under multiaxial nonproportional cyclic loading', *Computational materials science* **28**(3-4), 587–596.
- Downing, S. D. & Socie, D. (1982), 'Simple rainflow counting algorithms', *International journal of fatigue* **4**(1), 31–40.
- Faruq, N. Z. (2016), 'An elasto-plastic approach to estimate lifetime of notched components under variable amplitude fatigue loading: a preliminary investigation', *Frattura ed Integrita Strutturale* (37), 382–394.
- Fatemi, A. & Socie, D. F. (1988), 'A critical plane approach to multiaxial fatigue damage including out-of-phase loading', *Fatigue & Fracture of Engineering Materials & Structures* **11**(3), 149–165.
- Fatemi, A., Zeng, Z. & Plaseied, A. (2004), 'Fatigue behavior and life predictions of notched specimens made of qt and forged microalloyed steels', *International Journal of Fatigue* **26**(6), 663–672.
- Feroz, S. (2014), 'Aircraft fatigue failure', <http://aerofatiguefailure.blogspot.com/>,.
- Gates, N. & Fatemi, A. (2014), 'Notched fatigue behavior and stress analysis under multiaxial states of stress', *International Journal of Fatigue* **67**, 2–14.
- Gates, N. & Fatemi, A. (2016), 'Notch deformation and stress gradient effects in multiaxial fatigue', *Theoretical and Applied Fracture Mechanics* **84**, 3–25.
- Gates, N. R. & Fatemi, A. (2018), 'Multiaxial variable amplitude fatigue life analysis using the critical plane approach, part ii: notched specimen experiments and life estimations', *International Journal of Fatigue* **106**, 56–69.
- Glinka, G. (1985), 'Energy density approach to calculation of inelastic strain-stress near notches and cracks', *Engineering Fracture Mechanics* **22**(3), 485–508.
- Gough, H. (1949), 'Engineering steels under combined cyclic and static stresses', *Proceedings of the Institution of Mechanical Engineers* **160**(1), 417–440.
- Gough, H. (1950), 'Engineering steels under combined cyclic and static stresses', *Journal of Applied Mechanics-Transactions of the ASME* **17**(2), 113–125.
- Gough, H. & Pollard, H. (1935), 'The strength of metals under combined alternating stresses', *Proceedings of the institution of mechanical engineers* **131**(1), 3–103.
- Han, C., Chen, X. & Kim, K. (2002), 'Evaluation of multiaxial fatigue criteria under irregular loading', *International Journal of Fatigue* **24**(9), 913–922.
- Hertzberg, R. W., Vinci, R. P. & Hertzberg, J. L. (1996), *Deformation and fracture mechanics of engineering materials*, Vol. 89, Wiley New York.

- Hoffmann, M. & Seeger, T. (1985), 'A generalized method for estimating multiaxial elastic-plastic notch stresses and strains, part 1: Theory', *Journal of Engineering Materials and Technology* **107**(4), 250–254.
- Hoffmeyer, J., Döring, R., Seeger, T. & Vormwald, M. (2006), 'Deformation behaviour, short crack growth and fatigue lives under multiaxial nonproportional loading', *International journal of fatigue* **28**(5-6), 508–520.
- Hua, C. & Socie, D. (1985), 'Fatigue damage in 1045 steel under variable amplitude biaxial loading', *Fatigue & Fracture of Engineering Materials & Structures* **8**(2), 101–114.
- Ince, A. & Glinka, G. (2016), 'Innovative computational modeling of multiaxial fatigue analysis for notched components', *International Journal of Fatigue* **82**, 134–145.
- Jayaraman, N. & Ditmars, M. (1989), 'Torsional and biaxial (tension-torsion) fatigue damage mechanisms in waspaloy at room temperature', *International Journal of Fatigue* **11**(5), 309–318.
- Jiang, Y., Hertel, O. & Vormwald, M. (2007), 'An experimental evaluation of three critical plane multiaxial fatigue criteria', *International Journal of Fatigue* **29**(8), 1490–1502.
- Jiang, Y. & Sehitoglu, H. (1996), 'Modeling of cyclic ratchetting plasticity, part i: development of constitutive relations', *Journal of Applied Mechanics* **63**(3), 720–725.
- Jiang, Y.-y. (2000), 'A fatigue criterion for general multiaxial loading', *Fatigue and fracture of engineering materials and structures* **23**(1), 19–32.
- Kanazawa, K., Miller, K. & Brown, M. (1977), 'Low-cycle fatigue under out-of-phase loading conditions', *Journal of Engineering Materials and Technology* **99**(3), 222–228.
- Kanazawa, K., Miller, K. & Brown, M. (1979), 'Cyclic deformation of 1% cr-mo-v steel under out-of-phase loads', *Fatigue & Fracture of Engineering Materials & Structures* **2**(2), 217–228.
- Kim, K., Chen, X., Han, C. & Lee, H. (2002), 'Estimation methods for fatigue properties of steels under axial and torsional loading', *International journal of fatigue* **24**(7), 783–793.
- Kim, K., Park, J. & Lee, J. (1999), 'Multiaxial fatigue under variable amplitude loads', *TRANSACTIONS-AMERICAN SOCIETY OF MECHANICAL ENGINEERS JOURNAL OF ENGINEERING MATERIALS AND TECHNOLOGY* **121**, 286–293.
- Köttgen, V., Barkey, M. & Socie, D. (1995), 'Pseudo stress and pseudo strain based approaches to multiaxial notch analysis', *Fatigue & fracture of engineering materials & structures* **18**(9), 981–1006.
- Lazzarin, P. & Susmel, L. (2003), 'A stress-based method to predict lifetime under multiaxial fatigue loadings', *Fatigue & Fracture of Engineering Materials & Structures* **26**(12), 1171–1187.
- Lee, Y.-L., Pan, J., Hathaway, R. & Barkey, M. (2005), *Fatigue testing and analysis: theory and practice*, Vol. 13, Butterworth-Heinemann.

- Manson, S. S. (1954), 'Behavior of materials under conditions of thermal stress'.
- McDiarmid, D. (1991), 'A general criterion for high cycle multiaxial fatigue failure', *Fatigue & Fracture of Engineering Materials & Structures* **14**(4), 429–453.
- McDiarmid, D. (1994), 'A shear stress based critical-plane criterion of multiaxial fatigue failure for design and life prediction', *Fatigue & Fracture of Engineering Materials & Structures* **17**(12), 1475–1484.
- Meneghetti, G., Campagnolo, A., Berto, F. & Tanaka, K. (2018), 'Notched ti-6al-4v titanium bars under multiaxial fatigue: Synthesis of crack initiation life based on the averaged strain energy density', *Theoretical and Applied Fracture Mechanics* **96**, 509–533.
- Miner, M. (1945), 'Cumulative damage in fatigue', *J Appl Mech* **67**, A159–64.
- Mitchell, M. (1996), 'Fundamentals of modern fatigue analysis for design'.
- Morrow, J. (1965), Cyclic plastic strain energy and fatigue of metals, in 'Internal friction, damping, and cyclic plasticity', ASTM International.
- Neuber, H. (1958), 'Theory of notch stresses: principles for exact stress calculation of strength with reference to structural forms and materials', *AEC TR 4547*.
- Neuber, H. (1961), 'Theory of stress concentration for shear-strained prismatical bodies with arbitrary nonlinear stress-strain law', *Journal of Applied Mechanics* **28**(4), 544–550.
- Norma, A. (1998), 'E606-92 (1998) standard practice for strain-controlled fatigue testing', *Filadelfia (EE. UU.): American Society for Testing and Materials*.
- Palmgren, A. (1924), 'A. die lebensdauer von kugellagern'.
- Peterson, R. E. (1959), 'Notch sensitivity', *Metal fatigue* pp. 293–306.
- Pilkey, W. D. (2005), 'Advanced mechanical engineering solutions', http://www.amesweb.info/StressConcentrationFactor/U_ShapedCircumferentialGroove.aspx.
- Plumbridge, W. & Ryder, D. (1969), 'The metallography of fatigue', *Metallurgical reviews* **14**(1), 119–142.
- Prager, W. (1955), 'The theory of plasticity: a survey of recent achievements', *Proceedings of the Institution of Mechanical Engineers* **169**(1), 41–57.
- Ren, X., Wu, F., Xiao, F. & Jiang, B. (2015), 'Corrosion induced fatigue failure of railway wheels', *Engineering Failure Analysis* **55**, 300–316.
- Rolovic, R. & Tipton, S. M. (2000), 'Multiaxial cyclic ratcheting in coiled tubing part i: theoretical modeling', *Journal of engineering materials and technology* **122**(2), 157–161.
- Shamsaei, N., Fatemi, A. & Socie, D. F. (2011), 'Multiaxial fatigue evaluation using discriminating strain paths', *International Journal of Fatigue* **33**(4), 597–609.

- Shamsaei, N., Gladskyi, M., Panasovskyi, K., Shukaev, S. & Fatemi, A. (2010), 'Multiaxial fatigue of titanium including step loading and load path alteration and sequence effects', *International Journal of Fatigue* **32**(11), 1862–1874.
- Shang, D.-G., Sun, G.-Q., Deng, J. & Yan, C.-L. (2007), 'Multiaxial fatigue damage parameter and life prediction for medium-carbon steel based on the critical plane approach', *International Journal of Fatigue* **29**(12), 2200–2207.
- Smith, K. N. (1970), 'A stress-strain function for the fatigue of metals', *Journal of materials* **5**, 767–778.
- Socie, D. (1987), 'Multiaxial fatigue damage models.', *Transactions of the ASME. Journal of Engineering Materials and Technology* **109**(4), 293–298.
- Socie, D. (1997), 'Fatigue life analysis software', <https://www.hbm.com/en/3362/somat-infield-softwareoptimized-for-use-with-somat-hardware/>.
- Socie, D. F. & Marquis, G. B. (2000), *Multiaxial fatigue*, Society of Automotive Engineers Warrendale, PA.
- Socie, D. & Morrow, J. (1980), Review of contemporary approaches to fatigue damage analysis, in 'Risk and failure analysis for improved performance and reliability', Springer, pp. 141–194.
- Sonsino, C. (2007), 'Course of sn-curves especially in the high-cycle fatigue regime with regard to component design and safety', *International Journal of Fatigue* **29**(12), 2246–2258.
- Stephens, R. I., Fatemi, A., Stephens, R. R. & Fuchs, H. O. (2000), *Metal fatigue in engineering*, John Wiley & Sons.
- Suresh, S. (1991), 'Fatigue of materials (cambridge solid state science series)', *Cambridge: Press Syndicate of the University of Cambridge*.
- Susmel, L. (2004), 'A unifying approach to estimate the high-cycle fatigue strength of notched components subjected to both uniaxial and multiaxial cyclic loadings', *Fatigue & Fracture of Engineering Materials & Structures* **27**(5), 391–411.
- Susmel, L. (2008a), 'Multiaxial fatigue limits and material sensitivity to non-zero mean stresses normal to the critical planes', *Fatigue & Fracture of Engineering Materials & Structures* **31**(3-4), 295–309.
- Susmel, L. (2008b), 'The theory of critical distances: a review of its applications in fatigue', *Engineering Fracture Mechanics* **75**(7), 1706–1724.
- Susmel, L. (2009), *Multiaxial notch fatigue*, Elsevier.
- Susmel, L. (2010), 'A simple and efficient numerical algorithm to determine the orientation of the critical plane in multiaxial fatigue problems', *International Journal of Fatigue* **32**(11), 1875–1883.

- Susmel, L. (2014), 'Four stress analysis strategies to use the modified wöhler curve method to perform the fatigue assessment of weldments subjected to constant and variable amplitude multi-axial fatigue loading', *International Journal of Fatigue* **67**, 38–54.
- Susmel, L., Atzori, B., Meneghetti, G. & Taylor, D. (2011), 'Notch and mean stress effect in fatigue as phenomena of elasto-plastic inherent multi-axiality', *Engineering Fracture Mechanics* **78**(8), 1628–1643.
- Susmel, L. & Lazzarin, P. (2002), 'A bi-parametric wöhler curve for high cycle multi-axial fatigue assessment', *Fatigue & Fracture of Engineering Materials & Structures* **25**(1), 63–78.
- Susmel, L. & Taylor, D. (2003), 'Fatigue design in the presence of stress concentrations', *The Journal of Strain Analysis for Engineering Design* **38**(5), 443–452.
- Susmel, L. & Taylor, D. (2007), 'A novel formulation of the theory of critical distances to estimate lifetime of notched components in the medium-cycle fatigue regime', *Fatigue & Fracture of Engineering Materials & Structures* **30**(7), 567–581.
- Susmel, L. & Taylor, D. (2008), 'The modified wöhler curve method applied along with the theory of critical distances to estimate finite life of notched components subjected to complex multi-axial loading paths', *Fatigue & Fracture of Engineering Materials & Structures* **31**(12), 1047–1064.
- Susmel, L. & Taylor, D. (2010), 'An elasto-plastic reformulation of the theory of critical distances to estimate lifetime of notched components failing in the low/medium-cycle fatigue regime', *Journal of Engineering Materials and Technology* **132**(2), 021002.
- Susmel, L. & Taylor, D. (2011), 'The theory of critical distances to estimate lifetime of notched components subjected to variable amplitude uniaxial fatigue loading', *International Journal of Fatigue* **33**(7), 900–911.
- Susmel, L. & Taylor, D. (2012), 'A critical distance/plane method to estimate finite life of notched components under variable amplitude uniaxial/multi-axial fatigue loading', *International Journal of Fatigue* **38**, 7–24.
- Susmel, L., Tovo, R. & Benasciutti, D. (2009), 'A novel engineering method based on the critical plane concept to estimate the lifetime of weldments subjected to variable amplitude multi-axial fatigue loading', *Fatigue & Fracture of Engineering Materials & Structures* **32**(5), 441–459.
- Susmel, L., Tovo, R. & Socie, D. F. (2014), 'Estimating the orientation of stage i crack paths through the direction of maximum variance of the resolved shear stress', *International Journal of Fatigue* **58**, 94–101.
- Susmel & Taylor, D. (2015), 'Estimating lifetime of notched components subjected to variable amplitude fatigue loading according to the elastoplastic theory of critical distances', *Journal of Engineering Materials and Technology* **137**(1), 011008.
- Tavernelli, J. & Coffin, L. (1962), 'Experimental support for generalized equation predicting low cycle fatigue', *Journal of Basic Engineering* **84**(4), 533–537.

- Tipton, S. M. & Nelson, D. V. (1997), 'Advances in multiaxial fatigue life prediction for components with stress concentrations', *International Journal of Fatigue* **6**(19), 503–515.
- Tipton, S. & Nelson, D. (1989), 'Multiaxial fatigue life predictions for the sae specimen using stress based approaches', *Society of Automotive Engineers, Inc., Multiaxial Fatigue: Analysis and Experiments*, pp. 61–65.
- Van, K. D., Cailletaud, G., Flavenot, J., Le Douaron, A. & Lieurade, H. (1986), Criterion for high-cycle fatigue failure under multiaxial loading, in 'ICBMFF2'.
- Wang, Y. & Susmel, L. (2016), 'The modified manson–coffin curve method to estimate fatigue lifetime under complex constant and variable amplitude multiaxial fatigue loading', *International Journal of Fatigue* **83**, 135–149.
- Webber, D. (1970), Constant amplitude and cumulative damage fatigue tests on bailey bridges, in 'Effects of Environment and Complex Load History on Fatigue Life', ASTM International.
- Woo, S. (n.d.), 'Reliability design of mechanical system for mechanical civil engineer', <https://www.researchgate.net/publication/311856871-Reliability-Disasters-and-Its-Assessment-Significance>.

Appendix A

The developed Matlab Code to predict Multiaxial Fatigue ^[i]

A Matlab script is listed below to find Multiaxial fatigue damage of a notched component. The input data consists of local stress/strain states at a specific point inside a material being assessed in all directions (X, Y & Z). The input data were arranged in the form of a 12-column matrix. The corresponding stress-strain states were taken from the analysed FE model and consisted of $\sigma_x(t)$, $\epsilon_x(t)$, $\sigma_y(t)$, $\epsilon_y(t)$, $\sigma_z(t)$, $\epsilon_z(t)$, $\tau_{xy}(t)$, $\gamma_{xy}(t)$, $\tau_{yz}(t)$, $\gamma_{yz}(t)$, $\tau_{xz}(t)$ & $\gamma_{xz}(t)$. The reader would need to re-write the following script inside Matlab software with the same order and symbols stated below.

1. Creating [C] (the Variance and Covariance Matrix):

```
tic
strain=LocalStressStrainHistory(:, [2 4 6 8 10 12]);
strain(:,4)=strain(:,4)/2;
strain(:,5)=strain(:,5)/2;
strain(:,6)=strain(:,6)/2;
C_matrix=cov(strain,1);
```

2. Determine the potential critical planes:

```
N=0;
gamma_max=0;
for Fi=linspace(0,pi,37)
for Th=linspace(0,pi,37)
for Al=linspace(0,pi,37)
d=d.vec(Fi,Th,Al);
Var_strain_t=d'*(C_matrix*d);
gamma_a=2*(sqrt(2*Var_strain_t));
```

^[i]All calculations were performed using ANSYS® APDL Product Release 17.2 and MATLAB2017a running on an Intel i7 powered desktop PC with 8GB RAM, and running Windows 10 (64bit)

```

if gamma_a>=gamma_max
gamma_max=gamma_a;
N=N+1;
plane_max(N, :)=[Fi Th Al Var_strain_t gamma_a];
d_matrix(N, :)=[d' ];
end
end
end
end
toc

```

3. Determine Orientation of the correct Critical Plane:

```

tic
ConVal=estim(plane_max,d_matrix,C_matrix,N);
kapa=1000;
Var_old=0;
Div_Var_old=0;
for NN=1:N
Fi=plane_max(NN,1);
Th=plane_max(NN,2);
Al=plane_max(NN,3);
Var_strain_Al,Var_strain_Th,Var_strain_Fi,M=derive(Al,Th,Fi,C_matrix,d);
Fi=Fi+kapa*Var_strain_Fi;
Th=Th+kapa*Var_strain_Th;
Al=Al+kapa*Var_strain_Al;
Div_Var=d'*M;
if abs(Div_Var)>ConVal;
Fi_old=Fi;
Th_old=Th;
Al_old=Al;
Var_strain_Al,Var_strain_Th,Var_strain_Fi,M=derive(Al,Th,Fi,C_matrix,d);
Fi=Fi+kapa*Var_strain_Fi;
Th=Th+kapa*Var_strain_Th;
Al=Al+kapa*Var_strain_Al;
d=d.vec(Fi,Th,Al);
M=C_matrix*d;
Div_Var=d'*M;
elseif abs(Div_Var)<ConVal
Var_old=Var_strain_t;
Div_Var_old=Div_Var;
Fi_old=Fi;
Th_old=Th;
Al_old=Al;

```

```

d=d.vec(Fi_old,Th_old,Al_old);
Var_strain_t=d'*(C_matrix*d);
gamma_a=2*(sqrt(2*Var_strain_t));
end
Max_max_angles(NN,:)=[Fi_old Th_old Al_old gamma_a];
end
toc
MMM=0;
for nnn=1:NN
Fi=Max_max_angles(nnn,1);
Th=Max_max_angles(nnn,2);
Al=Max_max_angles(nnn,3);
d1=(sin(Th)*sin(2*Fi)*cos(Al)+sin(Al)*sin(2*Th)*(cos(Fi)^2))/2;
d2=(-sin(Th)*sin(2*Fi)*cos(Al)+sin(Al)*sin(2*Th)*(sin(Fi)^2))/2;
d3=-sin(Al)*sin(2*Th)/2;
d4=0.5*sin(Al)*sin(2*Fi)*sin(2*Th)-cos(Al)*cos(2*Fi)*sin(Th);
d5=sin(Al)*cos(Fi)*cos(2*Th)+cos(Al)*sin(Fi)*cos(Th);
d6=sin(Al)*sin(Fi)*cos(2*Th)-cos(Al)*cos(Fi)*cos(Th);
d=[d1; d2; d3; d4; d5; d6];
Var_strain_tt=d'*(C_matrix*d);
gamma_a=2*(sqrt(2*Var_strain_tt));
Max_max_strain(nnn,:)=[Fi*180/pi Th*180/pi Al*180/pi gamma_a d1 d2
d3 d4 d5 d6];
end

```

4. Sorting the order of the matrix result of the Critical Plane:

```

tic
gamma_a_unsorted=Max_max_strain(:,4);
order=sort(gamma_a_unsorted,'descend');
Sorted_solution=Max_max_strain(order,:);
toc

```

5. Calculating "rho" for each set of Calculated Angles (Potential Critical Planes):

```

tic
stress=LocalStressStrainHistory(:,[1 3 5 7 9 11]);
C_matrix_stress=cov(stress,1);
rat=pi/180;
for ii=1:NN
Fi=rat*Sorted_solution(ii,1);
Th=rat*Sorted_solution(ii,2);
Al=rat*Sorted_solution(ii,3);
n_vec=[sin(Th)*cos(Fi); sin(Th)*sin(Fi);
cos(Th)];

```

```

q_vec=[cos(A1)*sin(Fi)+sin(A1)*cos(Th)*cos(Fi);
-cos(A1)*cos(Fi)+sin(A1)*cos(Th)*sin(Fi);
-cos(A1)*sin(Fi)];
d1=(sin(Th)*sin(2*Fi)*cos(A1)+sin(A1)*sin(2*Th)*(cos(Fi)^2))/2;
d2=(-sin(Th)*sin(2*Fi)*cos(A1)+sin(A1)*sin(2*Th)*(sin(Fi)^2))/2;
d3=-sin(A1)*sin(2*Th)/2;
d4=0.5*sin(A1)*sin(2*Fi)*sin(2*Th)-cos(A1)*cos(2*Fi)*sin(Th);
d5=sin(A1)*cos(Fi)*cos(2*Th)+cos(A1)*sin(Fi)*cos(Th);
d6=sin(A1)*sin(Fi)*cos(2*Th)-cos(A1)*cos(Fi)*cos(Th);
d=[d1; d2; d3; d4; d5; d6];
for jj=1:length(stress(:,1))
sigma_general=local_mat(stress(jj,:));
epsilon_general=local_mat(strain(jj,:));
stress_nt(jj,1)=(n_vec'*sigma_general)*n_vec;
shear_qt(jj,1)=(q_vec'*sigma_general)*n_vec;
strain_nt(jj,1)=(n_vec'*epsilon_general)*n_vec;
gamma_qt(jj,1)=(q_vec'*epsilon_general)*n_vec;
end
var_stress_nt=var(stress_nt(:,1));
var_shear_qt=var(shear_qt(:,1));
Var_strain_td=d'*(C_matrix*d);
gamma_ad=2*(sqrt(2*Var_strain_td));
Var_tau_ad=d'*(C_matrix_stress*d);
tau_ad=(sqrt(2*Var_tau_ad));
tau_m=mean(shear_qt(:,1));
sigma_na=(sqrt(2*var_stress_nt));
stress_nm=mean(stress_nt(:,1));
max_normal=(stress_nm)+(sigma_na);
rho=((stress_nm)+(sigma_na))/((tau_ad));
All_calculation(ii,:)=[Fi*180/pi Th*180/pi Al*180/pi gamma_ad
tau_ad stress_nm sigma_na max_normal rho];
end
toc

```

6. Final Result:

```

tic
header='N', 'Fi', 'Th', 'Al', 'gamma_a', 'tau_a', 'sigma_nm',
'sigma_na', 'sigma_n_max', 'rho';
data_all=(1:size(All_calculation,1))' (All_calculation(:,1:9));
data_all=sortrows(data_all,[-5 -6 -10 -9]);
RESULTS=dataset(data_all,header:);

```

7. Determine Number of Cycles to Failure for Constant Amplitude Loading:


```

E=210000;
ve=0.3;
sgmf=852.3;
epsf=0.477;
b=-.105;
c=-.554;
tauf=460.6;
gamf=1.55;
b0=-.068;
c0=-.648;
Nf=nf_calc (RESULTS.gamma_a (1) , RESULTS.rho (1) , E, ve, sgmf, tauf, epsf,
gamf, b, b0, c, c0)
Function to find  $N_{fe}$ :
function [Nf]=nf_calc (gamma_a, rho, E, ve, sgmf, tauf, epsf, gamf, b, b0, c, c0)
tau_f_G=rho*(1+ve)*sgmf/E+(1-rho)*tauf/80800;
gamf_rho=rho*(1+0.5)*epsf+(1-rho)*gamf;
b_rho=b*b0/((b0-b)*rho+b);
c_rho=c*c0/((c0-c)*rho+c);
x=0.1;
y=1;
m=0;
while y>0.00001
clc
y=(tau_f_G)*xb_rho+gamf_rho*xc_rho-gamma_a;
if isreal(y);
break;
end
dy=b_rho*(tau_f_G)*x(b_rho-1)+c_rho*gamf*x(c_rho-1);
x=x-y/dy
if x<0;
break;
end
Nf=x/2;
m=m+1
end
clc
end

```

8. Determine Number of Cycles to Failure for Variable Amplitude Loading:

```

E=210000;
G=80800;
ve=0.3;
sgmf=852.3;

```

```

epsf=0.477;
b=-.105;
c=-.554;
tauf=460.6;
gamf=1.55;
b0=-.068;
c0=-.648;
ro = rho(1,1);
tic
for n=1:length(count.Amplitude)
rho_limit = 1.70;
if RESULTS.rho(1) > rho_limit
rho = rho_limit
elseif RESULTS.rho(1) < rho_limit
rho = RESULTS.rho(1)
end
Nf(n,1)=nf_calc(count.Amplitude(n),rho,E,ve,sgmf,tauf,epsf,gamf,b,b0,c,c0);
end
toc
order=sort(count.Amplitude,'descend');
Nf_vs_A=[Nf(order) count.Amplitude(order)];
figure1 = figure;
point1 = 10*(Nf_vs_A(1,1));
point2 = 2*Nf_vs_A(length(count),1);
elastic_MCCM=[point1
((ro*(1+0.5)*epsf+(1-ro)*gamf)*(point1)^(c*c0/((c0-c)*ro+c)));
1 ((ro*(1+0.5)*epsf+(1-ro)*gamf)*1^(c*c0/((c0-c)*ro+c))];
plastic_MCCM=[point2 ((ro*(1+ve)*sgmf/E+(1-ro)*tauf/G)*(point2)^(b*
b0/((b0-b)*ro+b)));
100 ((ro*(1+ve)*sgmf/E+(1-ro)*tauf/G)*100^(b*b0/((b0-b)*ro+b))];
interval = 1;
Nf_ext = 25;
start_Nf = Nf_vs_A(1,1);
while Nf_ext <= start_Nf
gamma_a_ext(interval) = ((ro*(1+ve)*sgmf/E+(1-ro)*tauf/G)*(2*Nf_ext)^(b*
b0/((b0-b)*ro+b)))+((ro*(1+0.5)*epsf+(1-ro)*gamf)*(2*Nf_ext)^(c*
c0/((c0-c)*ro+c)));
Nf_vs_ext(interval) = Nf_ext;
interval = interval+1;
Nf_ext = Nf_ext + 10;
end
axes1 =
axes('Parent',figure1,'YScale','log','YMinorTick','on',...

```

```

'YMinorGrid','on',...
'YGrid','on',...
'XScale','log',...
'XMinorTick','on',...
'XMinorGrid','on',...
'XGrid','on');
ylim(axes1,[0.0001 1]);
box(axes1,'on');
hold(axes1,'all');
loglog(2*Nf_vs_A(:,1),Nf_vs_A(:,2),'k','LineWidth',2);
loglog(2*Nf_vs_ext,gamma_a_ext,'k','LineWidth',2);
loglog(plastic_MCCM(:,1),plastic_MCCM(:,2),'--r');
loglog(elastic_MCCM(:,1),elastic_MCCM(:,2),'--r');
xlabel('2N_f');
ylabel('gamma_a');
Dcr=0.22;
D_tot=sum(1./Nf);
Nfe=sum(count.Cycles_No)*Dcr/D_tot;
figure2 = figure;
axes2 = axes('Parent',figure2,'YGrid','on','XGrid','on');
box(axes2,'on');
hold(axes2,'all');
plot(Nf_vs_A(:,2))
xlabel('Sigma(n)')
ylabel('gamma_a')
bar(Nf_vs_A(:,2),'FaceColor',[0 0 1]);
Function to find Nfe:
function[Nf]=nf_calc(gamma_a,rho,E,ve,sgmf,tauf,epsf,gamf,b,b0,c,c0)
tau_f_G=rho*(1+ve)*sgmf/E+(1-rho)*tauf/80800;
gamf_rho=rho*(1+0.5)*epsf+(1-rho)*gamf;
b_rho=b*b0/((b0-b)*rho+b);
c_rho=c*c0/((c0-c)*rho+c);
x=0.1;
y=1;
m=0;
while y>0.00001
clc
y=(tau_f_G)*xb_rho+gamf_rho*xc_rho-gamma_a;
if isreal(y);
break;
end
dy=b_rho*(tau_f_G)*x(b_rho-1)+c_rho*gamf*x(c_rho-1);
x=x-y/dy

```

```
if x<0;
break;
end
Nf=x/2;
m=m+1
end
clc
end
```

Appendix B

Fatigue Fracture Surface

Table B.1: Fatigue Fracture Surfaces of Notches under multiaxial CA/VA load with zero mean stress

	$r_n = 1.5mm$		$r_n = 3mm$		$r_n = 6mm$	
	Medium-Cycle	Low-Cycle	Medium-Cycle	Low-Cycle	Medium-Cycle	Low-Cycle
CAZMSIph						
CAZMSOPh						
VAZMSIph						
VAZMSOPh						

Table B.2: Fatigue Fracture Surfaces of Notched Specimens under Multiaxial V.A Fatigue load with involving mean stresses

	$r_n = 1.5mm$		$r_n = 3mm$		$r_n = 6mm$	
	Medium-Cycle	Low-Cycle	Medium-Cycle	Low-Cycle	Medium-Cycle	Low-Cycle
VANZMSIph [†]						
VANZMSOPh [†]						

[†]VA: Variable Amplitude, NZMS: Non-Zero mean Stress, **Iph**: In-phase, **OPh**: Out-of-phase, r_n :Notch Root Radius

Table B.3: Fatigue Fracture Surfaces of Notched Specimens under Multiaxial V.A Fatigue load - Different Frequencies

	$r_n = 1.5mm$		$r_n = 3mm$		$r_n = 6mm$	
	Medium-Cycle	Low-Cycle	Medium-Cycle	Low-Cycle	Medium-Cycle	Low-Cycle
AxFr0.5,TFr1.0 [†]						
AxFr1.0,TFr0.5 [†]						

[†]AxFr0.5,TFr1.0: Axial Load Frequency=0.5 & Torsional Frequency=1.0

[†]AxFr1.0,TFr0.5: Axial Load Frequency=1.0 & Torsional Frequency=0.5